DESIGN, FABRICATION, AND UTILIZATION OF SILICA INVERSE OPAL STRUCTURES FOR FLOW-THROUGH CATALYST SUPPORTS

By

Douglas B. Gornowich

A DISSERTATION

Submitted to
Michigan State University
in partial fulfillment of the requirements
for the degree of

Chemistry - Doctor of Philosophy

2013

ABSTRACT

DESIGN, FABRICATION, AND UTILIZATION OF SILICA INVERSE OPAL STRUCTURES FOR FLOW-THROUGH CATALYST SUPPORTS

By

Douglas B. Gornowich

Enzymes are used in a wide range of industries for various different chemical processes. Optimizing the performance of enzymes remains an area of high interest in many research labs. An enzyme is often immobilized on or within a support structure, which allows for the biocatalyst to be relatively easy to recover post-reaction. Immobilization can also increase the structural stability of the enzyme, which is beneficial from a cost standpoint because pure enzymes can be expensive. By choosing the appropriate support and immobilization chemistry, it is possible to maximize the efficiency of a biocatalyst. The purpose of this work was to design, fabricate and utilize inverse opal structures as a support for the immobilization of enzymes.

We have developed a flow-through silica inverse opal structure that was used for the immobilization of biocatalysts. The inverse opal structures were created using polystyrene nanospheres as a template, sol-gel chemistry to deposit silica in the interstitial spaces between the nanospheres, and solvent dissolution to remove the template. Scanning electron microscopy and dynamic light scattering were used to characterize the nanospheres and structures. The silica inverse opal structure has a relatively high surface area, and a surface that is amenable to a wide range of surface modification reactions. Two enzymes were chosen to evaluate our catalyst support structure; glucose oxidase and alkaline phosphatase. Absorbance and fluorescence measurements were used for the enzyme assays.

Our results show an enhancement in reactivity that is associated with enzyme immobilization and nano-confinement, and also underscore limitations inherent to this approach. Three different reaction formats were examined: solution phase, immobilized enzymes on planar supports, and enzymes immobilized on the flow-through inverse opal structure. Glucose oxidase exhibited an increase in reactivity when comparing planar vs. solution phase and inverse opal vs. planar structural formats. This finding indicated an enhancement due to the immobilization process and due to the nanoconfinement of the enzyme within the inverse opal structure. In contrast, alkaline phosphatase exhibited a reduced activity when comparing solution phase vs. enzyme immobilized on planar and inverse opal structures. This finding illustrated the importance of identifying immobilization chemistry that maintains the enzyme in an active form and binds the enzyme in a way that leaves the reactive site accessible. An enhancement was observed for the inverse opal structure vs. the planar support, indicating that there remains the positive effect associated with nano-confinement of the enzyme.

This project proved to be enlightening by showing the enhancements in activity for glucose oxidase, and also by showing that there are limitations that need to be addressed in the alkaline phosphatase results. There will be continued work to further characterize and optimize the flow-through inverse opal structures. In addition, it may be useful to examine the use of other materials for the inverse opal support itself. The results of this work are promising for the utilization of inverse opal structures to immobilize and optimize the performance of enzymes.

ACKNOWLEDGEMENTS

I would like to acknowledge a few people that have helped me grow as a scientist and a person over the course of my graduate career. First and foremost, I would like to thank my graduate research advisor, Dr. Gary J. Blanchard. His door was always open, which allowed for an open line of communication throughout my time spent at MSU. I appreciate the thoughtful insight that he provided as well as the constructive criticism that helped to mold me into the scientist that I am today. I would also like to thank my guidance committee for all of their assistance along the way; Dr. Greg Swain, Dr. Merlin Bruening and the late Dr. Greg Baker. In addition, I would like to thank Dr. John McCracken for stepping in as a committee member for my defense.

I would also like to thank all of the past and current Blanchard group members that were there to lend a helping hand. I would like to specifically thank the following past members; Dr. Monique Lapinski, Dr. Kelly Greenough, Dr. Janelle Newman, Dr. Alexis Blevins, Dr. Benjamin Oberts, Dr. Monika J. Dominska, Dr. Heather A. Pillman, and Dr. Margaretta Koster. I would also like to thank the following members of the group that have helped me throughout my time at MSU; Christine Hay, Iwan Setiawan, Chen Qiu, Fredy Pratama, Stephan Baumler, and Matthew Oliver.

I would also like to express gratitude to a list of groups and facilities that allowed me to utilize their instrumentation for my graduate work. I would like to thank the folks over at the Michigan State University Center for Advanced Microscopy facility for allowing me to use the scanning electron microscope. I would also like to thank Dr. Xuefei Huang and his research group for allowing me access to their dynamic light scattering instrument. Finally, I would like

to thank Mike Rich for granting me access to the instruments at the Composite Materials and Structure Center at MSU.

Last, but certainly not least, I would like to thank all of my family and friends that provided me with encouragement and support throughout my journey in graduate school. I would especially like to thank my wife, Sheila, for being understanding and positive when things were tough. I simply could not have done it without her support.

TABLE OF CONTENTS

LIST OF TABLES

LIST OF FIGURES

LIST OF SCHEMES

CHAPTER 1: Introduction to Enzyme Immobilization and Inverse Opal Structures

Introduction

Enzyme immobilization is a key area of interest in many research labs.[1,2] Enzymes are used in a wide variety of industries, including dairy (cheese), beverage (fermentation), biofuels (fermentation), and food safety (diagnostic test kits). Consequently, optimizing the performance of the various enzymes used in these processes is important. Maximizing the performance of an enzyme is a balance of maximizing reactivity and while maintaining long term stability of the enzyme. The two main areas of interest in this field are examining the different techniques used to immobilize the enzyme and the design of the material/support used to immobilize the enzyme. Designing a support that would increase the performance of a given enzyme would be a valuable contribution to science, and this dissertation reports on an investigation utilizing inverse opal structures as a scaffold to immobilize enzymes. This Chapter will discuss enzyme immobilization, give an overview of inverse opal structures, sometimes referred to as nanoporous solids (NS), and introduce the enzyme/NS combinations that were used in this work. Chapter 2 will focus on the fabrication of inverse opal structures on planar and porous supports. Chapters 3 and 4 provide examples of the utility and limitations of NS structures used as flow-through heterogeneous catalytic reactors for two different enzymes. Chapter 5 will include overall conclusions and future directions for this project.

Enzyme Immobilization

As mentioned above, the immobilization of enzymes often results in enhanced performance relative to that in the solution phase for a given protein. There are, however, a few areas of concern regarding the immobilization process. The standard by which enzymes are

evaluated in an industrial setting, to maximize the cost efficiency of a process, is a ratio quantitating the kg of product per kg of enzyme. Ideally, enzymes should not cost more than a few percent of the total production costs.[2] Immobilizing enzymes provides several advantages over solution phase enzymatic reactions including: facile separation of the enzyme and reactants/products, reduction of protein contamination in the product, ease of enzyme recovery and reuse, increased structural stability of the biocatalyst, and enzyme denaturation that may be caused by products formed during the reaction can be minimized when using a flow-through system. Another advantage to immobilizing the enzyme is the possibility of arranging sequences of enzymes in specific order(s) to perform cascaded chemical reactions.[3,4] The reactivity of the enzyme is often affected when it is tethered to a support structure. Depending on the manner in which the enzyme is immobilized, it is possible to enhance the reactivity of the biocatalyst relative to that in the solution phase.[5-7]

There are, however, some potential disadvantages to the immobilization process. The most prominent issue to contend with is ensuring that the immobilization method does not make the active site of the protein inaccessible to substrate molecules. If the enzyme is attached in a manner where the active site is not readily accessible, its reactivity will be decreased, sometimes markedly, relative to that in the solution phase. Another issue that may arise for certain biocatalysts is steric crowding of the proteins. This can be a problem if the steric effects alter the conformation of the enzyme in a way that changes the conformation of or access to the binding pocket. Using various surface chemistry immobilization techniques and inserting chemical spacers between enzymes can often minimize the aforementioned limitations encountered when biocatalysts are immobilized.[8]

There are three main techniques used for enzyme immobilization: binding to a prefabricated support structure, encapsulation or entrapment within a material, and aggregation of enzymes due to covalent cross-linking. The first two approaches can involve biocatalysts that are either physisorbed or bonded covalently to the support matrix. The main distinction between the two techniques is that the enzyme is attached to the support in sequential steps in the first case. For the entrapment method, the enzyme and support are formed simultaneously, resulting in an enzyme/support matrix. The cross-linking methodology is completely different than the other two techniques because the enzyme itself is used as the support structure. Fig. 1.1 provides a simple illustration of the different methods, and the following three paragraphs will discuss each system in more detail.

Enzymes bound to a pre-fabricated carrier exhibit certain advantages when it comes to immobilization. The biocatalysts can be either physisorbed or covalently attached to the surface, which ensures that the proteins are accessible to substrate molecules. However, the surface attachment used is an important factor in determining the conformation of the protein when it is attached to the surface, and this will be discussed later in this chapter. There have been several different prefabricated materials reported in the literature used for enzyme immobilization. These supports include acrylic resins,[9] hydrogels[10] and polymers.[11,12] A major focus has also been centered on utilizing selected inorganic supports as enzyme carriers, including nanoporous and mesoporous silica,[5-7,13,14] silica nanospheres,[15,16] zeolites,[17,18] alumina,[19] and macroporous titania.[20] Many of these support structures provide an active surface for the attachment of enzymes, but a major drawback for many of them are expense and difficulty in fabrication.

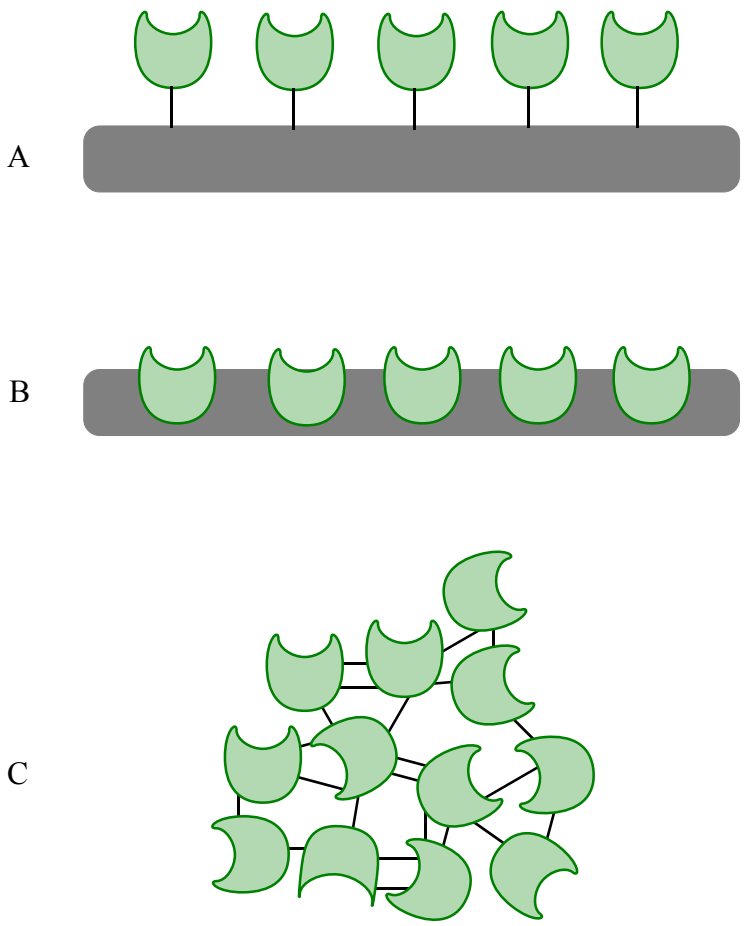

Figure 1.1: Illustration of three different enzyme immobilization techniques; binding to a prefabricated support (A), entrapment (B), and enzyme aggregation/crystals (C). Note, this is just to illustrate the different methods and is not drawn to scale. For interpretation of the reference to color in this and all other figures, the reader is referred to the electronic version of this dissertation.

The second method for immobilizing enzymes is entrapment of the biocatalyst.[21-27] For this technique, enzymes and the entrapping matrix material are typically co-assembled in a one-pot reaction. The primary advantage of this technique is that high enzyme loadings are achievable. The physical interactions between the enzyme and the material are relatively weak and, as a result, enzyme leakage can be a problem. The way many researchers get around this is to include reactive functional groups within the matrix to facilitate covalent attachment between the biocatalyst and the surrounding material. Entrapment is typically performed using organic polymers,[21,22] ionic liquids[23] or sol-gel based metal oxides.[24-27] The main limitation in this work is that due to the nature of the encapsulating process, a large amount of biocatalysts can be buried within the matrix. If the active sites are rendered inaccessible by virtue of enzyme entrapment within the matrix, much lower activity may be observed. Entrapment and prefabricated supports are often referred to the enzyme "carrier" matrix.

The third class of enzyme immobilization techniques is cross-linked enzyme aggregates or crystals (carrier-free) where the enzyme itself is the carrier.[28-31] For this method, bioactive proteins are cross-linked together to form insoluble aggregates or crystals that can be physically separated from solution.[28-31] This approach dates back to 1964 when it was discovered that surface NH_2 groups could be cross-linked using glutaraldehyde.[32,33] Since then, there have been several attempts at improving crystallization techniques, including control over the pore size in the crystals.[34] Other efforts have been made to simplify the separation of the crystals by attaching them to magnetic particles.[35] The main drawback to this approach is the crystallization process itself, because of the requirement of high purity enzymes and

consequently high cost. Another inherent disadvantage of this approach is a result of the physical issue of a large amount of enzyme residing within the crystal structure and thus being inaccessible. Such enzyme is essentially used as filler material and is not catalytically active.

A great deal of research is currently ongoing and focused on addressing the limitations of each of the three different approaches.[1,2] Carrier-bound techniques on pre-fabricated supports have been the gold standard over the past decades, and continue to be at the forefront of biocatalysis systems. Recent advances in encapsulation and aggregation techniques have shown promise. The next section of this Chapter will detail a novel approach that uses dielectric inverse opal materials as support structures for enzyme immobilization. There are several benefits that accrue from the use of this structural motif, including confinement of the enzymes in a nanoscale volume and the chemical functionality of the matrix itself for use in tethering enzymes.

Inverse opals

Inverse opal materials have been studied extensively over the last decade.[5,36-44] An inverse opal structure is fabricated using a process that is illustrated in Fig. 1.2. In general, the procedure of how such nanoporous solids are fabricated is described by the following steps: 1) nanospheres are deposited in an organized assembly on a support, 2) the interstitial space between the spheres is filled with a different material, and 3) the nanospheres are removed, leaving an inverse "image" of the nanosphere assembly which is characterized by openings (nanosphere touch points) that allow for facile flow through the structure. It is also possible to combine the first two steps and co-deposit the nanospheres in a suspension of the filler material. The properties of these materials will be discussed in this section, including the wide variety of options for composition of the matrix, the moderately high surface area, and control over the

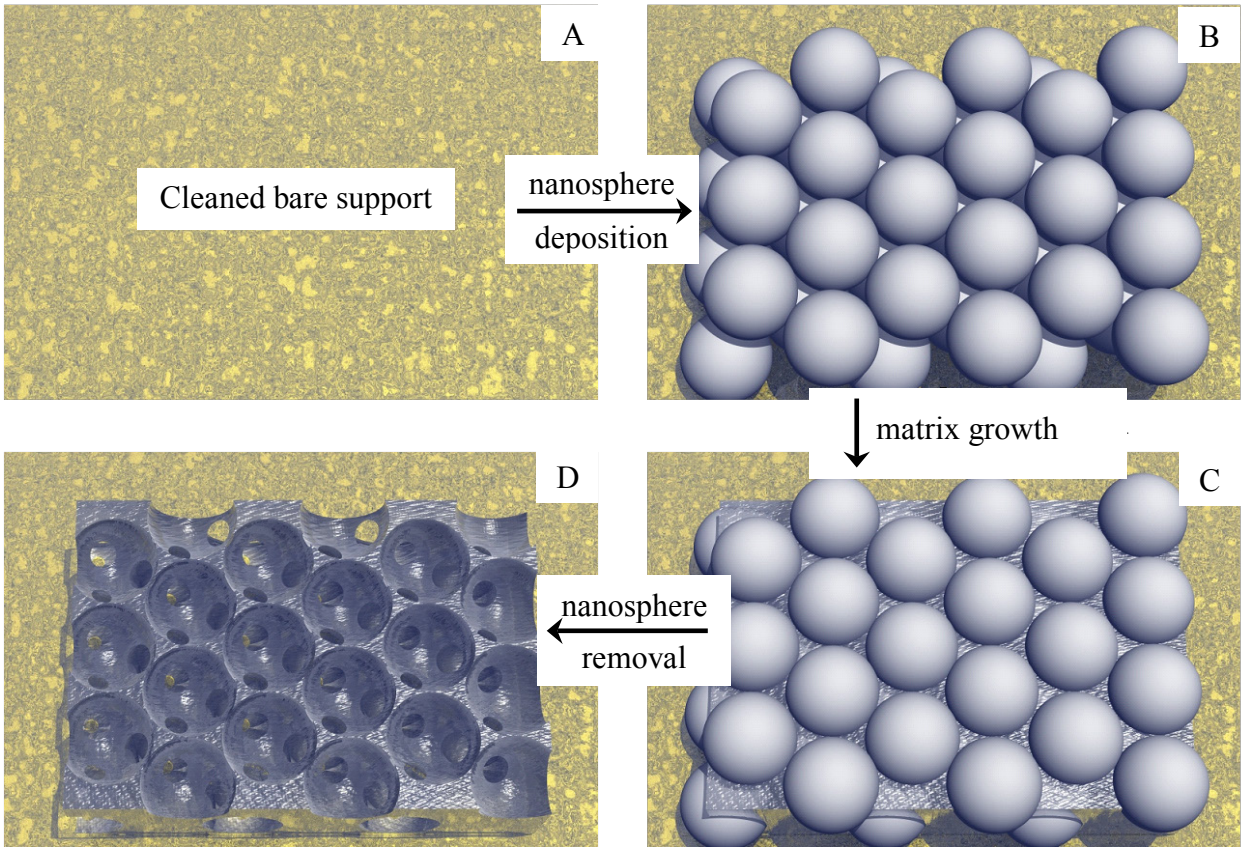

Figure 1.2: Illustration of the steps involved in the fabrication of an inverse opal structure.

pore size. The utility of inverse opals for use as supports for enzyme immobilization will be illustrated in Chapters 3 and 4. There are, of course, limitations to the use of such structures, and they are considered in this work as well.

There are many different possibilities for the nanosphere and filling matrix materials, allowing for the use of these structures in a variety of different applications. Typically, either organic polymer or inorganic oxide spheres are used for the formation of the nanosphere scaffold. Polystyrene and silica are the nanospheres used most widely.[5,39,41-45] There have been several different materials used to fill the void spaces between nanospheres. For dielectric materials, silica,[36,46] titania,[39,40,46-48] zirconia,[46,48] alumina,[46,48] and composites[49] have been reported. Metals have also been used widely, including Pt,[41-43,50-52] Pd,[41-43,51] Au,[37,52] Ni,[50,53,54] and Cu.[50] Inorganic oxide inverse opals are typically formed with the use of sol-gel chemistry, and metals are electrodeposited into the interstitial space. The ability to choose the matrix material makes inverse opal structures amenable for a variety of different uses.

Another characteristic property of inverse opals is that they have a relatively high surface-area-to-volume (SA/V) ratio. The surface area can be calculated based on the dimensions and geometric arrangement of the nanospheres comprising the scaffold structure. Voids are designated as the spaces vacated by the nanospheres that had been used as the scaffold, and the openings left by the nanosphere contact points are termed pores. The pore size is determined by the size of the spheres used for the scaffold, a relationship that implies very sensitive control over the characteristic openings within the matrix. Kuhn and coworkers have shown that the diameter of the pores are *ca*. 20% of the diameter of the nanospheres.[37] For a

hexagonal close-packed structure, each sphere on the first layer would have 9 contact points with neighboring spheres and one pore on the bottom (with the support), and each subsequent layer would have 12 contact points. The surface area (SA) of each void on the first layer can be calculated by $SA_{void} = (SA_{nanosphere} - 10A_{pore})$ and $SA_{void} = (SA_{nanosphere} - 12A_{pore})$ for subsequent layers. $SA_{nanosphere}$ is $4\pi r^2$ and the A_{pore} is estimated to be $0.2\pi r^2$ for the circular pores. For illustrative purposes, assume that an inverse opal structure is fabricated using nanospheres with a diameter of 500 nm. Consequently, the pores would have a diameter of 100 nm. For $1cm^3$ of material, there would be $2x10^4$ voids along each side of the material, resulting in $4x10^8$ voids per layer. Using the equations above, the surface area would be 1.57 cm^2 for the first layer and 1.26 cm^2 for each subsequent layer. With $2x10^4$ layers, the resulting total surface area is $2.5x10^4$ cm^2 per geometric cm^3 of material. It is worth noting that the surface area for each layer is independent of nanosphere size, however using smaller spheres will allow for more layers to be deposited in a given volume.

The relatively high surface area and wide range of matrix materials make inverse opals an auspicious carrier for enzyme immobilization. For all of the work presented in this dissertation, silica was used as the matrix material and it was deposited using sol-gel chemistry. The details of the NS structure fabrication are outlined in Chapter 2 of this dissertation. The focus in Chapter 1 is on the rationale for the design of the inverse opals used. The moderately high SA/V ratio affords a relatively high loading density of biocatalysts to be achieved in a limited volume despite the limitation of a single monolayer of coverage within the matrix (*vide infra*). In addition, silica is amenable to a wide range of surface modification chemistry for enzyme

immobilization. Most of the enzyme attachment strategies can be performed under relatively mild reaction conditions, minimizing enzyme denaturation during immobilization. Enzyme immobilization by glutaraldehyde (Fig. 1.3) cross-linking of primary amines on the support to primary amines on the surface of the enzyme molecules is a well-established and relatively efficient method.[55-60] Having the enzyme immobilized on a support structure is desirable because the enzyme can be stored in buffer and can have prolonged stability.[58]

Another appealing characteristic of NS structures is that they are sufficiently porous to allow for flow-through designs to be developed.[5] Confining proteins in small spaces has been shown to increase the stability of the molecule.[61] When substrate-containing solutions are flowed through the NS, it is possible that enhanced reactivity relative to that in the solution phase can be observed by increasing the number of substrate-enzyme interactions based on geometric confinement within the inverse opal structure. A plot of characteristic diffusion length of a substrate molecule relative to the diameter of the nanoscale void space of the inverse opal (Fig. 1.4), $2\sqrt{(Dt)}/d$ vs. d, illustrates the increased relative probability of reactive substrate-enzyme interactions for the NS systems, where D is the diffusion coefficient for the substrate molecule (cm^2/sec), t is time (sec), and d is the diameter of the nanospheres used. For the flow rates used in these experiments, residence times for the substrate molecules within the NS are on the order of 5-10 seconds. From this model it is clear that the smaller the void volume, the higher the probability of a substrate-enzyme reaction event occurring. Another important factor to consider in a flow-through structural motif is that the products of the reaction are swept away from the enzyme. This can be advantageous for certain enzymes such as glucose oxidase, where one of

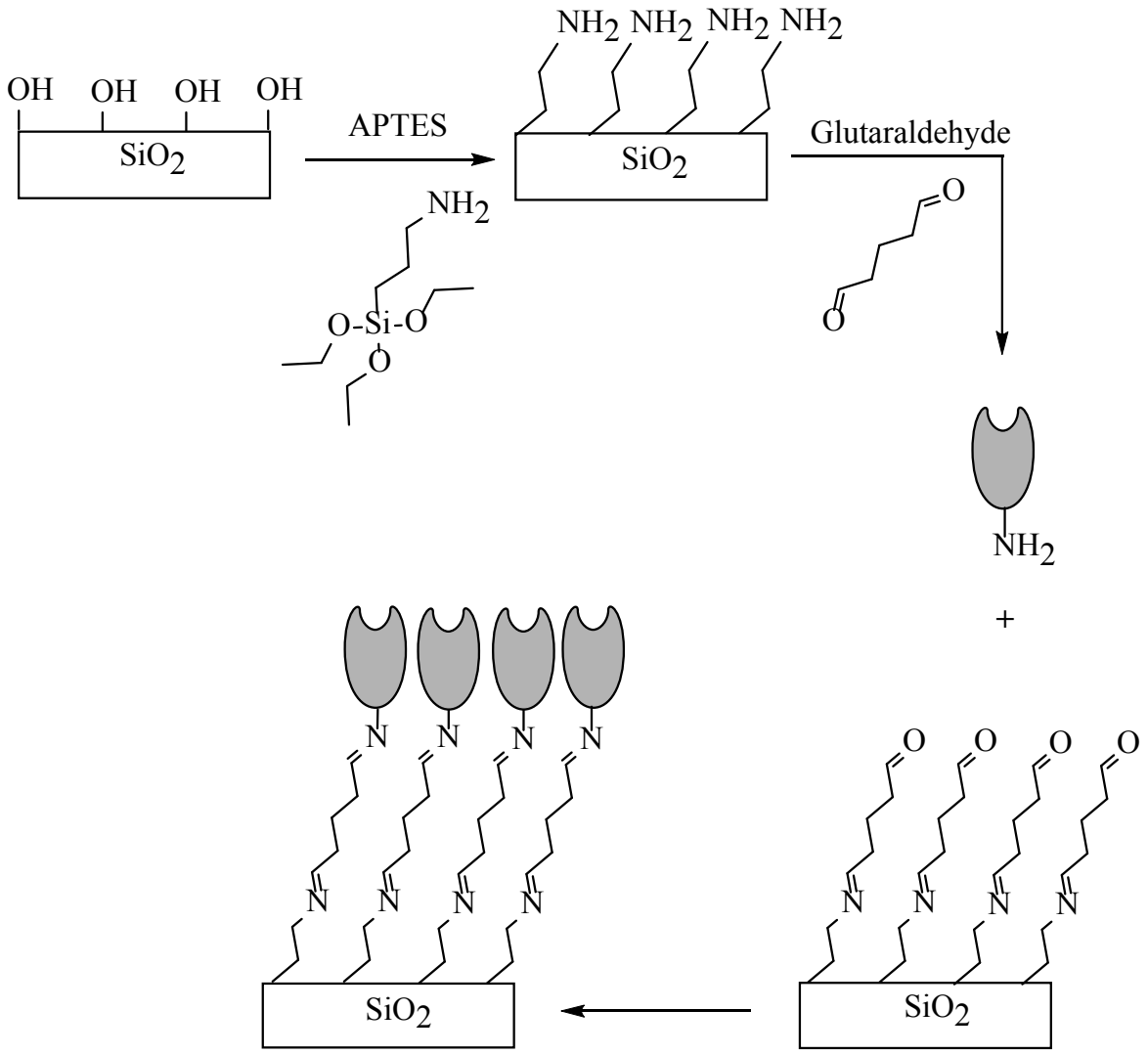

Figure 1.3: Enzyme immobilization using (3-aminopropyl)triethoxysilane (APTES) and glutaraldehyde to cross-link amine groups

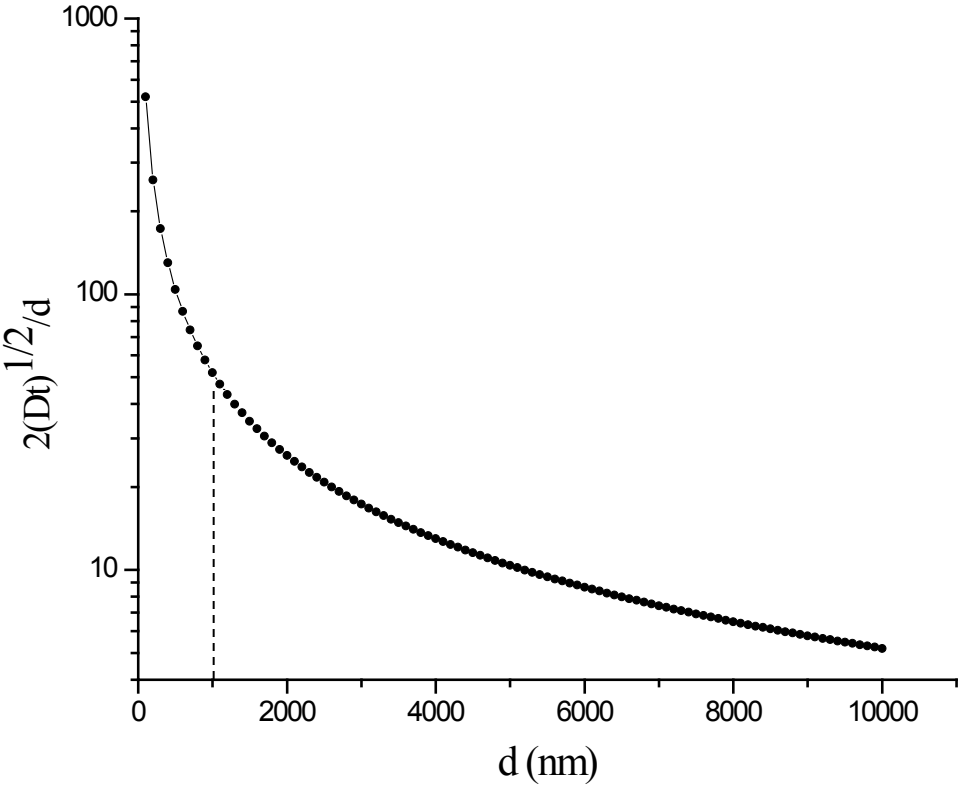

Figure 1.4: Plot of $2\sqrt{(Dt)}/d$ vs. d to indicate the enhanced probability of substrate-enzyme interactions (t = 1 sec). The dashed line highlights the d used for the experimental conditions in this work.

the products (H_2O_2) of the reaction can denature the native enzyme over prolonged exposure times.[62-64]

With all of the previously mentioned potential benefits in mind, there are a few limitations to the use of NS structures as support structures for the attachment of enzymes. The biggest challenge is to create the NS in a physically robust format that will allow a reactant stream to flow through the matrix. Inverse opal structures are very fragile by nature and a support is required to help maintain the integrity of the structure. Chapter 2 addresses this issue in more detail. Another limitation is associated with the fragile structure and small pore size that limits the flow-rates that can be used. An issue specific to dielectric inverse opals is the quantitation of the enzyme loading in the NS matrix. Spectroscopic techniques are difficult to employ due to the inverse opals acting as photonic crystals.[65] Due to the alternating dielectric constant within the matrix, photonic band gaps are seen at locations in the UV and visible spectrum, depending on the dimensions of the inverse opal structure. Thus performing quantitative spectroscopic measurements is a challenge in such media. Gravimetric methods can provide some quantitative data, but the measurements can be time consuming and challenging, in both execution and interpretation.

Model Enzymes

Glucose oxidase (GOx) and alkaline phosphatase (ALP) were chosen as model enzymes for our inverse opal flow-through catalytic nano-reactors. These two enzymes were not chosen with any specific industrial application in mind, but rather as starting points to illustrate the potential and limitations of this approach to the immobilization of biocatalytic systems. These enzymes are readily available for purchase and are relatively inexpensive. GOx (*Aspergillus*

niger) and ALP (bovine intestinal mucosa) are similar in size (160 kDa), yet they are different with respect to substrate specificity. GOx is an enzyme that exhibits a high specificity for β-D-glucose and the reaction is shown in Scheme 1.1. In contrast, ALP dephosphorylates phosphate monoesters into alcohols with very little substrate specificity (Scheme 1.2). It was our hope that these two enzymes would be sufficient to demonstrate our flow-through system and provide some insight into how this structural motif for flow-through supported catalytic reactions could be improved. Three different reaction formats were examined; free enzymes in solution, enzyme immobilized on planar solid supports, and enzyme attached to nanoporous solid structures. These results are presented in Chapter 3 for GOx and Chapter 4 for ALP and, taken together, they demonstrate some of the advantages and limitations associated with this approach to enzyme immobilization.

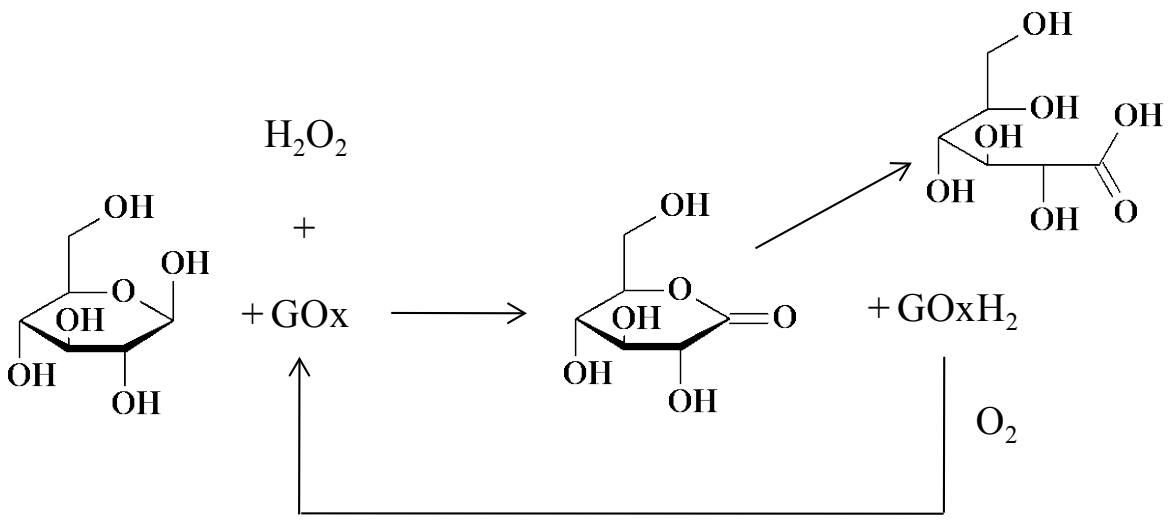

Scheme 1.1: GOx reaction, oxidation of β-D-glucose to form D-gluconolactone, which is then spontaneously hydrolyzed to D-gluconic acid. The reduced enzyme reacts with oxygen to regenerate GOx and produces hydrogen peroxide.

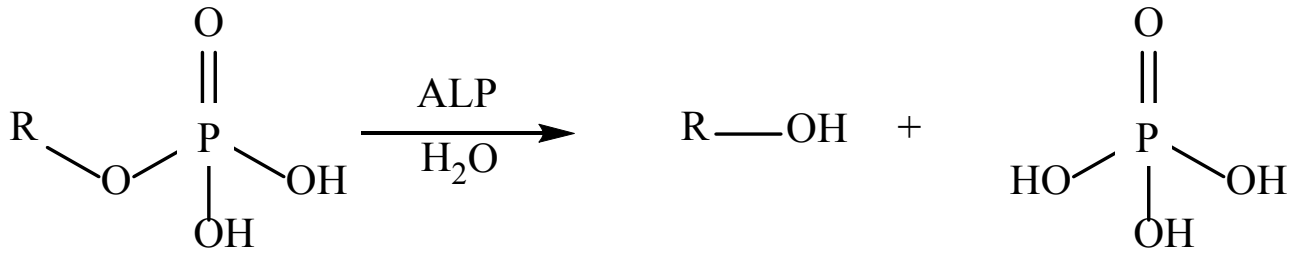

Scheme 1.2: Non-specific dephosphorylation of a phosphate monoester by reacting with alkaline phosphatase.

Literature Cited

Literature Cited

1. Hwang, E. T.; Gu, M. B. *Engineering in Life Sciences* **2013**, *13*, 49.

2. Sheldon, R. A. *Advanced Synthesis & Catalysis* **2007**, *349*, 1289.

3. Bruggink, A.; Schoevaart, R.; Kieboom, T. *Organic Process Research & Development* **2003**, *7*, 622.

4. Veum, L.; Hanefeld, U. *Chemical Communications* **2006**, *0*, 825.

5. Gornowich, D. B.; Blanchard, G. J. *The Journal of Physical Chemistry C* **2012**, *116*, 12165.

6. Lei, C.; Soares, T. A.; Shin, Y.; Liu, J.; Ackerman, E. J. *Nanotechnology* **2008**, *19*, 1.

7. Lei, C.; Shin, Y.; Liu, J.; Ackerman, E. J. *Journal of the American Chemical Society* **2002**, *124*, 11242.

8. Manta, C.; Ferraz, N.; Betancor, L.; Antunes, G.; Batista-Viera, F.; Carlsson, J.; Caldwell, K. *Enzyme and Microbial Technology* **2003**, *33*, 890.

9. Katchalski-Katzir, E.; Kraemer, D. M. *Journal of Molecular Catalysis B: Enzymatic* **2000**, *10*, 157.

10. Temiño, D. M.-R. D.; Hartmeier, W.; Ansorge-Schumacher, M. B. *Enzyme and Microbial Technology* **2005**, *36*, 3.

11. Ivanov, A. E.; Edink, E.; Kumar, A.; Galaev, I. Y.; Arendsen, A. F.; Bruggink, A.; Mattiasson, B. *Biotechnology Progress* **2003**, *19*, 1167.

12. de Oliveira, P. C.; Alves, G. M.; de Castro, H. F. *Biochemical Engineering Journal* **2000**, *5*, 63.

13. Moelans, D.; Cool, P.; Baeyens, J.; Vansant, E. F. *Catalysis Communications* **2005**, *6*, 307.

14. Borole, A.; Dai, S.; Cheng, C.; Rodriguez, M., Jr.; Davison, B. *Applied Biochemistry and Biotechnology* **2004**, *113*, 273.

15. Kim, M. I.; Ham, H. O.; Oh, S.-D.; Park, H. G.; Chang, H. N.; Choi, S.-H. *Journal of Molecular Catalysis B: Enzymatic* **2006**, *39*, 62.

16. Wang, Y.; Caruso, F. *Chemical Communications* **2004**, 1528.

17. Díaz, J. F.; Balkus Jr, K. J. *Journal of Molecular Catalysis B: Enzymatic* **1996**, *2*, 115.

18. Yan, A.-X.; Li, X.-W.; Ye, Y.-H. *Applied Biochemistry and Biotechnology* **2002**, *101*, 113.

19. Reshmi, R.; Sanjay, G.; Sugunan, S. *Catalysis Communications* **2006**, *7*, 460.

20. Zhu, Y.; Cao, H.; Tang, L.; Yang, X.; Li, C. *Electrochimica Acta* **2009**, *54*, 2823.

21. Besic, S.; Minteer, S. In *Enzyme Stabilization and Immobilization*; Minteer, S. D., Ed.; Humana Press: 2011; Vol. 679, p 113.

22. Kobayashi, J.; Mori, Y.; Kobayashi, S. *Chemical Communications* **2006**, *0*, 4227.

23. Nakashima, K.; Kamiya, N.; Koda, D.; Maruyama, T.; Goto, M. *Organic & Biomolecular Chemistry* **2009**, *7*, 2353.

24. Braun, S.; Rappoport, S.; Zusman, R.; Avnir, D.; Ottolenghi, M. *Materials Letters* **1990**, *10*, 1.

25. Avnir, D. *Accounts of Chemical Research* **1995**, *28*, 328.

26. Avnir, D.; Braun, S.; Lev, O.; Ottolenghi, M. *Chemistry of Materials* **1994**, *6*, 1605.

27. Gill, I. *Chemistry of Materials* **2001**, *13*, 3404.

28. Cao, L.; van Rantwijk, F.; Sheldon, R. A. *Organic Letters* **2000**, *2*, 1361.

29. Roy, J. J.; Abraham, T. E. *Journal of Molecular Catalysis B: Enzymatic* **2006**, *38*, 31.

30. St. Clair, N. L.; Navia, M. A. *Journal of the American Chemical Society* **1992**, *114*, 7314.

31. Zelinski, T.; Waldmann, H. *Angewandte Chemie International Edition in English* **1997**, *36*, 722.

32. Quiocho, F. A.; Richards, F. M. *Proceedings of the National Academy of Sciences of the United States of America* **1964**, *52*, 833.

33. Quiocho, F. A.; Richards, F. M. *Biochemistry* **1966**, *5*, 4062.

34. Talekar, S.; Shah, V.; Patil, S.; Nimbalkar, M. *Catalysis Science & Technology* **2012**, *2*, 1575.

35. Tudorache, M.; Nae, A.; Coman, S.; Parvulescu, V. I. *RSC Advances* **2013**, *3*, 4052.

36. Hatton, B.; Mishchenko, L.; Davis, S.; Sandhage, K. H.; Aizenberg, J. *Proceedings of the National Academy of Sciences* **2010**, *107*, 10354.

37. Szamocki, R.; Reculusa, S.; Ravaine, S.; Bartlett, P. N.; Kuhn, A.; Hempelmann, R. *Angewandte Chemie International Edition* **2006**, *45*, 1317.

38. Abramova, V.; Sinitskii, A. *Superlattices and Microstructures* **2009**, *45*, 624.

39. Cao, Y.; Wang, Y.; Zhu, Y.; Chen, H.; Li, Z.; Ding, J.; Chi, Y. *Superlattices and Microstructures* **2006**, *40*, 155.

40. Yu, H. M.; Yim, J.-H.; Choi, K. Y.; Lim, J. S. *The Journal of Supercritical Fluids* **2012**, *67*, 71.

41. Dimos, M. M.; Blanchard, G. J. *The Journal of Physical Chemistry C* **2010**, *114*, 6019.

42. Dimos, M. M.; Blanchard, G. J. *Journal of Electroanalytical Chemistry* **2011**, *654*, 13.

43. Dimos, M. M.; Blanchard, G. J. *The Journal of Physical Chemistry C* **2011**, *115*, 11247.

44. Gornowich, D. B.; Blanchard, G. J. *The Journal of Physical Chemistry C* **2013**, in preparation.

45. Mu, W.; Hwang, D.-K.; Chang, R. P. H.; Ketterson, J. B. *Journal of Raman Spectroscopy* **2011**, *42*, 941.

46. Holland, B. T.; Blanford, C. F.; Do, T.; Stein, A. *Chemistry of Materials* **1999**, *11*, 795.

47. Turner, M. E.; Trentler, T. J.; Colvin, V. L. *Advanced Materials* **2001**, *13*, 180.

48. Holland, B. T.; Blanford, C. F.; Stein, A. *Science* **1998**, *281*, 538.

49. Zhou, Q.; Dong, P.; Cheng, B. *Journal of Crystal Growth* **2006**, *292*, 320.

50. Jiang, P.; Cizeron, J.; Bertone, J. F.; Colvin, V. L. *Journal of the American Chemical Society* **1999**, *121*, 7957.

51. Bartlett, P. N.; Birkin, P. R.; Ghanem, M. A. *Chemical Communications* **2000**, 1671.

52. Bartlett, P. N.; Baumberg, J. J.; Birkin, P. R.; Ghanem, M. A.; Netti, M. C. *Chemistry of Materials* **2002**, *14*, 2199.

53. Sumida, T.; Wada, Y.; Kitamura, T.; Yanagida, S. *Langmuir* **2002**, *18*, 3886.

54. Huang, Y.-J.; Lai, C.-H.; Wu, P.-W.; Chen, L.-Y. *Materials Letters* **2009**, *63*, 2393.

55. Robinson, P. J.; Dunnill, P.; Lilly, M. D. *Biochimica et Biophysica Acta (BBA) - Enzymology* **1971**, *242*, 659.

56. Van Aken, B.; Ledent, P.; Naveau, H.; Agathos, S. *Biotechnology Letters* **2000**, *22*, 641.

57. Betancor, L.; López-Gallego, F.; Alonso-Morales, N.; Dellamora, G.; Mateo, C.; Fernandez-Lafuente, R.; Guisan, J. M. 2006; Vol. 22, p 57.

58. López-Gallego, F.; Betancor, L.; Mateo, C.; Hidalgo, A.; Alonso-Morales, N.; Dellamora-Ortiz, G.; Guisán, J. M.; Fernández-Lafuente, R. *Journal of Biotechnology* **2005**, *119*, 70.

59. Surinenaite, B.; Bendikiene, V.; Juodka, B. *Prog. Biotechnol.* **1998**, *15*, 577.

60. Subramanian, A.; Kennel, S. J.; Oden, P. I.; Jacobson, K. B.; Woodward, J.; Doktycz, M. J. *Enzyme and Microbial Technology* **1999**, *24*, 26.

61. Zhou, H.-X.; Dill, K. A. *Biochemistry* **2001**, *40*, 11289.

62. Kleppe, K. *Biochemistry* **1966**, *5*, 139.

63. Krishnaswamy, S.; Kittrell, J. R. *Biotechnology and Bioengineering* **1978**, *20*, 821.

64. Malikkides, C. O.; Weiland, R. H. *Biotechnology and Bioengineering* **1982**, *24*, 2419.

65. Yablonovitch, E. *Physical Review Letters* **1987**, *58*, 2059.

CHAPTER 2: Fabrication of Inverse Opal Structures

Introduction

Inverse opal structures have gained the interest of several research groups over the past decade.[1-20] There are many different procedures for preparing the NS. There are a vast range of materials that can be used as templates and as the matrix itself. A schematic for the construction of a NS is illustrated in Fig. 2.1. The basic process involved in the fabrication of this type of materials starts with layers of polymer or silica spheres deposited on a support. The interstitial space between the spheres is then backfilled with a different material, and finally the sphere template is removed either by dissolution or thermal decomposition. There are different methods associated with the deposition of the spheres. The size of the spheres used can be changed according to the desired application, offering a high degree of control over the pore size of the system. The material that is deposited in between the spheres can also be chosen based on the application that is intended for the resulting NS.

The Blanchard group has experience using metal inverse opal structures.[3-5] In that work, silica nanosphere assemblies were used as the scaffold to build the NS and metals were electrodeposited in the interstitial space. The silica spheres were then removed by dissolution with hydrofluoric acid (HF). Platinum and palladium were both used to create NS structures and the methods used in that work provided highly ordered NS structures. One of the main limitations of that work was the construction of the NS on a planar, non-permeable support. Consequently, any chemical reactions that take place on the surface of the nanoporous metal are strictly limited by diffusion of reactive species in the NS, and flow is not possible.

Using this knowledge for inverse opal preparation, the work described in this research required constructing inverse opal structures using dielectric materials. To take this one step

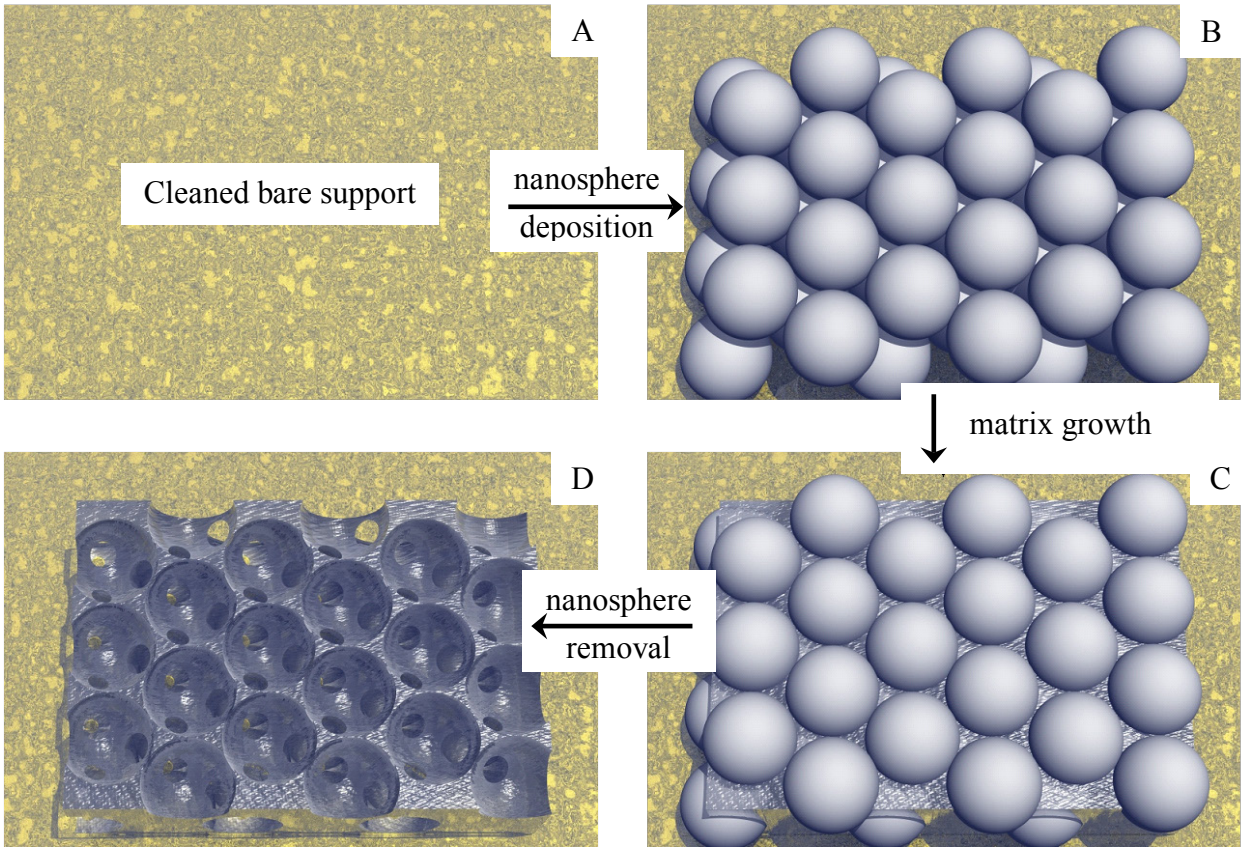

Figure 2.1: Schematic for the fabrication of an inverse opal on a planar substrate.

further and to eliminate the limitations associated with diffusion as the only means of transport, the focus of this work also shifted to creating a NS material that would afford the ability to flow a stream of reactant containing solution through the structure. The first section of this Chapter focuses on forming NS structures on planar supports, and concludes with utilizing a combination of techniques to form flow-through inverse opal structures. Polystyrene spheres (PS) were used in the construction of scaffold structures for the NS and silica was deposited in the interstitial space between the spheres by means of sol-gel chemistry. Once formed, the resulting matrix was amenable to a wide range of surface modifications using several different chemical reactions.

Polystyrene Sphere Synthesis

The first step in the process of fabricating dielectric inverse opals is to synthesize polymer spheres. For this work, polystyrene was chosen for two reasons. The first is that there are multiple synthetic procedures available for the preparation of spheres in a wide range of sizes that yield a monodisperse size distribution.[21-32] Nanosphere monodispersity is important for the growth of well-organized inverse opal structures. In addition, polystyrene spheres are relatively simple to remove using solvent dissolution or heating methods. It is important to note that all polystyrene spheres used in this work were non-cross-linked polymers. Cross-linked spheres were synthesized, but they are not as soluble in solvents such as toluene or ethyl acetate. Removing the cross-linked spheres from the matrix would be too difficult for solvent dissolution and, as a result only non-cross-linked polymers were used.

There are a number of options for synthesizing polymer spheres.[21-32] Two common approaches that are utilized are dispersion and emulsion polymerization reactions.[21-32] These syntheses are one-pot reactions and both yield polymer spheres in the size range of 0.1-15 μm in

diameter depending on the reaction conditions.[26] Both approaches were utilized in this work, and the characterization of the resulting spheres will be described in detail in the following sections.

Dispersion polymerization in an alcoholic medium has been studied extensively in recent decades.[21,24-33] This one pot reaction requires a stabilizer, initiator, monomer, and solvent. The most common stabilizers used are (hydroxypropy1)cellulose, poly(acry1ic acid), or poly(*N*-vinylpyrrolidone) (PVP).[30,31] The stabilizer enables the formation of latex spheres, however the understanding of the details involved in this process are qualitative.[28,34] For this work, PVP (MW = 55,000) was used for all dispersion reactions. The initiator triggers the polymerization of the monomers in solution. The most common initiators break down upon heating, forming free radical species in solution. Benzoyl peroxide and azobisisobutyronitrile (AIBN) are two common free radical sources for dispersion polymerization,[24,26,27] and AIBN was used for all reactions reported in this work. Polystyrene and poly(methyl methacrylate) (PMMA) are two common polymers used to synthesize spheres. Polystyrene was used for the work contained in this dissertation. An important component of dispersion polymerization is the reaction medium, and in most cases alcohols are used as the solvent. Methanol and ethanol were both utilized in this research. The overall reaction scheme for the dispersion polymerization reaction used for this work is illustrated in Scheme 2.1. The stabilizer identity and concentration, initiator concentration, monomer concentration, and reaction medium all play important roles in determining the size and polydispersity of the resulting polymer spheres.[31]

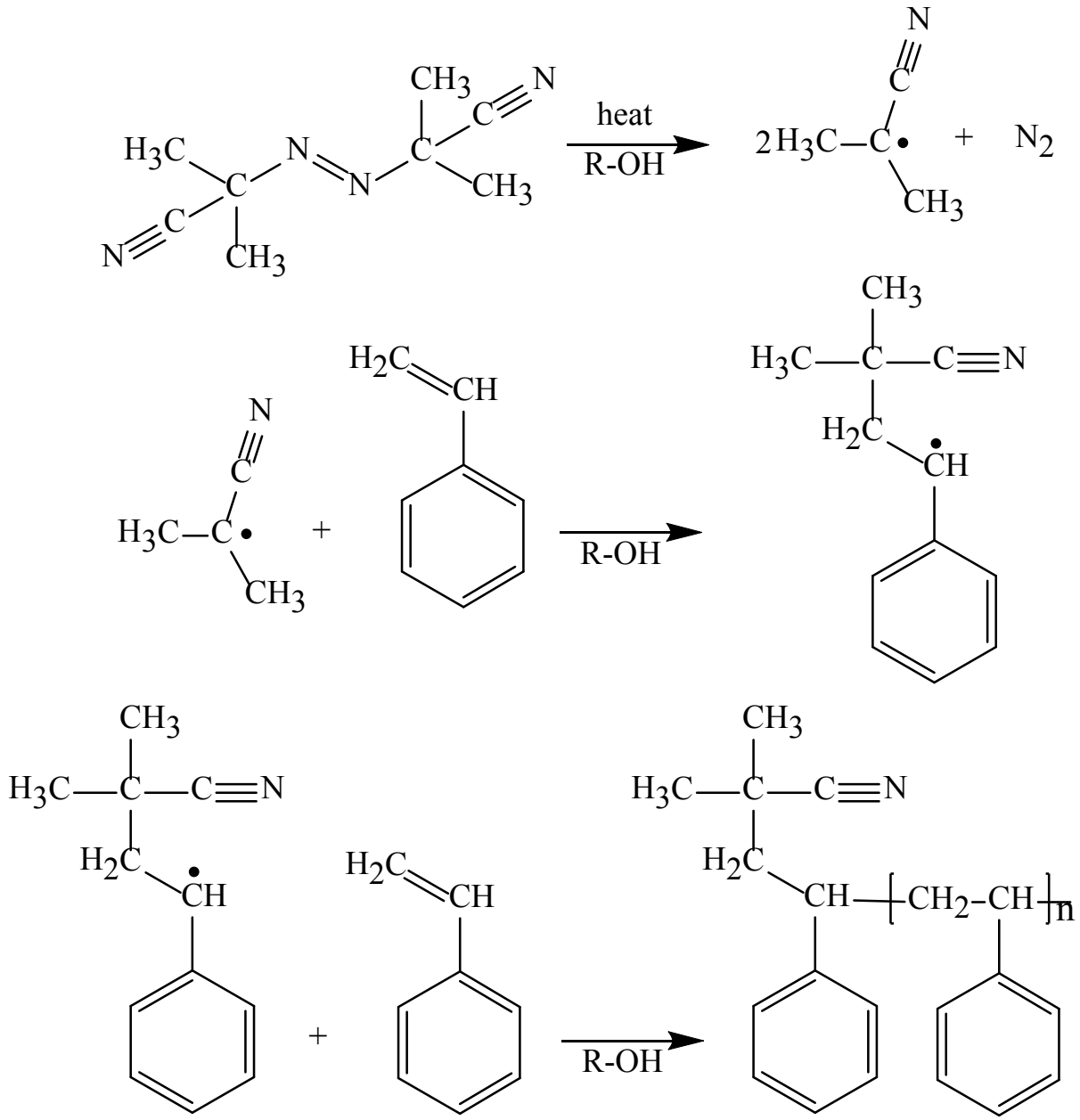

Scheme 2.1: Reaction schematic for a free radical dispersion polymerization reaction for polystyrene sphere synthesis. PVP was present in the reaction mixture as a stabilizer.

For a typical reaction, the initiator (AIBN) was added to a round-bottom flask containing ethanol. The reaction flask was then heated to reflux at a temperature of 80°C for approximately 30 minutes. Then the stabilizer (PVP) and monomer (polystyrene) were added to the reaction flask. The reaction was allowed to proceed with stirring at 80°C under reflux for 24 hours, and then allowed to cool to room temperature. The spheres were washed three times with ethanol via centrifugation at 3900 rpm. The ethanol was allowed to evaporate, and the spheres were suspended in aqueous solutions at various w/w concentrations for deposition onto planar support surfaces.

The first key component to synthesizing monodisperse polymer spheres is to use purified chemicals. Styrene monomer is available commercially, but it contains a stabilizer to prevent polymerization while in storage. Consequently, this stabilizer must be removed prior to use. There are two approaches to removing the stabilizer; washing with a strong base or distillation of the monomer. It was found that distilling the monomer was the most effective way, because this method purified the reactant just prior to use and resulted in comparatively monodisperse spheres. If care was not taken to remove the stabilizer from the styrene, a bimodal distribution of spheres was the typical result, as shown in Fig. 2.2. Spheres with a wide size distribution are not ideal to use as a scaffold for NS construction because they do not assemble in a highly ordered manner.

As noted previously, all of the constituents in the dispersion polymerization reaction play a role in determining the size of the polymer spheres. The first component that was varied was the alcohol solvent used for the reaction medium. Methanol, ethanol, and isopropanol were all used as reaction media for dispersion polymerization reactions. A solution containing 45 mL of alcohol, 5 mL of water, 5 mL of styrene monomer, 50 mg of AIBN, and 0.6 g of PVP was used

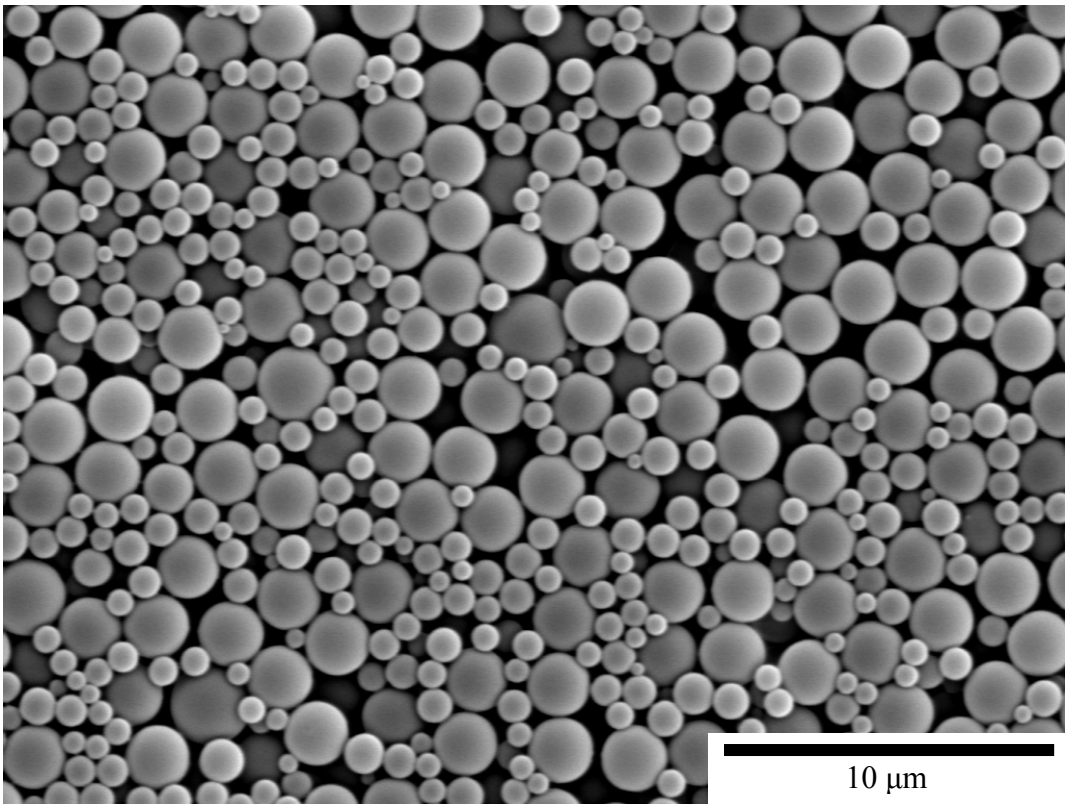

Figure 2.2: SEM image of polystyrene spheres with a bimodal size distribution.

for the each reaction following the procedure previously described. Nitrogen was bubbled into the mixture throughout the reaction. The PS sphere sizes were *ca*. 900 nm, 1.1 μm, and 2.2 μm for methanol, ethanol, and isopropanol, respectively. These data suggest a correlation between alcohol aliphatic chain length and nanosphere diameter. The methanol (Fig. 2.3) and ethanol (Fig. 2.4) reactions yield monodisperse spheres, while the isopropanol (Fig. 2.5) produces a bimodal distribution with some irregularly shaped polymer structures.

The amount of stabilizer was also varied for a series of reactions with ethanol as the solvent. Reactions were performed using 0.2%, 0.8% and 1.2% (w/v) PVP and the diameters of the spheres were 2.3, 1.5 , and 1.1 μm, respectively. The amount of ethanol, initiator (AIBN), styrene, and water were all held constant at 45 mL, 50 mg, 5 mL, and 5 mL, respectively. The results reveal an inverse relationship between polymer sphere size and PVP concentration (Fig. 2.6). Higher steric stabilizer concentrations yield smaller spheres, consistent with literature reports.[31] While the other constituents of the dispersion reaction solution could be varied, the spheres synthesized with the previously mentioned methods were suitable for the purposes of this work.

Another type of polymerization reaction was investigated briefly in an effort to obtain smaller spheres, on the order of a few hundred nanometers in diameter. Emulsion polymerization was utilized for this work, and has been previously characterized in the literature.[22,23,35] In this reaction format, potassium persulfate is used as the initiator for the polymerization. A solution of 50 mL of methanol, 20 mL of water, 4 mL of styrene, and 100 mg of potassium persulfate was used for this reaction. The mixture was heated under reflux at 70°C in an oil bath for 24 hours under nitrogen. The SEM image of PS spheres with an average diameter of 180 nm synthesized using this technique is presented in Fig. 2.7. Using the two

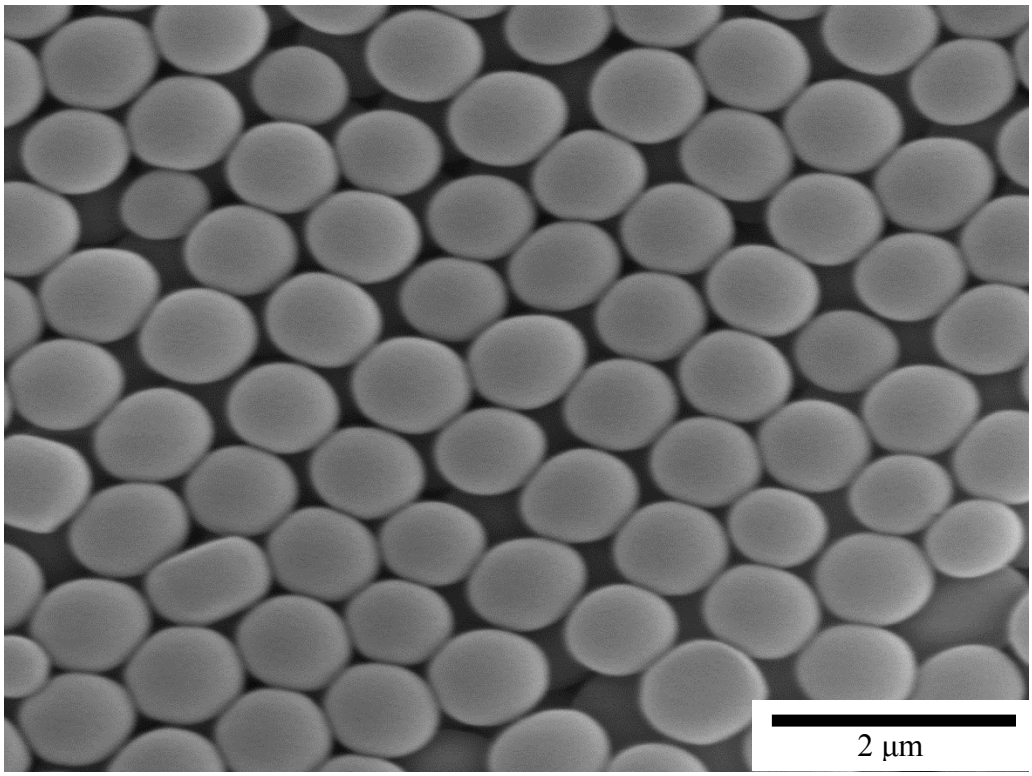

Figure 2.3: SEM image of polystyrene spheres with an average diameter of 900 nm synthesized using methanol as the solvent.

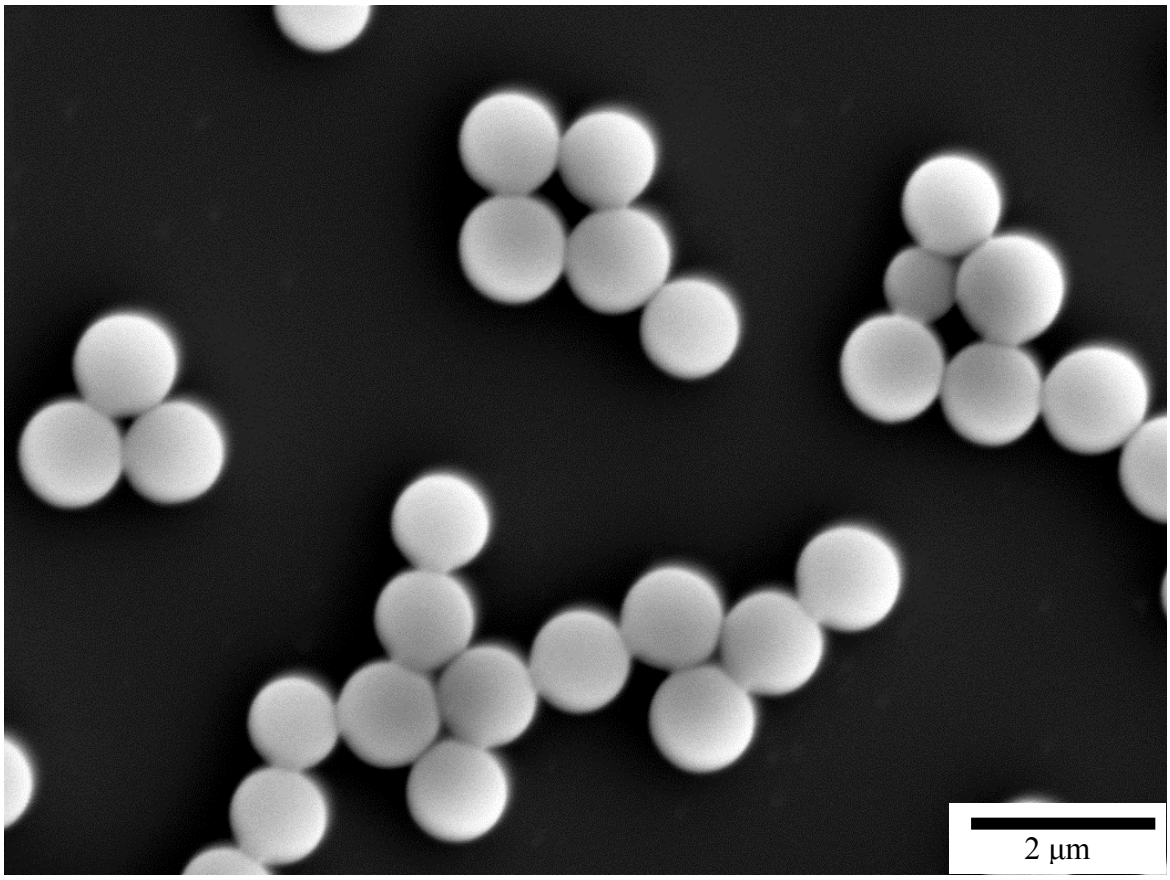

Figure 2.4: SEM image of polystyrene spheres with an average diameter of 1.1 μm synthesized using ethanol as the solvent.

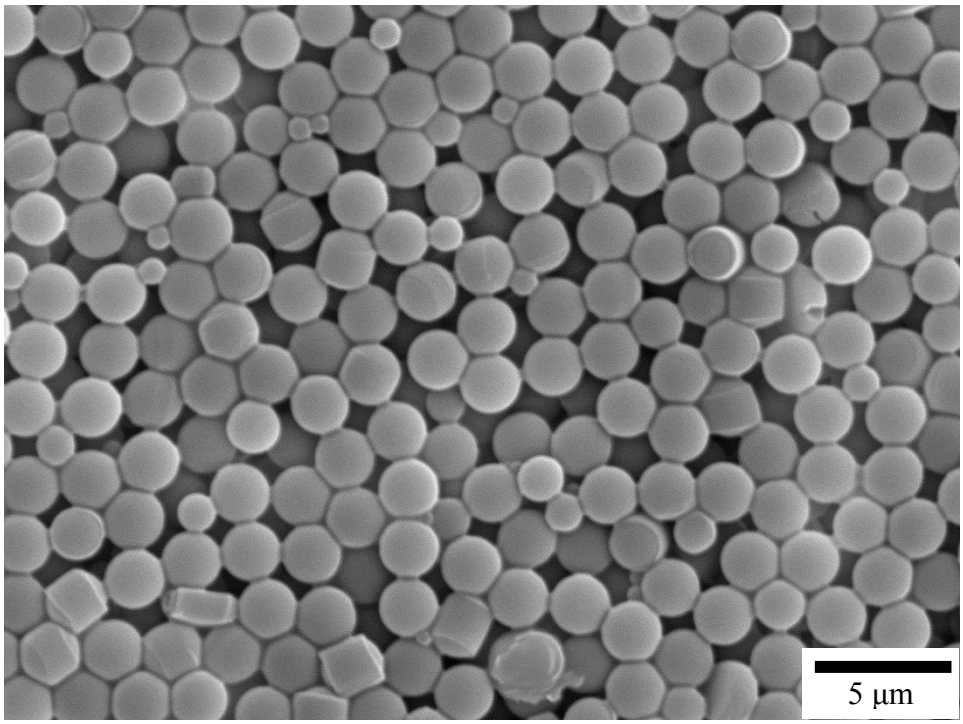

Figure 2.5: SEM image of polystyrene spheroidal structures with an average diameter of 2.2 µm synthesized using ethanol as the solvent.

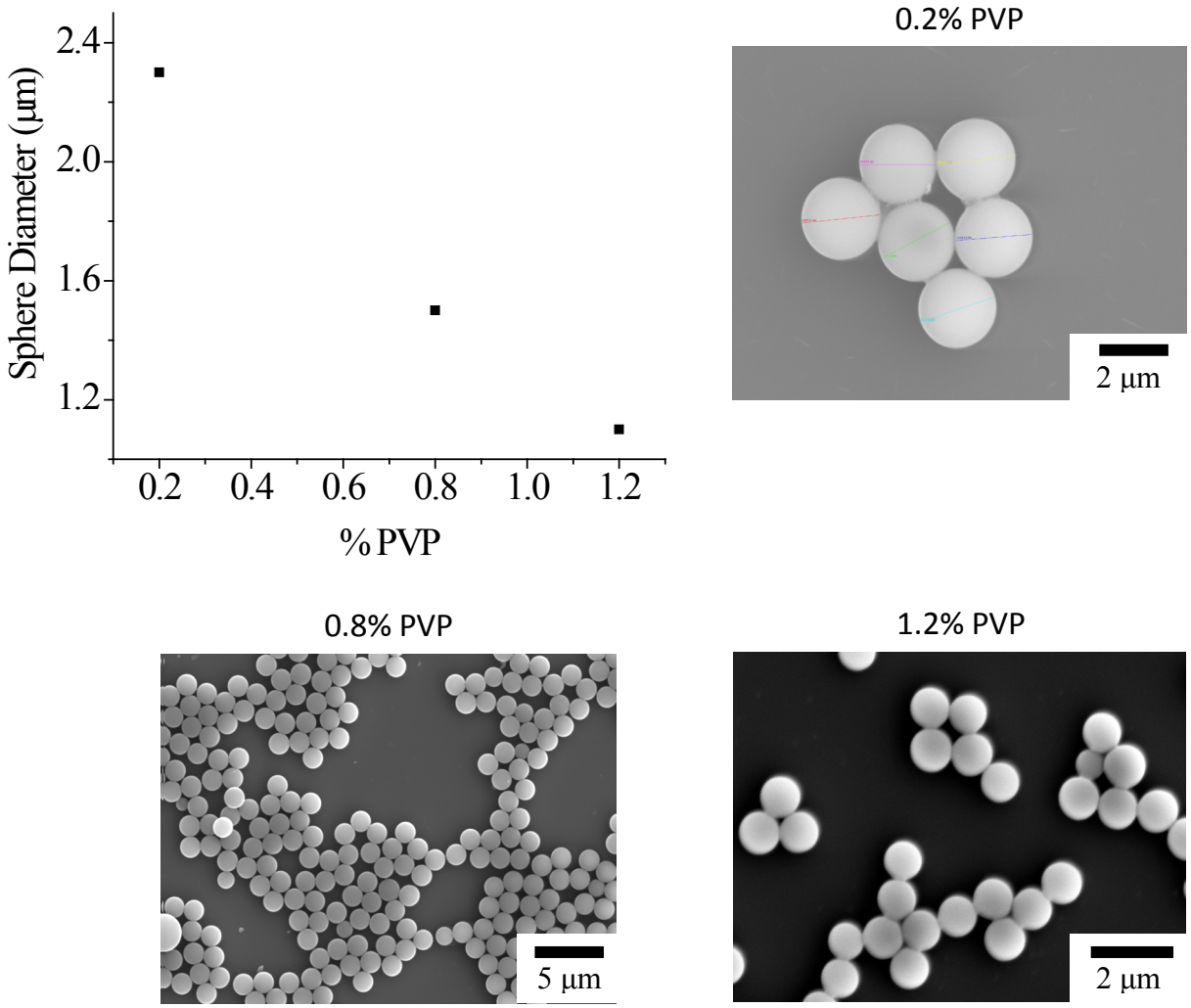

Figure 2.6: Plot of polystyrene sphere size vs. steric stabilizer concentration (top left) for free radical dispersion polymerization reactions with ethanol as the solvent. SEM images (top right and bottom) of polystyrene spheres at each PVP concentration.

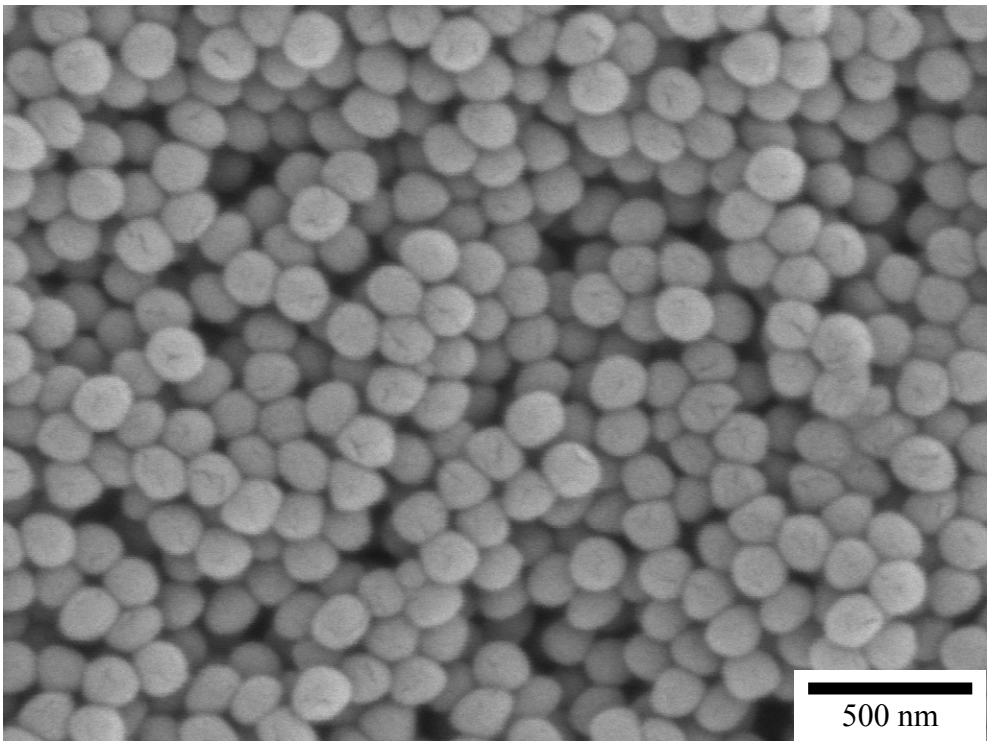

Figure 2.7: SEM image of polystyrene spheres with an average diameter of 180 nm synthesized using an emulsifier polymerization reaction method.

synthetic techniques described previously, a wide size range of PS spheres (180 nm – 2 μm diameter) were synthesized and used throughout the NS fabrication experiments.

The polymer spheres were characterized using two different techniques, scanning electron microscopy (SEM) and dynamic light scattering (DLS). For a highly ordered NS to be formed, the spheres for the scaffold must have a monodisperse size distribution. Fig. 2.8 is a SEM image of polystyrene spheres with a diameter of *ca*. 1 μm that were deposited on a glass microscope slide. All samples were coated with gold using an Emscope SC500 sputter coater with a deposition current of 20 mA for 3 minutes in preparation to be analyzed using SEM. At 20 mA, the gold deposition rate results in a thickness of 7 nm/minute.[36] All micrographs were obtained using a JEOL 6400V microscope with a LaB_6 emitter at an accelerating voltage of 12 kV.

The size of the PS spheres was measured using a Malvern Zetasizer Nano ZS. Fig. 2.9 contains dynamic light scattering (DLS) data for polystyrene spheres, with an average diameter of 1.15 μm and the distribution of particle sizes. This instrument is equipped with backscatter detection technology which measures scattered light at an angle of 173° relative to the axis of light propagation. This detection method provides several advantages over traditional DLS techniques, where scattering is measured from light that passes through the sample. With backscatter detection geometry, the (scattered) light does not have to pass through the sample, allowing for strongly scattering samples to be analyzed. Backscatter detection geometry reduces the effect known as multiple scattering, where light scattered by one particle is subsequently scattered by other particles. Particulate contamination issues are also reduced by collecting the data in backscatter configuration because particulate contaminants are often relatively large compared to the size of the nanospheres. Larger particles scatter in the forward direction mostly,

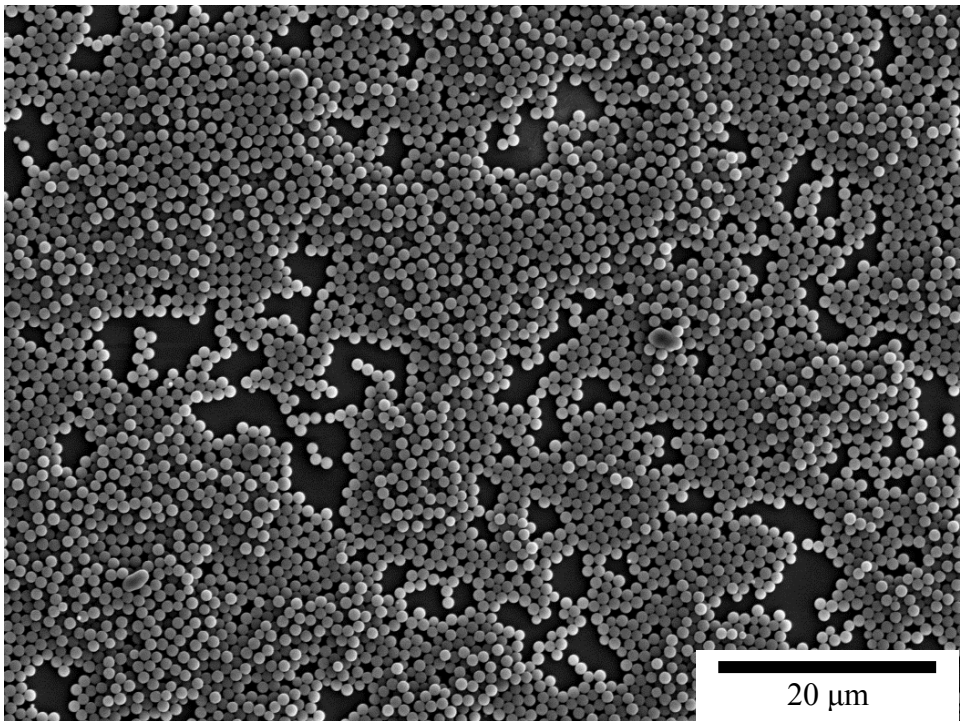

Figure 2.8: SEM image of polystyrene spheres with a diameter of *ca*. 1 μm deposited on a glass microscope slide that were synthesized using a free radical dispersion polymerization method.

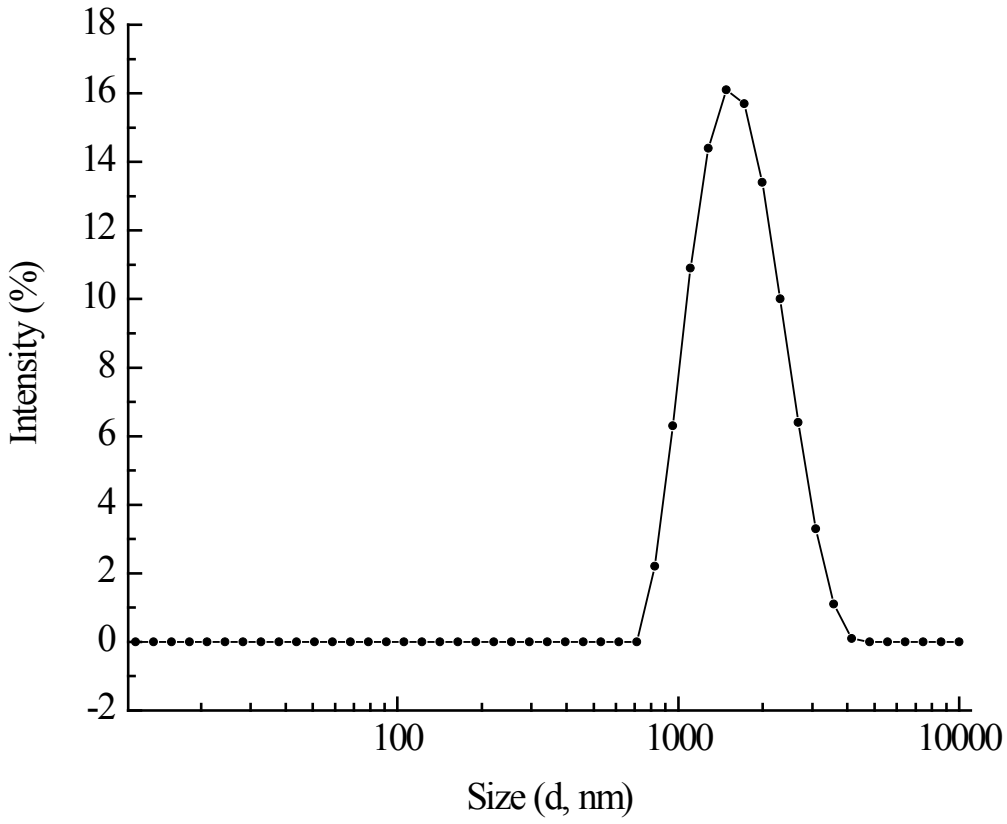

Figure 2.9: Dynamic light scattering data showing the particle size distribution of the polystyrene spheres with an average diameter of 1.15 μm.

so collecting in backscatter mode greatly reduces signals from contaminants that may be present in the sample.[37] For all of this work, the polystyrene spheres were suspended in a 1% wt./wt. aqueous solution. Prior to each DLS analysis, the aqueous suspension of spheres was sonicated for 30 minutes to break apart any aggregates that may have formed during storage.

Polystyrene Sphere Deposition Techniques

Once the PS spheres have been synthesized and characterized, the next step in the process of building inverse opal structures is to deposit the spheres in an organized manner onto a support. Three different techniques were used for this purpose. The first and most elementary method used was solvent evaporation. A microscope slide was cut so that it would fit on a SEM stub and cleaned using piranha solution (3:1 sulfuric acid:hydrogen peroxide). An aqueous or alcoholic suspension of PS spheres was then added to the slide drop wise and the solvent was allowed to evaporate at room temperature. Fig 2.10 is a representative SEM image of PS spheres deposited using this technique. This technique was able to produce opal structures, but there is limited control over the spreading and evaporation of the solution on the support. Consequently, it was difficult to reproduce the same thickness from sample to sample. A second deposition technique was spin-coating. Glass microscope slides were placed on a spin-coater (Headway Research Inc.), and sphere suspensions were placed onto the surface while spinning at velocities ranging from 1000-3000 rpm. Fig 2.11 is a SEM image of PS spheres that were deposited onto a slide using a spin-coater. High quality packing of the spheres was not observed for the range of parameters used for this work, so this method was not used for inverse opal preparation.

The third method used for sphere deposition was vertical dipping.[3-5] For this technique, a SDI Nanodip Coater (nanodipper) was used to slowly withdraw a planar substrate from an

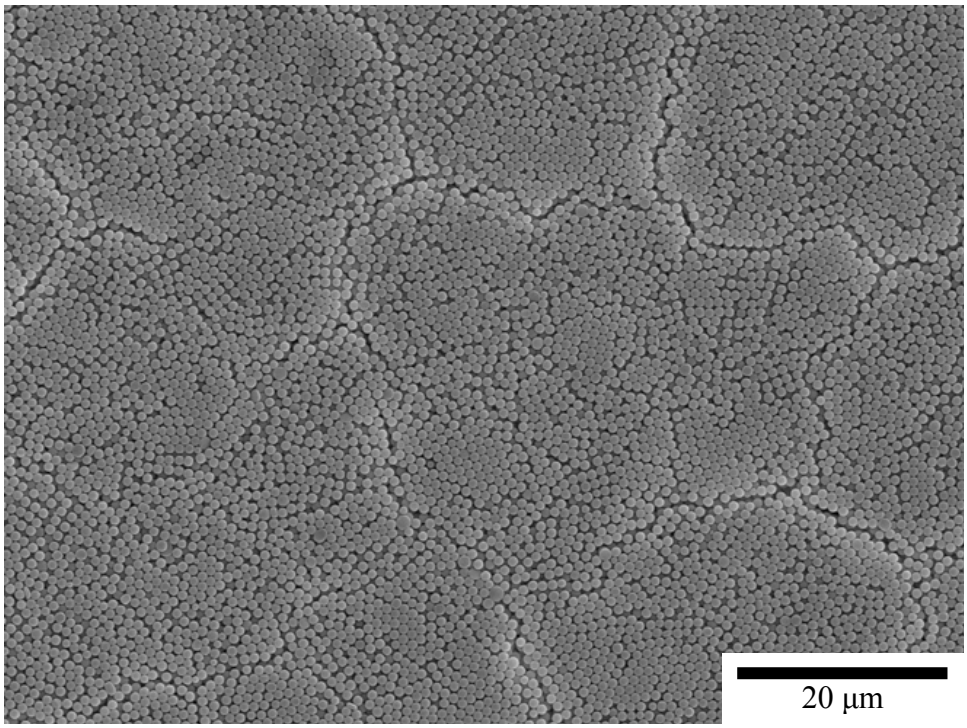

Figure 2.10: SEM image of polystyrene spheres with an average diameter of 1 μm deposited on a glass microscope slide using solvent evaporation.

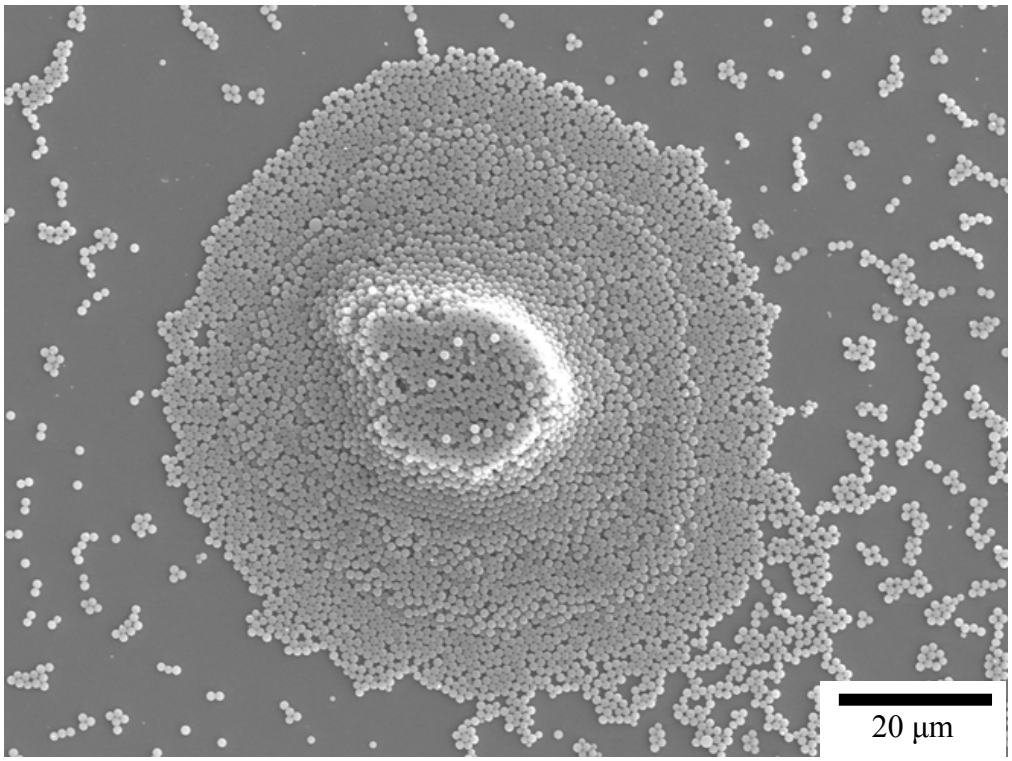

Figure 2.11: SEM image of polystyrene spheres with an average diameter of 1 μm deposited on a glass microscope slide using a spin-coater.

aqueous sphere suspension. Capillary forces at the meniscus cause a multi-layer assembly of spheres to be deposited on the substrate as it is withdrawn from the solution. Withdrawal speeds of 1 μm/sec up to 25 μm/sec were used for this work. A rate of 2 μm/sec yielded the best packing for size of PS spheres used in this work, and was used for most of the routine work that utilized the nanodipper. Fig. 2.12 is a SEM micrograph of PS spheres that were deposited on a clean glass microscope slide at a rate of 2 μm/sec. Examining the three methods shows that spin-coating yields a highly disordered arrangement of PS spheres that is not useful to use for building NS materials. The solvent evaporation and vertical dipping techniques both yield suitable scaffolds for NS construction. It was also found that sintering the spheres at 60-70°C for *ca*. 1 hour fuses the scaffold together to form a more robust structure. Vertical dipping results in an assembly with the highest proportion of hexagonally closed packed regions and is the method of choice for planar substrates. Vertical dipping also affords control over the number of layers of spheres deposited on the support. Multiple dipping cycles can be performed, adding layers of spheres with each cycle. Highly ordered structures with multiple layers formed by vertical dipping is consistent with literature reports.[38]

Sol-gel Methods for Silica Deposition

Sol-gel chemistry was used to fill the interstitial space between the PS spheres. Silica was chosen as the dielectric material because of its well understood sol-gel reactions and because it is amenable to a wide range of surface modification reactions. Scheme 2.2 is an overall schematic for the sol-gel reaction using tetraethyl orthosilicate (TEOS) as the precursor.[39] TEOS undergoes hydrolysis in the presence of water, and subsequent water and alcohol condensation reactions form siloxane bonds. As the precursor gels, an interconnected silica network is formed around the PS sphere scaffold. This sol-gel reaction is catalyzed by both

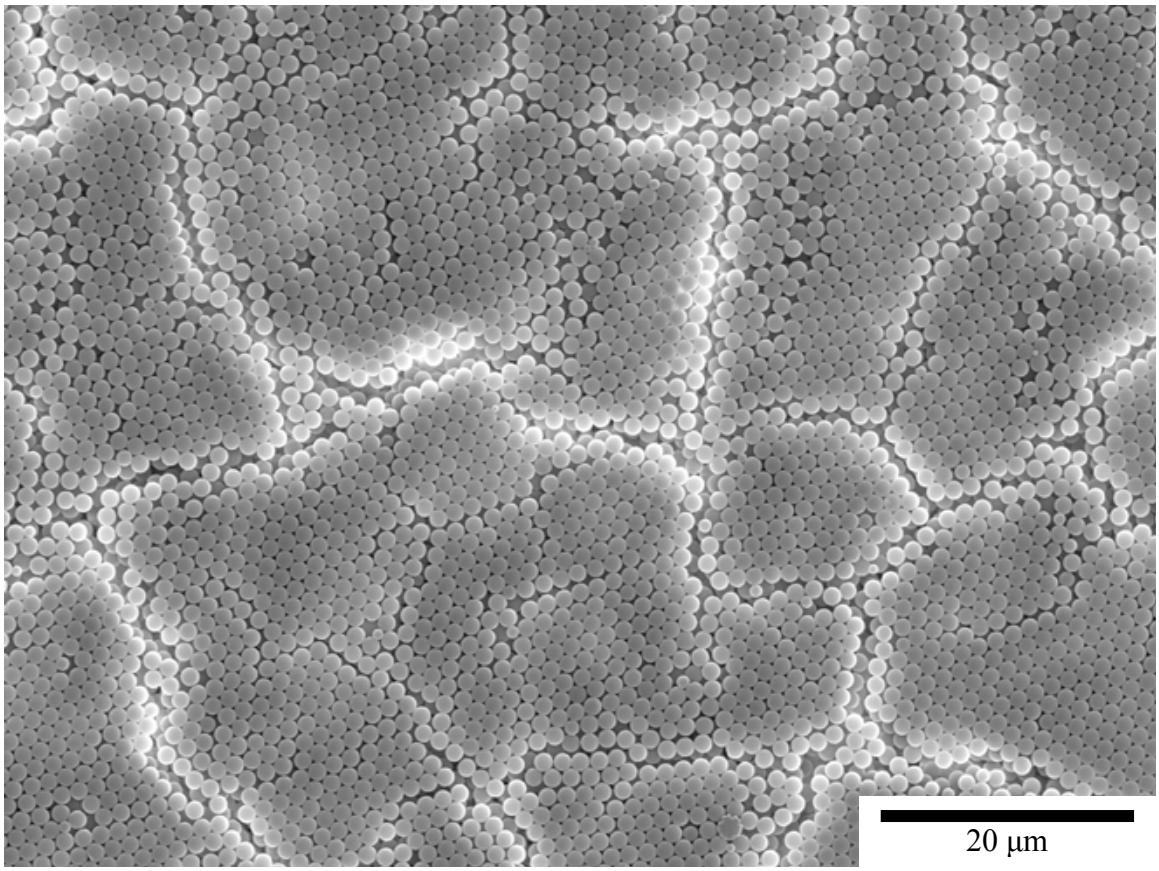

Figure 2.12: SEM image of polystyrene spheres with an average diameter of 1 μm deposited on a glass microscope slide using the nanodipper at a rate of 2 μm/sec.

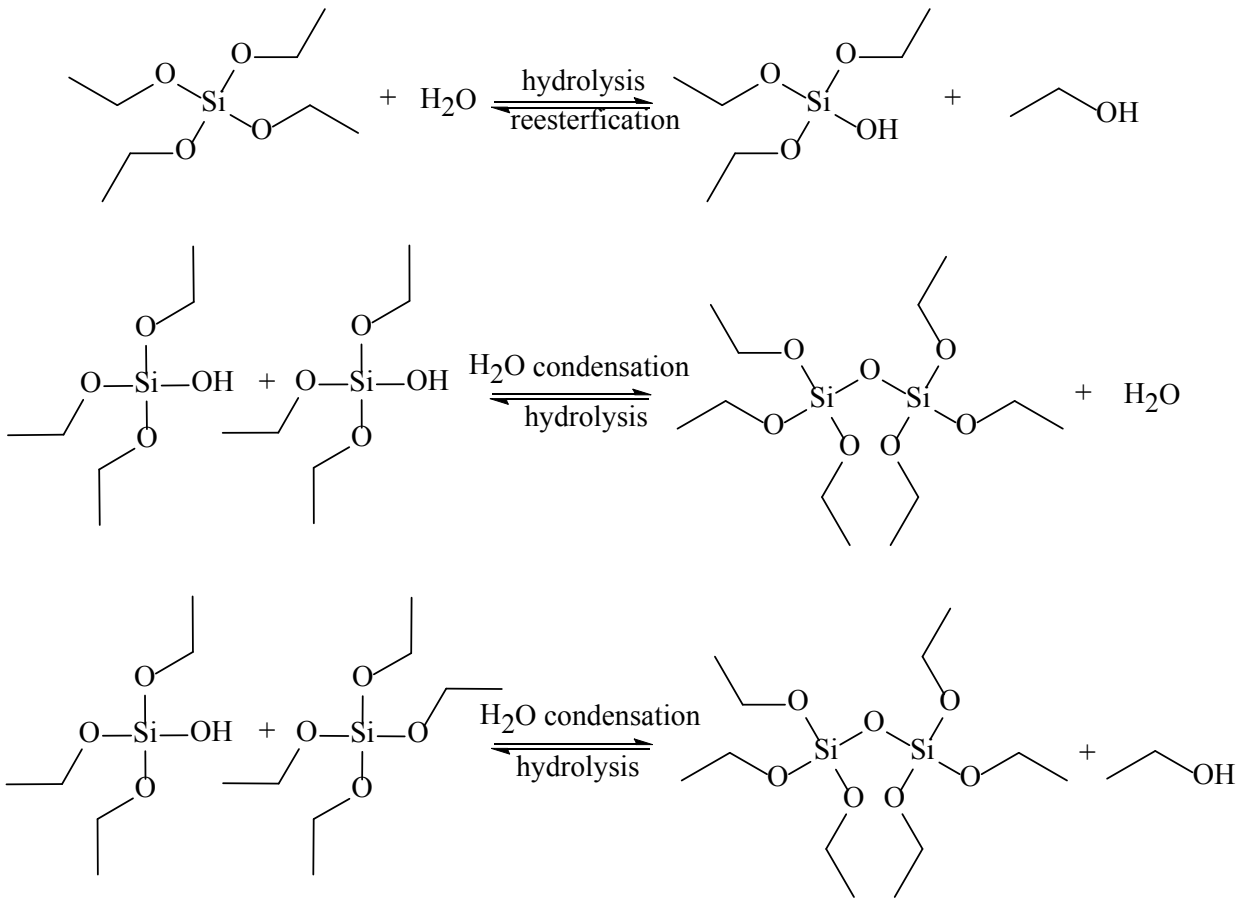

Scheme 2.2: Overall reaction schematic for the sol-gel process used to fill in the interstitial space with a TEOS precursor solution. Hydrolysis (top), water condensation (middle), and alcohol condensation (bottom) reactions.

acids and bases through different mechanisms. An acid catalyzed system was utilized for all of the work described in this dissertation. The precursor solution was prepared by combining 72 mL of water and 8 mL of ethanol, adjusting to pH 2 with concentrated hydrochloric acid, adding 4 mL of TEOS, and allowing the solution to stir for one hour. Two methods utilized for this process were by adding the sol-gel precursor solution drop-wise onto the PS scaffold, and vertical dipping using the nanodipper. Fig 2.13 contains SEM images for the evaporation method and Fig. 2.14 is a representative image of a NS fabricated using the nanodipper at a rate of 2 μm/sec. The PS sphere assemblies had been sintered for *ca*. 1 hour at 65°C before being submerged into the sol-gel solution. Both techniques worked well for utilizing silica sol-gel chemistry to fill in the interstitial regions between PS spheres.

Polystyrene Sphere Removal

There are two options available to remove the polymer spheres from within the matrix after it has solidified; heating to high temperatures to remove the spheres by thermal degradation or dissolving the spheres using a suitable solvent. Both approaches were studied, and each technique has advantages and disadvantages. For the heating technique, a temperature program was created using a high temperature furnace. The PS sphere/silica composite structure was placed in the furnace, the temperature was ramped from room temperature to 500°C at a rate of 5°C/min, the temperature then held constant at 500°C for 2 hours, and allowed to cool to room temperature. For the solvent dissolution technique, the composite structure was soaked in toluene for a period of 24-48 hours at room temperature. The heating method is much less time consuming and it guarantees that all of the polystyrene is removed from the matrix. However, this process typically resulted in significant cracking (see Fig. 2.15) of the NS structure and shrinkage of the silica network. Heating also results in a completely dehydrated silica network,

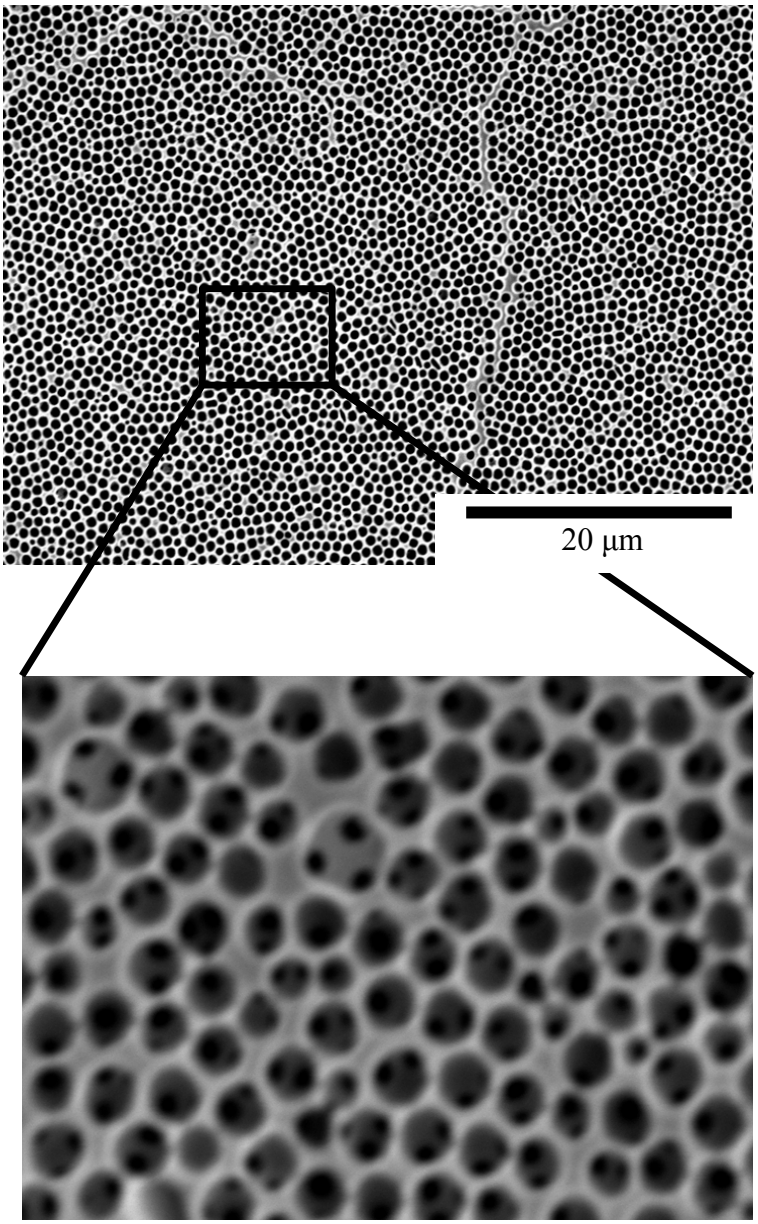

Figure 2.13: SEM images of silica inverse opal structures on a glass microscope slide. The spheres and sol-gel chemistry were performed in subsequent steps by adding solvent evaporation and adding the precursor solution on drop wise.

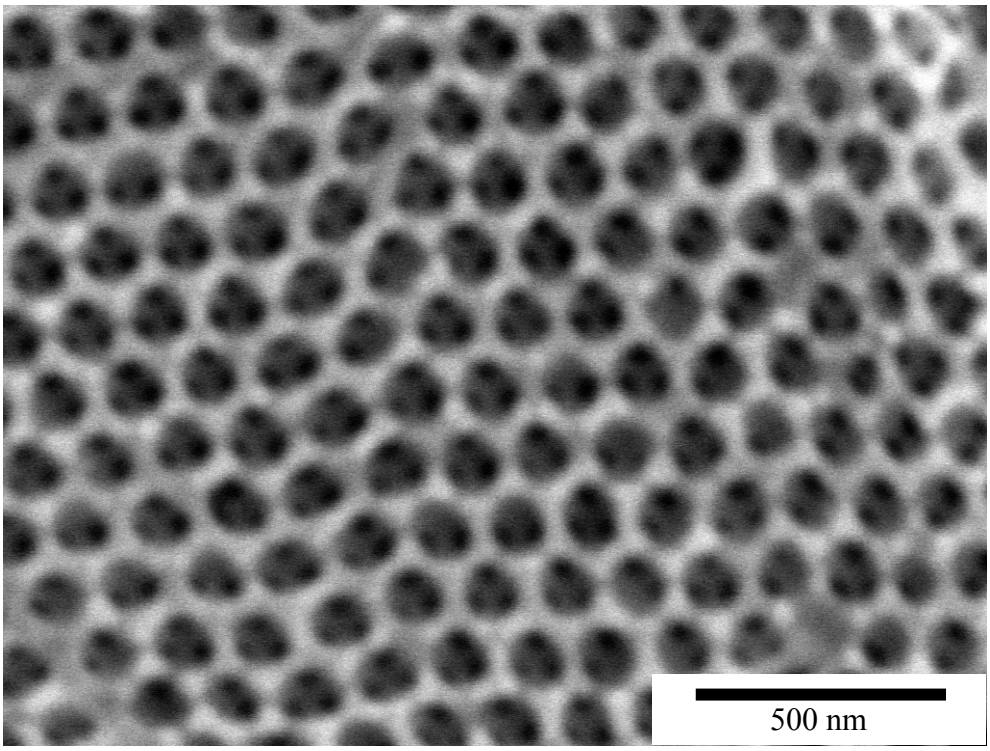

Figure 2.14: SEM image of a silica inverse opal structure on a glass microscope slide. The spheres and sol-gel chemistry were performed in subsequent steps using the nanodipper at 2 μm/sec. The spheres were deposited using 3 consecutive withdrawals from a suspension, sintered at 65°C for 1 hour, and then withdrawn from the sol-gel precursor solution 1 time. Toluene was used to remove the spheres.

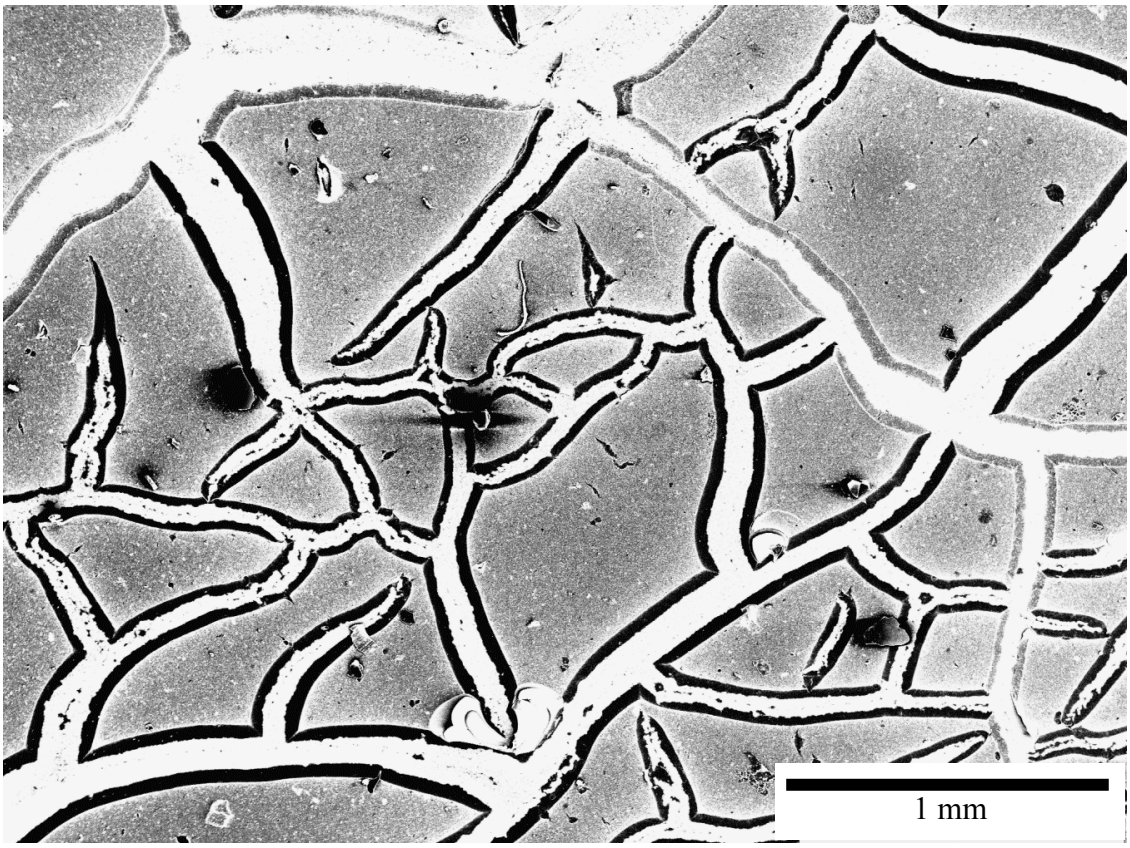

Figure 2.15: SEM image of an inverse opal that utilized heat to remove the polystyrene scaffold. This image was taken at low magnification to show the major cracking caused by the burning procedure.

rendering it much less reactive than the structure resulting from sphere dissolution with toluene. The toluene method was less destructive, however only spheres that are accessible to the solvent are removed from the matrix. Any polymer residue buried within the matrix will remain in the NS.

Flow-through Nanoporous Solid Structure Fabrication

Using the knowledge and experience gained in the process of constructing NS on planar substrates, we designed a NS structure appropriate for flow-through applications. Using a combination of the techniques previously described in this chapter, two different supports were used in an attempt to create a flow-through system. The first support matrix used was transmission electron microscopy (TEM) grids. The other support used for this work was porous alumina supports (PAS). The TEM grids and PAS are both commercially available materials that had three specific qualities important to this work. These are that they are relatively inert to the reactions we perform in their presence, that they are tolerant of a wide range of solvents, and they are able to withstand high temperatures. Both supports will be described in this section.

The first attempts at a flow-through system were made using 1500-2000 mesh TEM grids. A grid was mounted on a clean gold substrate, and the same dipping techniques that were described previously were used to deposit the spheres and fill in the void space with silica. Moderate success was made with the TEM grids using this method. The grid spaces were filled in with the NS matrix (Fig. 2.16), however a large portion of them remained partially filled or completely empty. This would provide an unrestricted path for a reactant containing solution to bypass the nanoporous solid structure, which was not desirable. In addition, the TEM grids are extremely delicate and require great care to be taken when handling them. As a result, it was concluded that TEM grids were not going to work for flow-through applications.

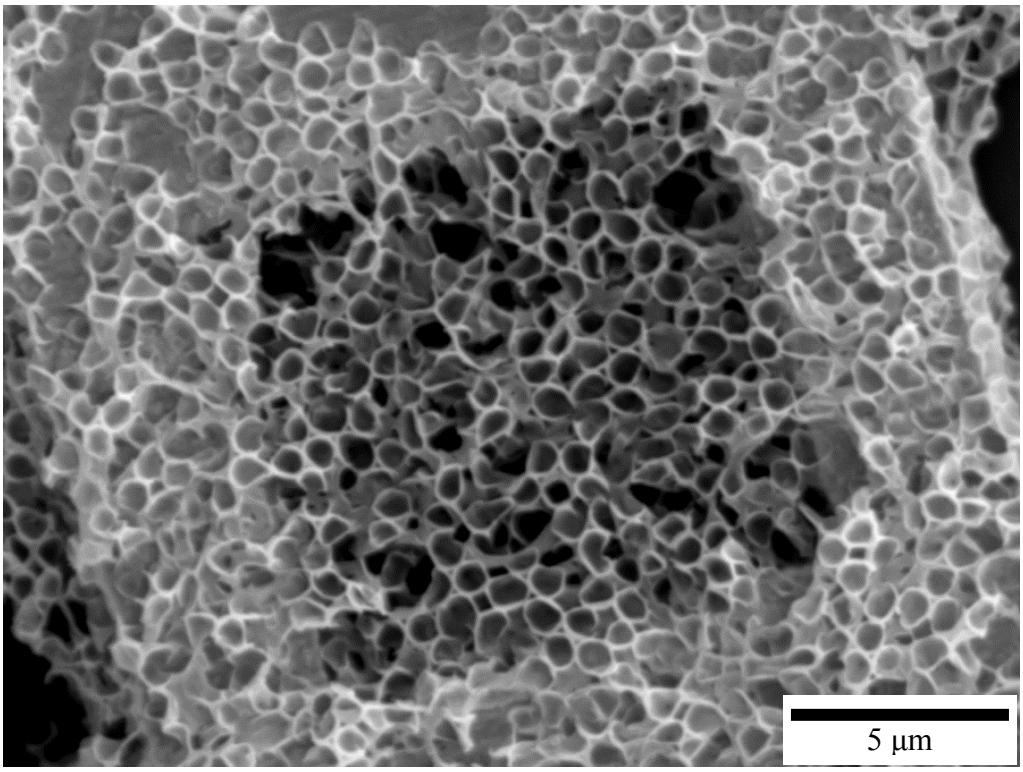

Figure 2.16: SEM image of an inverse opal that was synthesized on a gold TEM grid (1500 mesh).

At this point, we turned to PAS for the support matrix for the NS materials. The PAS are available commercially in a wide range of diameters and pore sizes. For all of the work presented in this dissertation, PAS with a diameter of 22 mm, thickness of 60 μm, and pore size of 200 nm (Whatman) were used. Due to the thinness and relatively fragile nature of the PAS, using the nanodipper was not an option for deposition of the spheres. As a result, the PAS were placed in an Advantec glass microanalysis filter holder with a porous glass frit as a structural support. Two different methods were examined for the NS fabrication on the PAS. The first involved performing steps analogous to the planar support. A 0.5 mL aliquot of aqueous 1% (wt./wt.) PS sphere suspension was deposited on the PAS and allowed to dry for 24 hours. Subsequently a 0.5 mL aliquot of sol-gel precursor solution was added drop-wise onto the PS scaffold. The sol-gel solution consisted of TEOS, ethanol, water and concentrated hydrochloric acid in a 4:6:3:1 mass ratio, respectively. A vacuum was applied using a water aspirator, and the PS/silica matrix was allowed to dry at room temperature for 24 hours. The second method involved using a co-assembly technique where PS spheres were suspended in the sol-gel precursor solution, and both the PS spheres and silica network were deposited simultaneously. For this method, 0.5 mL of an aqueous 1% (w/w) PS sphere solution was combined with 0.5 mL of a sol-gel precursor solution containing TEOS, ethanol, water and concentrated hydrochloric acid in a 4:6:3:1 mass ratio, respectively. The PS sphere/sol-gel mixture was then deposited on the PAS. A vacuum was applied using a water aspirator, and the sample was allowed to dry for 24 hours. The PS/silica matrix was then removed from the filter holder and soaked in toluene for 24 hours to remove the PS scaffold for structures prepared by both methods. Fig. 2.17 contains SEM images of structures prepared by both techniques to be used for flow-through applications. It was found that the method utilizing sequential steps often resulted in “capping” of the silica

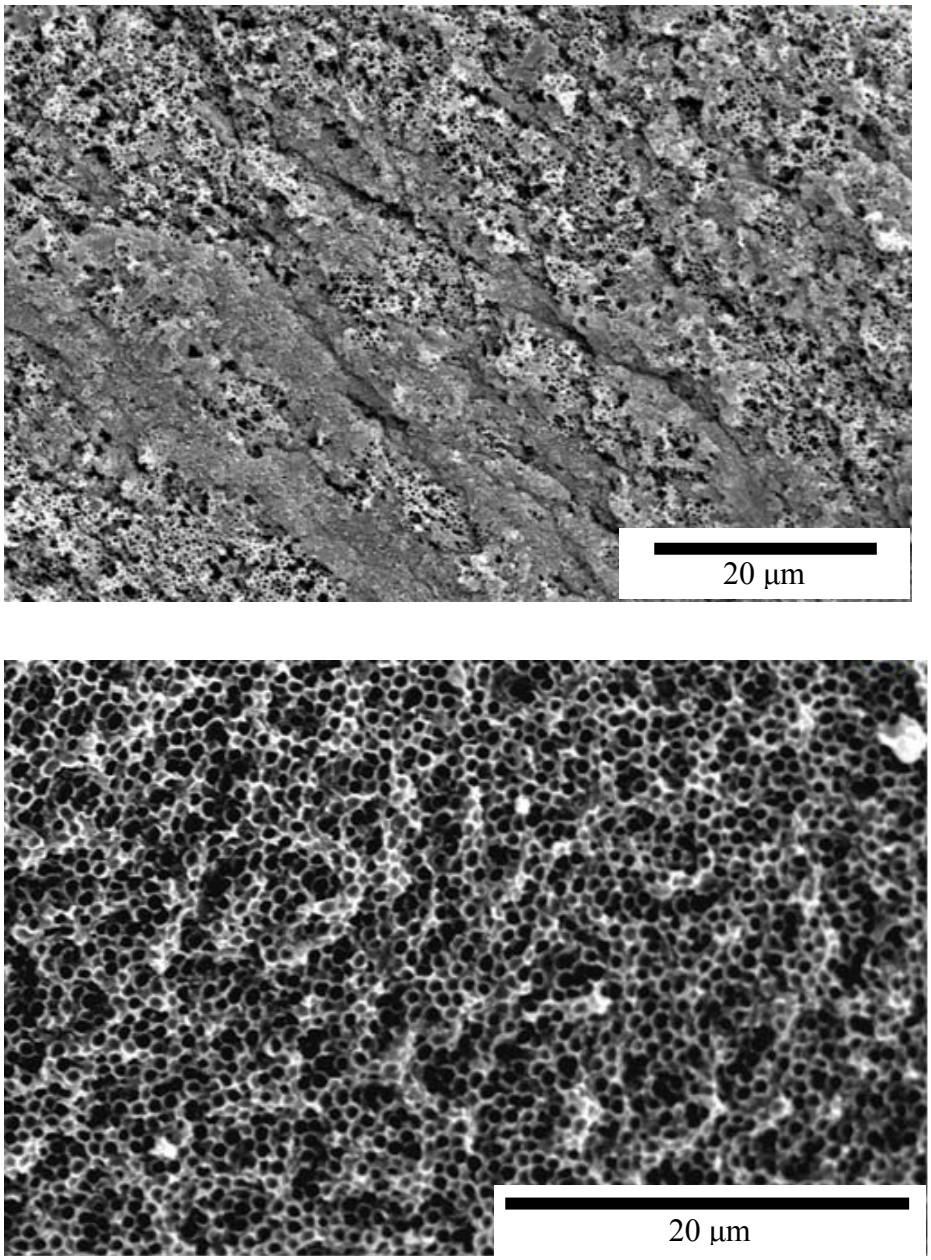

Figure 2.17: SEM images of an inverse opal structures that were synthesized on PAS. The top image represents an inverse opal formed using subsequent steps for the sphere and sol-gel depositions, and the bottom micrograph represents an inverse opal formed using the co-assembly technique.

network. The NS was present underneath the layer of silica, but the pores were blocked by a layer of silica. The co-assembly technique resulted in a NS with the pores fully exposed at the surface. As a result, the co-assembly technique was used for all of the NS/PAS matrices in the flow-through experiments throughout this work.[2] A co-assembly technique has been reported to result in crack-free inverse opal structures on planar substrates in the literature,[8] however our results have shown some areas of cracking remain.

Conclusions

This chapter was intended to provide an overview of the procedures used in the fabrication of silica inverse opal structures. Silica NS structures were constructed on a variety of supports, including glass microscope slides, TEM grids, and PAS. The knowledge gained through the process of fabricating NS on planar substrates was translated and modified to create NS structures on a porous support system. The goal of creating flow-through nanoporous solids was achieved using a PAS and a modified co-assembly technique. With this foundation, the decoration of these structures with catalytic species will form the foundation for the studies presented in this dissertation.

Literature Cited

Literature Cited

1. Nishijima, Y.; Ueno, K.; Juodkazis, S.; Mizeikis, V.; Misawa, H.; Tanimura, T.; Maeda, K. *Optics Express* **2007**, *15*, 12979.

2. Gornowich, D. B.; Blanchard, G. J. *The Journal of Physical Chemistry C* **2012**, *116*, 12165.

3. Dimos, M. M.; Blanchard, G. J. *The Journal of Physical Chemistry C* **2010**, *114*, 6019.

4. Dimos, M. M.; Blanchard, G. J. *Journal of Electroanalytical Chemistry* **2011**, *654*, 13.

5. Dimos, M. M.; Blanchard, G. J. *The Journal of Physical Chemistry C* **2011**, *115*, 11247.

6. Szamocki, R.; Reculusa, S.; Ravaine, S.; Bartlett, P. N.; Kuhn, A.; Hempelmann, R. *Angewandte Chemie International Edition* **2006**, *45*, 1317.

7. Szamocki, R.; Velichko, A.; Mücklich, F.; Reculusa, S.; Ravaine, S.; Neugebauer, S.; Schuhmann, W.; Hempelmann, R.; Kuhn, A. *Electrochemistry Communications* **2007**, *9*, 2121.

8. Hatton, B.; Mishchenko, L.; Davis, S.; Sandhage, K. H.; Aizenberg, J. *Proceedings of the National Academy of Sciences* **2010**, *107*, 10354.

9. Kim, J. K.; Moon, J. H.; Lee, T.-W.; Park, J. H. *Chemical Communications* **2012**, *48*, 11939.

10. Abramova, V.; Sinitskii, A. *Superlattices and Microstructures* **2009**, *45*, 624.

11. Cao, Y.; Wang, Y.; Zhu, Y.; Chen, H.; Li, Z.; Ding, J.; Chi, Y. *Superlattices and Microstructures* **2006**, *40*, 155.

12. Holland, B. T.; Blanford, C. F.; Do, T.; Stein, A. *Chemistry of Materials* **1999**, *11*, 795.

13. Holland, B. T.; Blanford, C. F.; Stein, A. *Science* **1998**, *281*, 538.

14. Holland, B. T.; Blanford, C. F.; Stein, A. *Science* **1998**, *281*, 538.

15. Turner, M. E.; Trentler, T. J.; Colvin, V. L. *Advanced Materials* **2001**, *13*, 180.

16. Yang, P.; Deng, T.; Zhao, D.; Feng, P.; Pine, D.; Chmelka, B. F.; Whitesides, G. M.; Stucky, G. D. *Science* **1998**, *282*, 2244.

17. Yu, H. M.; Yim, J.-H.; Choi, K. Y.; Lim, J. S. *The Journal of Supercritical Fluids* **2012**, *67*, 71.

18. Ma, J.; Parajuli, B. R.; Ghossoub, M. G.; Mihi, A.; Sadhu, J.; Braun, P. V.; Sinha, S. *Nano Letters* **2013**, *13*, 618.

19. Mathew, S. S.; Ma, S.; Kretzschmar, I. *Journal of Materials Research* **2013**, *28*, 369.

20. Wu, M.; Zheng, A.; Deng, F.; Su, B.-L. *Applied Catalysis B: Environmental* **2013**, *138–139*, 219.

21. Goodwin, J. W.; Hearn, J.; Ho, C. C.; Ottewill, R. H. *Colloid & Polymer Science* **1974**, *252*, 464.

22. Ottewill, R.; Shaw, J. *Colloid & Polymer Science* **1967**, *215*, 161.

23. Zhang, J.; Chen, Z.; Wang, Z.; Zhang, W.; Ming, N. *Materials Letters* **2003**, *57*, 4466.

24. Bamnolker, H.; Margel, S. *Journal of Polymer Science Part A: Polymer Chemistry* **1996**, *34*, 1857.

25. Jiang, S.; David Sudol, E.; Dimonie, V. L.; El-Aasser, M. S. *Journal of Applied Polymer Science* **2008**, *107*, 2453.

26. Kawaguchi, S.; Ito, K.; Okubo, M., Ed.; Springer Berlin / Heidelberg: 2005; Vol. 175, p 299.

27. Lu, Y. Y.; El-Aasser, M. S.; Vanderhoff, J. W. *Journal of Polymer Science Part B: Polymer Physics* **1988**, *26*, 1187.

28. Paine, A. J. *Journal of Colloid and Interface Science* **1990**, *138*, 157.

29. Paine, A. J. *Macromolecules* **1990**, *23*, 3109.

30. Paine, A. J. *Journal of Polymer Science Part A: Polymer Chemistry* **1990**, *28*, 2485.

31. Paine, A. J.; Luymes, W.; McNulty, J. *Macromolecules* **1990**, *23*, 3104.

32. Tseng, C. M.; Lu, Y. Y.; El-Aasser, M. S.; Vanderhoff, J. W. *Journal of Polymer Science Part A: Polymer Chemistry* **1986**, *24*, 2995.

33. Im, S. H.; Khalil, G. E.; Callis, J.; Ahn, B. H.; Gouterman, M.; Xia, Y. *Talanta* **2005**, *67*, 492.

34. Barrett, K. E. J. *Dispersion polymerization in organic media, edited by K. E. J. Barrett. With a foreword by C. H. Bamford*; Wiley: London, New York, 1974.

35. Liu, Z.; Jin, Z.; Li, W.; Qiu, J. *Materials Research Bulletin* **2006**, *41*, 119.

36. Flegler, S. L.; Heckman, J. W.; Klomparens, K. L. *Scanning and Transmission Electron Microscopy: An Introduction*; 1st ed.; Oxford University Press: New York, New York, 1993.

37. In *Zetasizer Nano User Manual*; Malvern Instruments Ltd.: Worcestershire, 2007; Vol. MAN0317, p 14.1.

38. Gu, Z.-Z.; Fujishima, A.; Sato, O. *Chemistry of Materials* **2002**, *14*, 760.

39. Brinker, J. C., Scherer, G. W. *Sol-Gel Science: The Physics and Chemistry of Sol-Gel Processing*; Academic Press, Inc.: San Diego, CA, 1990.

CHAPTER 3: Enhancement of GOx Activity by Confinement in an Inverse Opal Structure

Introduction

The immobilization of enzymes on support structures has proven to be an attractive research area for both fundamental and pragmatic reasons. Among the motivations for using immobilized enzymes are the minimization of post-reaction cleanup and the ability to recover and reuse the enzyme. From a more fundamental perspective, it has been shown that immobilization can either enhance or diminish the reactivity of an enzyme, depending on the specific system and manner of immobilization,[1,2] and that the long-term stability of the enzyme can be improved by immobilization.[3] The two methods used most widely are binding the enzyme to a pre-fabricated matrix and entrapment of the enzyme within a polymer. A variety of support materials have been demonstrated, including synthetic resins,[4] mesoporous silica,[5-7] silica nanospheres,[8,9] and zeolites.[10,11] Each of these supports offers advantages and disadvantages. The support-related issues of most importance to this work are (a) the ability to bind enzymes to the support surface covalently under mild reaction conditions, (b) high porosity to enable efficient reactant stream flow, and (c) relatively high surface area. Inverse opal structures satisfy all of these requirements and possess several potential structurally-based advantages. This material format is seeing increased utilization for the immobilization of enzymes,[12-15] with promising results having been reported recently that illustrate the range of utility of inverse opals for the immobilization of enzymes.[16,17]

We are interested in exploring inverse opal structures as catalyst supports. We have examined the efficiency of the catalytic conversion of glucose to gluconic acid and hydrogen peroxide with glucose oxidase (GOx) immobilized on a silica inverse opal structure. The ability to perform this reaction in a flowing mode is important because hydrogen peroxide denatures GOx, thereby terminating the reaction.[18,19] In a flow-through system, the product(s) are separated from the enzyme on a continuous basis, minimizing the adverse effect(s) of prolonged exposure of the enzyme to H_2O_2. We have chosen to use the glucose/GOx system because it is a well characterized reaction and the selectivity of GOx for glucose precludes the operation of more than one chemical reaction. Inverse opals are attractive for such studies because of the control one can exert over the internal void space and pore dimensions, and the ability to create these structures using a variety of oxide materials.[20-25] Inverse opals, sometimes referred to as nanoporous solids (NS), used in this work were constructed in our labs using assemblies of polystyrene spheres as a scaffold. Silica was deposited in the void spaces by a sol-gel growth method, and the polymer spheres were subsequently removed by dissolution. The resulting matrix is an interconnected structure that has a high surface area-to-volume (S/V) ratio (*ca*. 1.22 x 10^5 cm^2/cm^3 for an inverse opal constructed using 1 μm diameter spheres) and is amenable to a wide range of surface modifications that can be used for enzyme attachment. For inverse opals the pore diameter between void regions is taken to be 20% of the diameter of the spheres used in the formation of the structure, affording synthetic control over flow properties.[26]

Nanoporous solids offer the potential to enhance the catalytic activity of GOx due the high S/V and physical dimensions of the structure of the solid matrix. The high S/V ratio provides a large support area for the deposition of GOx in a structural format that produces a

high local density of catalyst. The nanoporous structure is conducive to frequent substrate-enzyme interactions, thus enhancing the turnover rate of the enzyme relative to solution phase enzymes or the enzyme bound to a planar surface. Our data show that the turn-over rate of GOx bound to inverse opal structures is enhanced relative to GOx bound to a planar silica surface or free in solution, and we understand these findings in the context of geometric confinement, surface binding of the enzyme and the kinetics of the GOx/glucose reaction.

Experimental

Nanoporous solid fabrication: Polystyrene spheres (PS) with an average diameter of 1.15 μm were synthesized using an adaptation of a free radical polymerization method.[27] Styrene monomer (99%, *Aldrich*) was distilled at 80°C to remove the stabilizer. The purified styrene was then added to a reaction flask with ethanol, 2,2'-azobisisobutyronitrile (AIBN, 98%, *Aldrich*), and polyvinylpyrrolidone (PVP, M_w ~ 55,000, *Aldrich*). The reaction solution was refluxed at 80°C for 24 hours. The resulting polystyrene spheres were then washed by centrifuging 3 times with ethanol rinses. The solvent was then allowed to evaporate, and a 2% (w/w) suspension of the polystyrene spheres was prepared in water (Milli-Q). The sphere suspension was sonicated for 30 minutes prior to each use to disperse any polystyrene aggregates that may have formed.

The method used for the sol-gel inverse opal formation procedure (*vide infra*) was adapted from the literature.[28] The sol consisted of tetraethylorthosilicate (TEOS, 99%, *Aldrich*), ethanol (anhydrous), water (Milli-Q) and concentrated hydrochloric acid (12 M, *CCI*) in a 4:6:3:1 mass ratio, respectively (total volume 10 mL). The sol was allowed to stir for 1 hour at room temperature prior to use.

To form the inverse opal structure, 0.5 mL of the sol was combined with 0.5 mL of the 2% (w/w) nanosphere solution. The resulting mixture was deposited on a porous alumina support (PAS, d = 22 mm, thickness = 60 μm, Whatman) with a 200 nm nominal pore diameter. The PAS was placed in an Advantec glass microanalysis filter holder with a porous glass frit as a structural support. Using a water aspirator, a vacuum was applied under the PS/sol/PAS and the resulting nanosphere assembly was left to dry at room temperature for a period of 24 hours. The nanosphere/sol structure mounted on the PAS was then removed from the filtration apparatus and placed in toluene (≥99.5%, *Mallinckrodt*) to remove the polystyrene nanospheres from the sol matrix. It was possible to flow toluene through the matrix after 24 hours of soak time.

Nanoporous solid surface modification: Glucose oxidase derived from *Aspergillus niger* (lyophilized powder, *Aldrich*) was immobilized on the surface of the nanoporous solid using a method adapted from the literature.[29] The NS/PAS assembly was first immersed in a solution containing 10% (v/v) 3-aminopropyltriethoxysilane (APTES, 99%, *Aldrich*) in toluene for a period of 30 minutes at 35°C. A cross-linking moiety was then added to the surface by placing the matrix in a 1% (v/v) aqueous glutaraldehyde solution.[30] The NS/PAS assembly was then incubated in a 1 mg/mL GOx solution containing 50 m*M* sodium acetate buffer (pH 4) for 24 hours at 4°C. The resulting GOx-modified NS/PAS was stored in sodium acetate buffer at 4°C when not in use.

Flow-through experiment: An in-house-made Teflon® flow cell was used to hold the NS/PAS in place for the flow-through experiments. β-D-Glucose in sodium acetate buffer solutions in a series of concentrations was flowed through the assembly at flow-rates ranging from 25-50 μL/min. The eluent was collected in 1 mL fractions and analyzed for H_2O_2.

GOx assay: Fenton's assay[31,32] was used to determine the concentration of hydrogen peroxide formed as a result of GOx catalytic oxidation of β-D-glucose to gluconolactone, which spontaneously hydrolyzes to form D-gluconic acid and H_2O_2. Fenton's reagent (FR) is 1 mM $FeSO_4$ in sodium acetate buffer (pH 4). We estimate from the data reported by Woodward *et al.* ε_{340} = 3,000 L/mol-cm for Fenton's reagent.[32] Hydrogen peroxide oxidizes Fe^{2+} to Fe^{3+} resulting in an increase in a near UV absorption band which is monitored at 340 nm. A 3 mL aliquot of FR was added to a quartz cuvette along with 20 μL of the sample to perform the assay. Absorbance measurements were made using a Cary 300 UV-visible double beam absorption spectrometer.

Free GOx in solution analysis: A 1.5 mL aliquot of a 1 mg/mL GOx in sodium acetate buffer solution was combined with 1.5 mL of FR in a cuvette. A 20 μL aliquot of an aqueous solution containing glucose was injected into the cuvette and the solution was stirred continuously throughout the measurement. Absorbance spectra were obtained at 2 minute intervals.

GOx immobilized on planar support: A 5 mm x 5 mm silicon wafer with a *ca*. 15 Å SiO_x layer was cleaned by sonication in water, acetone, and ethanol for 15 minutes each and dried in an oven.[29] The clean support wafer was then treated in the same manner as previously described for the immobilization of GOx on the NS/PAS. The GOx containing wafer was then placed in a cuvette along with 3 mL of FR. A 20 μL aliquot of an aqueous solution containing controlled amounts of glucose was injected into the cuvette and absorbance spectra were obtained in 5 minute intervals.

Scanning Electron Microscopy (SEM): All samples were coated with gold using an Emscope SC500 sputter coater with a deposition current of 20 mA for 3 minutes. All images were obtained using a JEOL 6400V microscope with a LaB_6 emitter at an accelerating voltage of 12 kV.

Dynamic Light Scattering (DLS): The size of the polystyrene spheres was measured using a Malvern Zetasizer Nano ZS. The spheres were suspended in an aqueous solution for analysis.

Thermogravimetric Analysis (TGA): The TGA analysis was performed using a Perkin Elmer TGA-7 thermogravimetric analyzer and TAC 7 thermal analysis controller. The temperature program involved three steps; heat from room temperature to 120°C at 10°C/min, hold at 120°C for 30 minutes, and heat from 120°C to 800°C at 10°C/min.

Results and Discussion

As noted above, the use of inverse opal (nanoporous solid, NS) structures as catalyst supports is attractive for several reasons. We have found experimentally that this structural motif gives rise to enhanced catalytic performance in the electrocatalytic oxidation of methanol with Pt as the matrix material.[33-35] In that work we found evidence for a geometrically-based performance enhancement and indications that the formation of the Pt inverse opal structure gave rise to a different distribution of crystalline faces than the deposition of a planar Pt surface. We are also interested in catalytic processes in systems where the support material does not function as the catalyst. For such systems, where the physical support is chemically inert, it is possible to decorate the support surface with a catalyst such as GOx. We focus in this work on our results for GOx bound to a silica inverse opal structure. We compare the reaction turnover rate for the GOx/glucose reaction for the inverse opal-bound enzyme to that for solution phase reaction and

for the enzyme bound to a planar silica substrate. Through these comparisons we can evaluate the relative contributions of different system properties. Our data demonstrate enhancements in the catalytic behavior of GOx for both steric and geometric reasons.

The construction of an inverse opal structure requires the use of spheres with a relatively narrow size distribution for constructing the scaffold. We have examined the size distribution of our spheres using dynamic light scattering (DLS) and SEM measurements. Results from these measurements are consistent, showing an average diameter of 1.15 μm with a relative polydispersity of 2.25% (Fig. 3.1). These spheres were used for all inverse opal preparation described in this work.

The construction of an inverse opal structure on a porous alumina substrate is an essential step in our ability to evaluate the enzymatic activity of GOx. We show in Fig. 3.2 a schematic of the NS/PAS assembly, with SEM micrographs of the inverse opal, the PAS and the interfacial region for a PAS where the two structures have separated. We show in the bottom panel a side-view of a NS/PAS assembly where physical separation between the two materials is beginning to occur. The NS assembly is *ca*. 27 layers thick. It is instructive given this information to estimate the surface area of the inverse opal structure. The surface area can be approximated geometrically. For a hexagonal close-packed arrangement, the surface area of each void is given by $A_{void} = A_{nanosphere} - 10A_{pore}$ for the first layer and $A_{void} = A_{nanosphere} - 12A_{pore}$ for each subsequent layer. The reason for the difference between the first and subsequent layers has to do with the points of contact a given nanosphere makes. For the first layer there are three contact points with the second layer, six neighboring contact points in the layer and one contact point with the support for a total of 10. For the second and subsequent layers, there are three contact points with each adjacent layer of nanospheres and six contact points with in-plane neighbors for

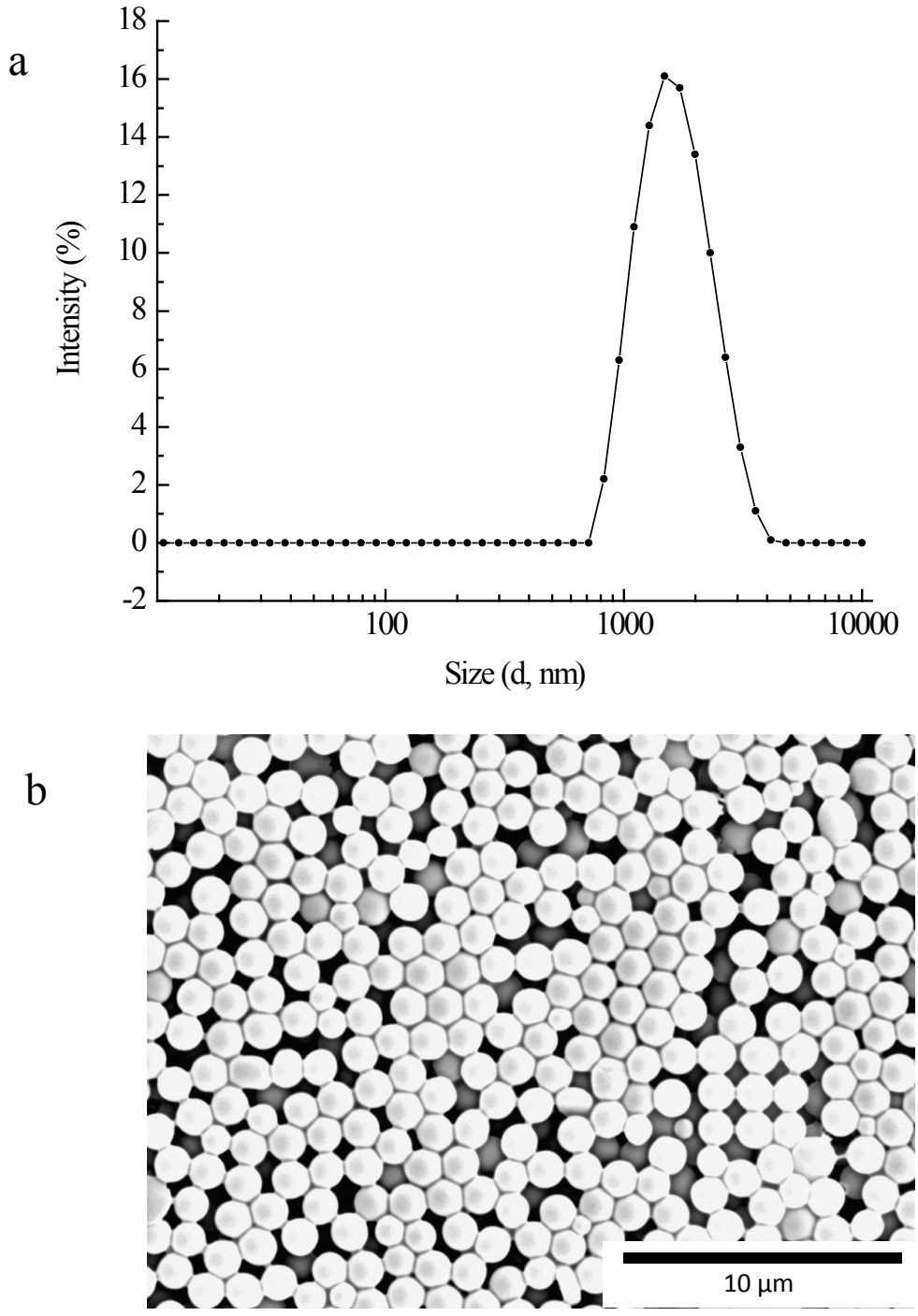

Figure 3.1: (a) Dynamic light scattering data showing the particle size distribution of the polystyrene spheres used to template the inverse opal structures used as enzyme supports. (b) SEM micrograph of the polystyrene spheres.

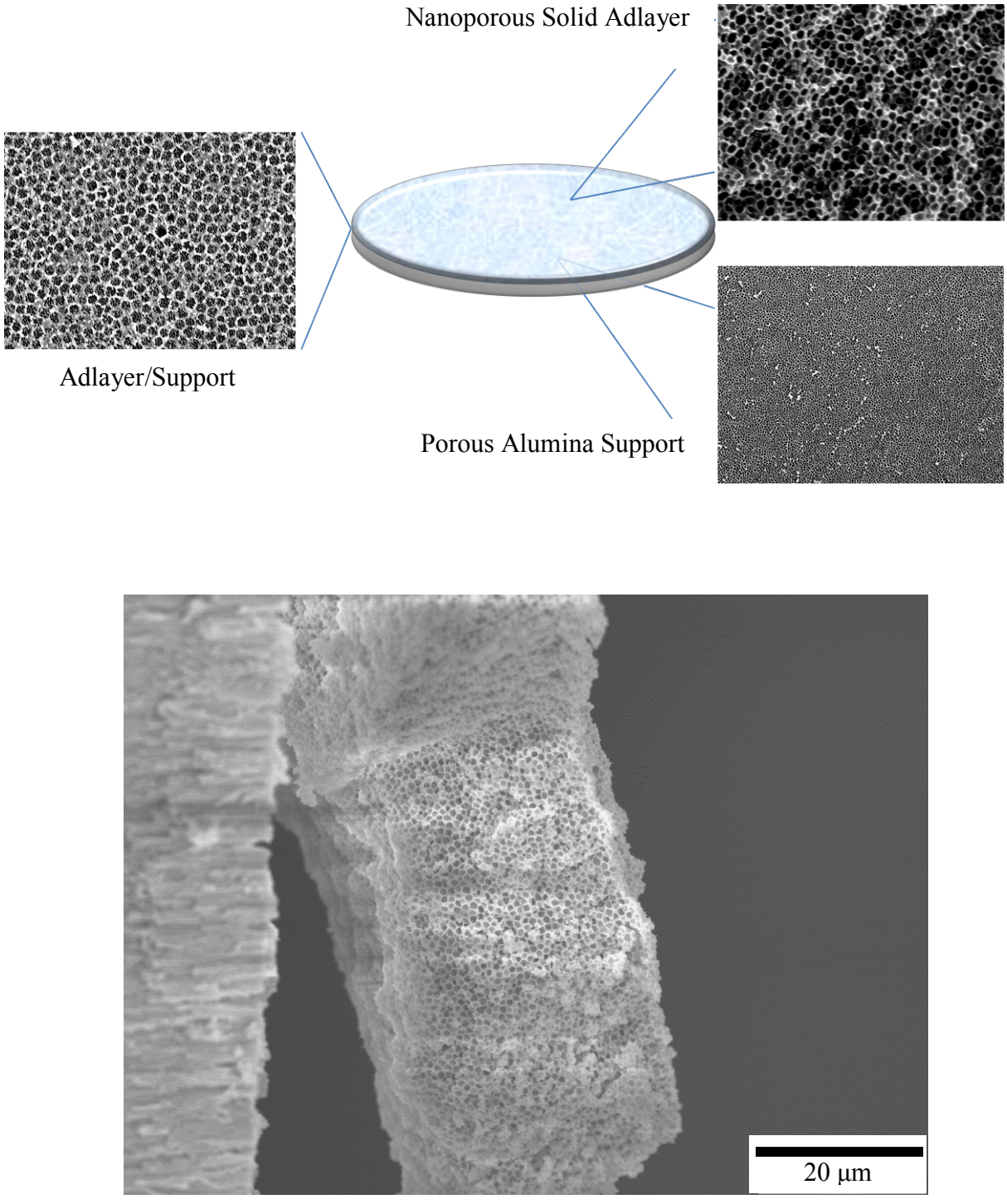

Figure 3.2: Schematic of the NS/PAS assembly. Top, SEM micrographs of inverse opal, PAS, and interfacial region, and bottom, SEM micrograph of an on-edge view of the NS/PAS that was fractured.

a total of 12. For nanospheres of radius *r*, we approximate the area to be $\pi(0.2r)^2$ for each circular pore. For spheres with a diameter of 1.15 μm and a PAS deposition area of 1.33 cm^2 the surface areas are 3.73 cm^2 and 3.65 cm^2 for the first and subsequent layers, respectively. For a 27 layer structure (Fig. 3.2), we estimate the total surface area to be 98.6 cm^2. With this information in hand, it is important to evaluate the amount of GOx present on/in the NS/PAS assembly.

The hydrodynamic radius of GOx has been reported[36] as 43 Å. Assuming a spherical shape, the "footprint" of GOx would be $A = \pi r^2 = 5.81 \times 10^{-13}$ cm^2/GOx, or a monolayer surface coverage of 1.70×10^{14} GOx for our nanoporous solid structures. Evaluation of the amount of GOx poses a substantial experimental challenge. Because silica is not conductive, we cannot use electrochemical means to evaluate the amount of GOx present. Spectroscopic measurements also pose a challenge owing to the diffractive nature of the inverse opal (photonic crystal). Another issue that is not amenable to either spectroscopic or electrochemical characterization is the amount of GOx that is bound or adsorbed to the PAS. For these reasons, we have used gravimetric analysis to evaluate surface loading in our systems.

For the TGA measurements on NS/PAS assemblies, three different samples were analyzed; NS/PAS with GOx immobilized (sample), NS/PAS with no GOx present (blank), and the PAS with GOx (control). The data shown in Fig. 3.3 were normalized first to zero mass at 640°C, then the NS/PAS with and without GOx were matched at 520°C to avoid the physically unrealistic result of negative mass. The step-wise decrease we see for the upper two scans at 120°C is the result of dehydration; the sample is held at this temperature for 30 minutes prior to

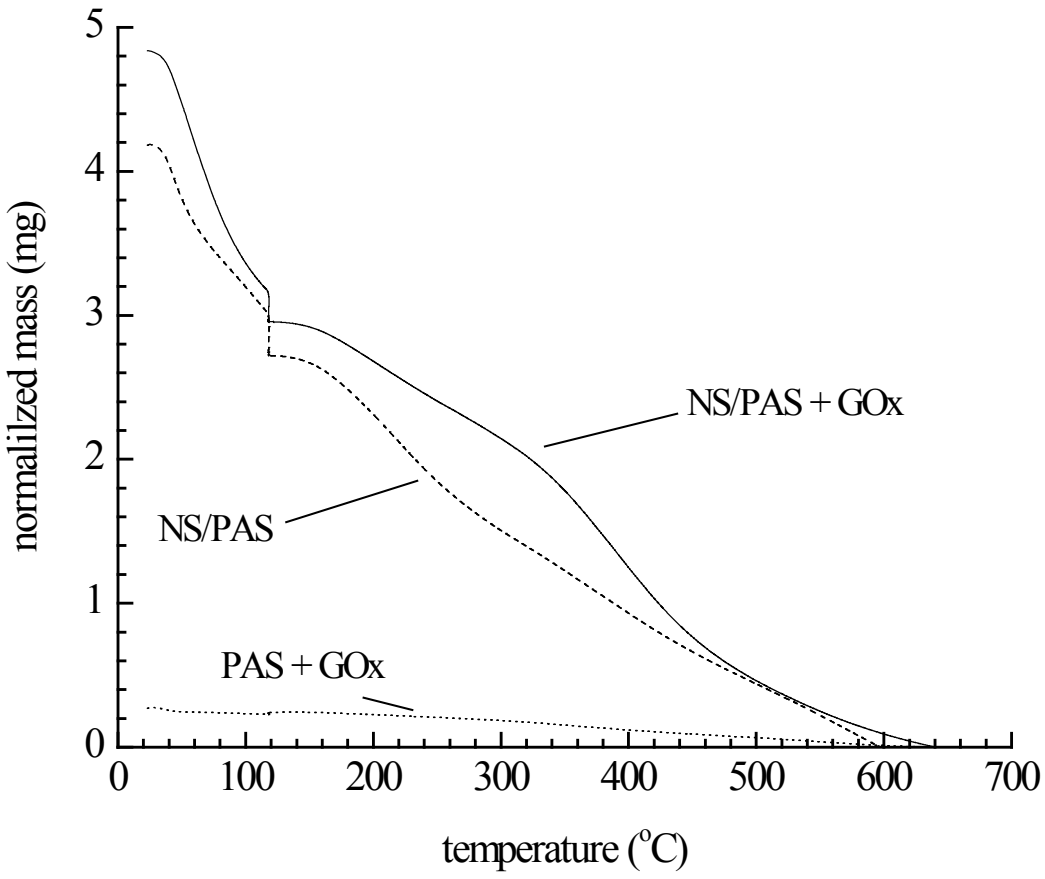

Figure 3.3: TGA data for NS/PAS. The data were normalized to zero mass at 640°C.

scanning to higher temperatures. Subtracting the blank and control mass loss from the mass loss associated with the NS/PAS with GOx immobilized resulted in an experimental enzyme loading of *ca*. 35 μg, or 1.32 x 10^{14} GOx molecules. This value indicates that *ca*. 0.77 monolayer of GOx is present on the surface of the NS. It is significant that the TGA data show some GOx is immobilized within the PAS. We performed control experiments to determine the activity of the GOx contained in the PAS and found that it was inactive. This finding indicates that enzyme activity of GOx is associated with enzyme that is bound to the NS matrix and not to the PAS. It is has been shown that enzymes immobilized on alumina can exhibit varying levels of reactivity.[37-39] Our TGA data indicate a significant amount of GOx trapped within the PAS, but the enzyme assay indicates an absence of enzymatic activity. The GOx in the PAS must either be denatured by the alumina or the active sites of the native enzyme must not be accessible to substrate (glucose). The important point of this finding is that the enzymatic activity we observe is associated with GOx bound to the surface of the inverse opal, and not associated with enzyme on/in the PAS.

With the surface-loading of GOx established for our NS/PAS assemblies, we consider next the reactivity of the bound GOx. Solutions containing a range of β-D-glucose concentrations in sodium acetate buffer were flowed at selected rates through the NS/PAS using a syringe pump. For all of these measurements, a pH 4 buffer was used to avoid the formation of iron oxide. We recognize that this is not the optimum pH for GOx enzymatic activity, but the enzyme exhibits sufficient activity at pH 4 to allow the measurements to be made.[32,40] Our results provide two key findings. The first is that the enzyme activity is dependent on the reactant flow-rate. Second, GOx immobilized on the NS exhibits a higher turnover rate than

solution phase GOx. There are a number of possible explanations for these findings, but it is clear that the inverse opal matrix plays a significant role in mediating the enzymatic activity of GOx. We consider below the factors that give rise to this observed enhancement.

It is instructive to consider the turnover rate of GOx under several experimental arrangements. Data comparing the reactivity of GOx in aqueous solution to its reactivity when bound to planar and nanoporous solid surfaces are shown in Table 3.1. For a 100 mM glucose solution we measure a turnover rate of 2.2 per second determined by Fenton's assay for GOx (present in solution at 1 mg/mL, pH 4). For GOx bound to a planar silica surface we observe a rate of 19 turnovers per second for a 100 mM glucose solution, an enhancement of a factor of 8.6 due to surface binding by the reaction we have used. This finding is consistent with other literature reports that show an increase in enzyme reactivity for bound enzymes relative to free enzymes in solution.[1,2]

It is important to evaluate the comparability of data from these two experimental configurations. For the solution phase measurements, the ratio of glucose/GOx = 1.6×10^4 and for GOx bound to planar silica, the ratio glucose/GOx = 1.9×10^4. For these two systems there is a large and functionally equal stoichiometric excess of glucose given the rate constant for this reaction,[41] rendering the turnover rate results comparable. It is also useful to consider the possible role of iron in solution. To evaluate the possibility that the presence of $Fe^{2+/3+}$ affects the activity of GOx, assays were performed both with and without iron present during the reaction. The data in Figure 3.4 show that $Fe^{2+/3+}$ does not affect the activity of GOx to within the experimental uncertainty. The efficiency of the GOx reaction for a bound enzyme relative to

Table 3.1 Comparison of GOx reactivity for selected catalytic systems. For all measurements reported in this Table, the glucose concentration was 100 mM.

Sample format	Flowrate (μL/min)	GOx	TO/sec.	TO Enhancement relative to solution phase reactivity
NS/PAS	25	0.77 ML[b]	192	87.3
NS/PAS	37.5	0.77 ML[b]	97	44.1
NS/PAS	50	0.77 ML[b]	28	12.7
Planar solid	--	1 ML	19	8.6
Solution phase	--	0.5 mg/mL	2.2[a]	1
PAS with GOx	50	0.241 mg	undetectable	undetectable

[a] solution phase turnover rate extrapolated to initial rate at t = 0

[b] 0.77 ML = 0.77 monolayer. Based on TGA data and surface area calculation.

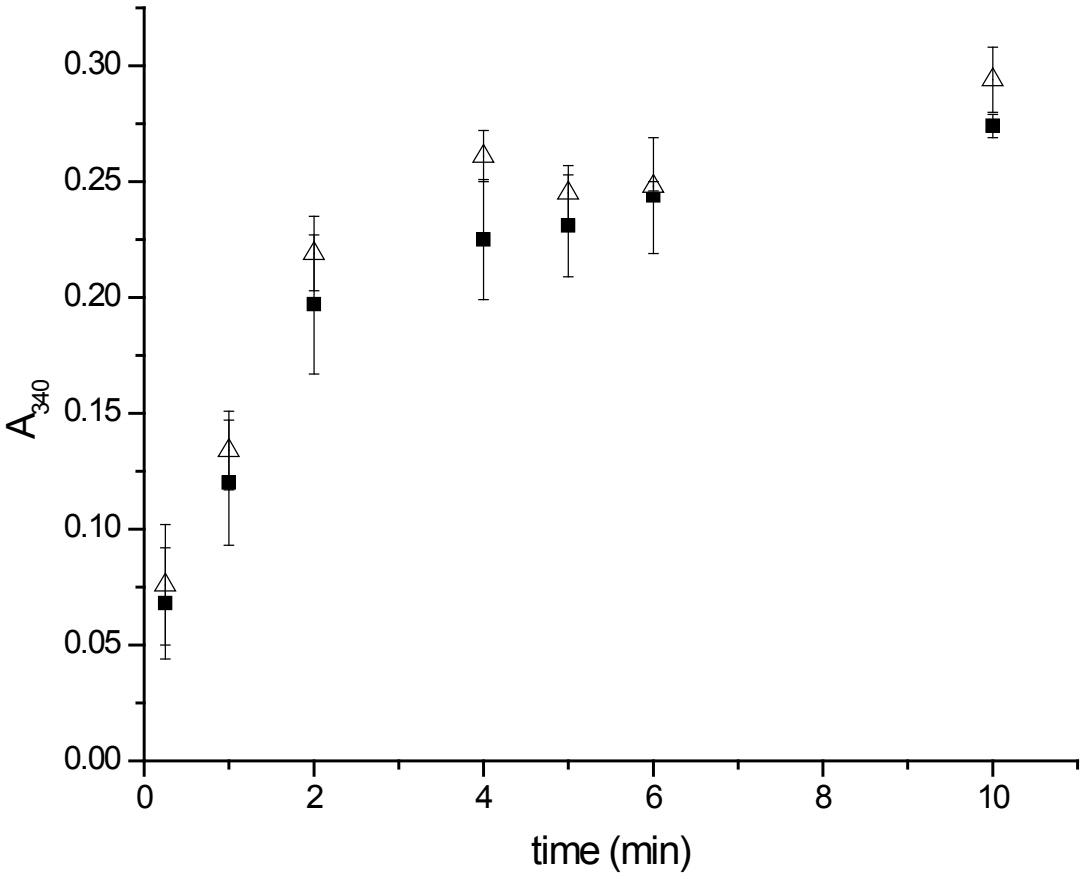

Figure 3.4: Investigation of the effect of $Fe^{2+/3+}$ on GOx activity. Solution phase measurements with $Fe^{2+/3+}$ present during reaction (■) and in the absence of $Fe^{2+/3+}$ (Δ).

the solution phase enzyme cannot be explained in the context of access to the reactive site of GOx. Rather, this enhancement can be understood in the context of the surface binding of the enzyme locking it into a more reactive distribution of conformers than exists in the solution phase. Another possible explanation is that there is a higher concentration of oxygen at the surface where the reaction occurs for the immobilized enzyme. The concentration of oxygen plays an important role in the kinetics of the reaction; however no oxygen concentration studies were performed for these experiments.

Examination of the data for the NS/PAS assembly shows that for this flow-based system the turnover rate (mean values) depends on the flow rate of the glucose solution (Fig. 3.5), although the uncertainties indicate that they are not statistically different. For all of the experiments on this structural format, the turnover rate is substantially higher than that seen for either the solution phase or planar solid-supported GOx. The flow rate dependence demonstrates that the kinetics of the glucose/GOx reaction are modest, consistent with known data on this reaction, $k \sim 1.7 \times 10^{-4}\ s^{-1}$ in solution.[41] What is more significant, however, is that the turnover rate for GOx bound to the NS/PAS assembly is higher than it is for GOx bound to the planar silica surface using the same binding chemistry. There is thus, in addition to the enhancement associated with binding GOx to a silica surface, an enhancement in turnover rate that derives from the inverse opal structure. We understand this effect based on the inverse opal structure functioning as an assembly of nanoreactors.[34] The effect is based on the action of diffusion within the nanoporous solid structure. As a reactant molecule passes through the nanoporous solid structure, it will execute diffusive motion. If the distance between the walls of the nano-confining volume in the nanoporous solid is less than the characteristic diffusion length, $2(Dt)^{1/2}$, then the reactant will experience multiple interactions with the catalyst-coated walls of

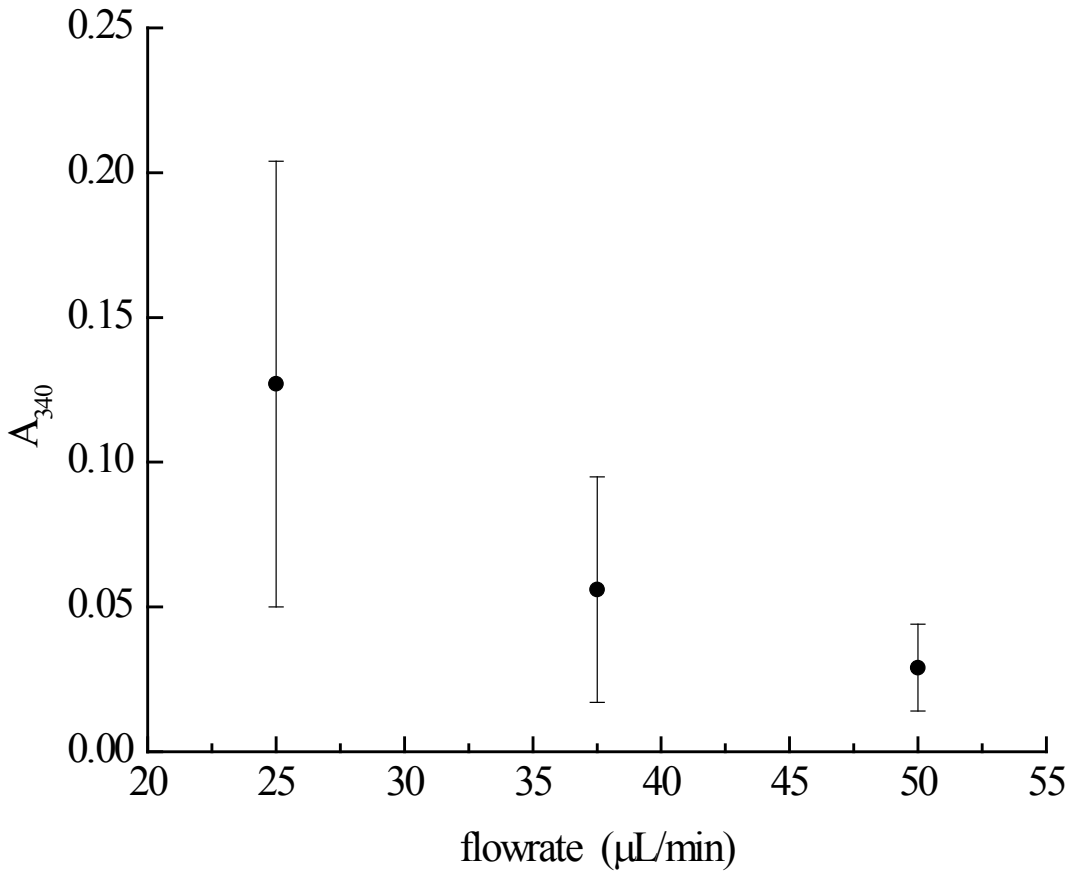

Figure 3.5: Absorbance values at 340 nm for the NS/PAS at different flowrates.

the nanoporous solid. We assert that the probability of a reaction event occurring is proportional to the number of reactant-enzyme interactions. The smaller the confining volume of the nanoporous solid, the higher the reaction probability. For our experimental conditions, flow rates of 25, 37.5 and 50 μL/minute correspond to 10.2, 6.8 and 5.1 second residence times, respectively, in the nanoporous solid structure. D for glucose in aqueous solution is 6.75×10^{-6} cm^2/s [42] and *d* for our assemblies is 1.15×10^{-4} cm. The quantity $2(Dt)^{1/2}/d$ provides a gauge of the geometric enhancement for the NS/PAS assembly compared to the planar surface. We calculate these enhancements to be 144 for 25 μL/min flow rate, 118 for 37.5 μL/min flow rate and 100 for 50 μL/min flow rate. We observe experimentally these enhancements to be 10, 5.1 and 1.5 for the three flow rates. The difference between experimental and calculated enhancements lies partly in the admitted over-simplification of the geometric estimate we have used and partly in the kinetic limitations to the turnover rates we report for the flow-through NS/PAS system.

The flow rates we have used in this work were selected for two reasons. The first is that the glucose/GOx reaction is kinetically limited, and fast flow rates lead to comparatively low reaction efficiency. The second reason is that we are limited to slower flow rates due to the fragile NS and PAS structures. We have attempted flow rates up to 1 mL/min, with the typical result being fractures in the NS/PAS matrix. Such mechanical breakage allows leakage through the NS/PAS without exposure to bound enzyme, producing results with negligible apparent turnover rates. It is also important to note that the overall efficiency of the conversion of glucose to hydrogen peroxide is *ca*. 6% for the 25 μL/min flow rate. This finding indicates that glucose can pass through the matrix unreacted, likely due to the reaction rate and the large stoichiometric excess of glucose used. Either the unreacted glucose makes it through the NS matrix without

contacting an enzyme or there are defect regions within the NS matrix that provide the reactant with an open path to the PAS. Using a NS matrix fabricated from smaller PS spheres may give some insight into which of these possibilities is responsible for the observed reaction efficiency.

The enhancements we report for GOx immobilized on silica inverse opal structures are higher than the values reported for mesoporous silica matrices.[6,7] The enhanced reactivity we observe for GOx immobilized on the planar silica support is similar to the values reported in that work. We believe the increased turnover rate observed in that work is due to the fact that the previous work was performed under diffusion-limited conditions. Having the ability to flow the reactant through the supported catalyst structure increases the frequency of enzyme-substrate interactions, resulting in a higher turnover rate. In addition to flow, the GOx molecules in our NS may be immobilized in a way that results in a higher number of available active sites due to the surface binding chemistry used.

Conclusions

The NS/PAS flow-through catalyst support we have demonstrated is a potentially useful matrix for enzyme immobilization that is capable of producing enhanced turnover rates. We report a GOx turnover enhancement of 87.3 for a 25 μL/min flow rate relative to solution phase reactivity and an enhancement of 8.6 for the planar solid relative to solution phase. The enhancement associated with the nanoporous solid matrix is due to both structural stabilization of the enzyme and geometric advantages associated with the inverse opal structure. 1.15 μm Diameter polystyrene spheres were chosen as inverse opal templates to allow facile flow through the structure. We are in the process of investigating the effect(s) of templating sphere size as well as the matrix material and enzyme binding chemistry to elucidate the parameter-dependence and optimum configuration, and to understand the potential of this structural motif for even

greater catalytic turnover rate enhancement. An important consideration is the improvement of the structural integrity of the NS/PAS assembly to allow higher reactant flow rates. This issue will be critical for systems where the catalyst possesses relatively fast reaction kinetics.

Literature Cited

Literature Cited

1. Minton, A. P. *Journal of Biological Chemistry* **2001**, *276*, 10577.

2. Zhou, H.-X.; Dill, K. A. *Biochemistry* **2001**, *40*, 11289.

3. Gupta, M. N. *Thermostability of enzymes*; Springer-Verlag: Secaucus, New Jersey, 1993.

4. Katchalski-Katzir, E.; Kraemer, D. M. *Journal of Molecular Catalysis B: Enzymatic* **2000**, *10*, 157.

5. Borole, A.; Dai, S.; Cheng, C.; Rodriguez, M.; Davison, B. *Applied Biochemistry and Biotechnology* **2004**, *113*, 273.

6. Lei, C.; Soares, T. A.; Shin, Y.; Liu, J.; Ackerman, E. J. *Nanotechnology* **2008**, *19*, 1.

7. Lei, C.; Shin, Y.; Liu, J.; Ackerman, E. J. *Journal of the American Chemical Society* **2002**, *124*, 11242.

8. Kim, M. I.; Ham, H. O.; Oh, S.-D.; Park, H. G.; Chang, H. N.; Choi, S.-H. *Journal of Molecular Catalysis B: Enzymatic* **2006**, *39*, 62.

9. Wang, Y.; Caruso, F. *Chemical Communications* **2004**, 1528.

10. Díaz, J. F.; Balkus, K. J. *Journal of Molecular Catalysis B: Enzymatic* **1996**, *2*, 115.

11. Yan, A.-X.; Li, X.-W.; Ye, Y.-H. *Applied Biochemistry and Biotechnology* **2002**, *101*, 113.

12. Zhu, Y.; Cao, H.; Tang, L.; Yang, X.; Li, C. *Electrochimica Acta* **2009**, *54*, 2823.

13. Walcarius, A.; Kuhn, A. *TrAC Trends in Analytical Chemistry* **2008**, *27*, 593.

14. Szamocki, R.; Velichko, A.; Mücklich, F.; Reculusa, S.; Ravaine, S.; Neugebauer, S.; Schuhmann, W.; Hempelmann, R.; Kuhn, A. *Electrochemistry Communications* **2007**, *9*, 2121.

15. Bon Saint Côme, Y.; Lalo, H.; Wang, Z.; Etienne, M.; Gajdzik, J.; Kohring, G.-W.; Walcarius, A.; Hempelmann, R.; Kuhn, A. *Langmuir* **2011**, *27*, 12737.

16. Wang, Z.; Etienne, M.; Kohring, G.-W.; Bon-Saint-Côme, Y.; Kuhn, A.; Walcarius, A. *Electrochimica Acta* **2011**, *56*, 9032.

17. Qu, F.; Nasraoui, R.; Etienne, M.; Côme, Y. B. S.; Kuhn, A.; Lenz, J.; Gajdzik, J.; Hempelmann, R.; Walcarius, A. *Electrochemistry Communications* **2011**, *13*, 138.

18. Kleppe, K. *Biochemistry* **1966**, *5*, 139.

19. Krishnaswamy, S.; Kittrell, J. R. *Biotechnology and Bioengineering* **1978**, *20*, 821.

20. Holland, B. T.; Blanford, C. F.; Stein, A. *Science* **1998**, *281*, 538.

21. Holland, B. T.; Blanford, C. F.; Do, T.; Stein, A. *Chemistry of Materials* **1999**, *11*, 795.

22. Yan, H.; Blanford, C. F.; Holland, B. T.; Parent, M.; Smyrl, W. H.; Stein, A. *Advanced Materials* **1999**, *11*, 1003.

23. Turner, M. E.; Trentler, T. J.; Colvin, V. L. *Advanced Materials* **2001**, *13*, 180.

24. Wijnhoven, J. E. G. J.; Vos, W. L. *Science* **1998**, *281*, 802.

25. Yang, P.; Deng, T.; Zhao, D.; Feng, P.; Pine, D.; Chmelka, B. F.; Whitesides, G. M.; Stucky, G. D. *Science* **1998**, *282*, 2244.

26. Szamocki, R.; Reculusa, S.; Ravaine, S.; Bartlett, P. N.; Kuhn, A.; Hempelmann, R. *Angewandte Chemie International Edition* **2006**, *45*, 1317.

27. Im, S. H.; Khalil, G. E.; Callis, J.; Ahn, B. H.; Gouterman, M.; Xia, Y. *Talanta* **2005**, *67*, 492.

28. Hatton, B.; Mishchenko, L.; Davis, S.; Sandhage, K. H.; Aizenberg, J. *Proceedings of the National Academy of Sciences* **2010**, *107*, 10354.

29. Subramanian, A.; Kennel, S. J.; Oden, P. I.; Jacobson, K. B.; Woodward, J.; Doktycz, M. J. *Enzyme and Microbial Technology* **1999**, *24*, 26.

30. Lopez-Gallego, F.; Betancor, L.; Mateo, C.; Hidalgo, A.; Alonso-Morales, N.; Dellamora-Ortiz, G.; Guisan, J. M.; Fernandez-Lafuente, R. *Journal of Biotechnology* **2005**, *119*, 70.

31. Woodward, J.; Lennon, K. W.; Zanin, G.; Wagner, M.; Scott, M. A. *Biotechnology Letters* **1985**, *7*, 197.

32. Woodward, J.; Wagner, M.; Lennon, K. W.; Zanin, G.; Scott, M. A. *Enzyme and Microbial Technology* **1985**, *7*, 449.

33. Dimos, M. M.; Blanchard, G. J. *The Journal of Physical Chemistry C* **2010**, *114*, 6019.

34. Dimos, M. M.; Blanchard, G. J. *Journal of Electroanalytical Chemistry* **2011**, *654*, 13.

35. Dimos, M. M.; Blanchard, G. J. *The Journal of Physical Chemistry C* **2011**, *115*, 11247.

36. Nakamura, S.; Hayashi, S.; Koga, K. *Biochimica et Biophysica Acta (BBA) - Enzymology* **1976**, *445*, 294.

37. Bosley, J.; Peilow, A. *Journal of the American Oil Chemists' Society* **1997**, *74*, 107.

38. de Oliveira, P. C.; Alves, G. M.; de Castro, H. F. *Biochemical Engineering Journal* **2000**, *5*, 63.

39. Tzanov, T.; Costa, S. A.; Gübitz, G. M.; Cavaco-Paulo, A. *Journal of Biotechnology* **2002**, *93*, 87.

40. Bright, H. J.; Appleby, M. *J. Biol. Chem.* **1969**, *244*, 3625.

41. Odebunmi, E. O.; Owalude, S. O. *Journal of Applied Science and Environmental Management* **2007**, *11*, 95.

42. Gladden, J. K.; Dole, M. *Journal of the American Chemical Society* **1953**, *75*, 3900.

CHAPTER 4: Evaluating the Catalytic Efficiency of Alkaline Phosphatase Confined in an Inverse Opal Structure

Introduction

Enzyme immobilization on support structures is an area of significant research activity because of its potential for improvements in chemical processing and catalyst recovery. Stabilization, regeneration, and the ability to easily separate the enzyme from the reaction products are three of the most commonly targeted areas for improvement in the field. A variety of support structures have been investigated, ranging from organic polymers to inorganic supramolecular structures such as zeolites,[1,2] mesoporous silica,[3-5] and silica nanospheres.[6,7] It has also been reported that enzymes can exhibit increased stability when immobilized in a confined space.[8-11] We have reported previously on the immobilization and enhanced reactivity of glucose oxidase confined in a silica inverse opal structure.[12] Other groups have also reported on the immobilization of enzymes using inverse opal structures,[11,13-15] suggesting that this matrix format may be a useful material for biocatalysis applications.[16,17] There are a number of potential issues associated with the immobilization of enzymes in this structural motif, and it the purpose of this work to explore some of these issues.

Inverse opal structures, sometimes referred to as nanoporous solids (NS), have characteristics that make them an attractive choice for enzyme immobilization when used in a flow-through system. Nanoporous solids have a relatively high surface area-to-volume ratio (*ca*. 1.22 x 10^5 cm^2/cm^3 for a NS constructed using 1 μm diameter spheres)[12] affording a useful loading density for enzymes. While other materials exist with higher surface area-to-volume ratios, the combination of structural regularity, relative ease of formation and a usefully high

achievable loading density make inverse opal NS structures attractive for our purposes. The regularity of the nanoscale confinement afforded by NS materials allows for predictable enhancements in catalytic activity relative to catalysts bound to a planar surface.[12] The geometric confinement provided by NS materials leads to a higher frequency of interactions between the substrate and the enzyme, thus increasing the probability of a reactive event. The manner in which the NS materials are constructed allows for significant control over the pore size within these materials.[15] Finally, the ability to utilize these materials in a flow-through mode reduces the exposure of the enzyme to reaction product(s), which have been shown in some cases to denature the enzyme.[18,19]

We reported previously on the immobilization of glucose oxidase (GOx) on a silica NS matrix.[12] In that work we found that the reactivity of NS-immobilized GOx was higher than either solution phase GOx or GOx immobilized on a planar silica surface. In this work we focus on the reactivity of alkaline phosphatase (ALP) immobilized on a silica inverse opal structure and compare its reactivity when immobilized in this manner to its solution phase and planar surface-bound reactivity. ALP derived from bovine intestinal mucosa is a dimeric zinc metallo-enzyme containing two identical subunits.[20] We chose ALP because it non-specifically dephosphorylates a wide range of phosphate monoesters, resulting in an alcohol and phosphate. A non-specific enzyme affords the ability to choose a variety of substrate molecules, which allows for the interrogation the active site(s) of ALP to see if any information can be gained regarding substrate specificity. Our experimental data address both the issue of substrate-dependent reactivity for this enzyme and the effect of immobilizing ALP. Our findings suggest that the immobilization of ALP reduces its activity relative to that of the solution phase enzyme,

in contrast to our findings for GOx, even though the enhancement associated with immobilization in a NS material relative to a planar surface remains the same. Taken collectively, these data demonstrate the important structural and enzyme-specific issues associated with this approach to enzyme immobilization.

Experimental

Nanoporous solid fabrication: Polystyrene spheres with an average diameter of 1.15 μm were synthesized using an adaptation of a free radical polymerization method. Styrene monomer (99%, *Aldrich*) was distilled at 80°C to remove the stabilizer. The purified styrene was then added to a reaction flask with ethanol, 2,2'-azobisisobutyronitrile (AIBN, 98%, *Aldrich*), and polyvinylpyrrolidone (PVP, M_w ~ 55,000, *Aldrich*). The reaction solution was refluxed at 80°C for 24 hours. The resulting polystyrene spheres were then washed by centrifuging 3 times with ethanol rinses. The solvent was then allowed to evaporate, and a 2% (w/w) suspension of the polystyrene spheres was prepared in water (Milli-Q). The sphere suspension was sonicated for 30 minutes prior to each use to disperse any polystyrene aggregates that may have formed.

The same method used for the sol-gel inverse opal formation from previous work[12] was used for this work. The sol consisted of tetraethylorthosilicate (TEOS, 99%, *Aldrich*), ethanol (anhydrous), water (Milli-Q) and concentrated hydrochloric acid (12 M, *CCI*) in a 4:6:3:1 mass ratio, respectively (total volume 10 mL). The sol was allowed to stir for 1 hour at room temperature prior to use.

To form the NS structure, 0.5 mL of the sol was combined with 0.5 mL of the 2% (w/w) nanosphere solution. The resulting mixture was deposited on a porous alumina support (PAS, d = 22 mm, thickness = 60 μm, *Whatman*) with a 200 nm nominal pore diameter. The PAS was placed in an Advantec glass microanalysis filter holder with a porous glass frit as a structural

support. Using a water aspirator, a vacuum was applied under the NS/PAS and the resulting nanosphere assembly was left to dry at room temperature for a period of 24 hours. The nanosphere/sol structure mounted on the PAS was then removed from the filtration apparatus and placed in toluene (≥99.5%, *Mallinckrodt*) to remove the polystyrene nanospheres from the sol matrix. It was possible to flow toluene through the matrix after 24 hours of soak time.

ALP materials: All of the following chemicals were purchased from Sigma Aldrich and used without further purification; 1-naphthol (≥99%), 2-naphthol (99%), 4-methylumbelliferone (4-MB, ≥98%), 1-naphthyl phosphate (1-NP, disodium salt), 2-naphthyl phosphate (2-NP, disodium salt, 97%), 4-methylumbelliferyl phosphate (4-MBP, disodium salt, premium grade), alkaline phosphatase (ALP, derived from bovine intestinal mucosa, lyophilized powder, MW ~160 kDa), and diethanolamine (DEA, reagent grade, ≥98%).

ALP immobilization: A 5 mm × 5 mm silicon wafer with a *ca*. 15 Å SiO_x layer was cleaned by immersing the chip in a piranha solution (3:1 concentrated sulfuric acid:30% hydrogen peroxide) for 30 minutes. The PAS was used without further modification. ALP was immobilized on the surface of a planar silicon support, PAS (control), and NS/PAS using a combination of methods adapted from the literature.[21-23] The various supports were first immersed in a solution containing 10% (v/v) 3-aminopropyltriethoxysilane (APTES, 99%, *Aldrich*) in toluene for a period of 30 minutes at 35°C. A linking moiety was then added to the surface by placing the matrix in a 1% (v/v) aqueous glutaraldehyde solution. The supports were then incubated in a 1 mg/mL ALP solution containing 1.0 *M* DEA buffer (pH adjusted to 9.8 with 6 *M* HCl) and 0.50 m*M* magnesium chloride for 24 hours at 4°C. The resulting ALP-modified supports were stored in DEA buffer at 4°C when not in use. The DEA buffer was prepared fresh on a weekly basis and stored in the fridge.

Flow-through ALP on PAS/NS format: An in-house-made Teflon® flow cell was used to hold the NS/PAS in place for the flow-through experiments. Each PAS and PAS/NS were flushed with DEA buffer for 30 minutes to remove any nonspecifically bonded ALP from within the matrix. After the substrates were rinsed, separate $1x10^{-4}$ *M* 4-MBP, 1-NP, and 2-NP in DEA buffer solutions were flowed through the PAS and PAS/NS at 50 μL/min. Samples were collected in 2 mL fractions and analyzed using fluorescence measurements.

Fluorescence assays for ALP activity: All fluorescence measurements were conducted using a Jobin-Yvon Fluorolog III spectrometer. The spectral resolution for the fluorescence experiments was 3 nm for all measurements. All fluorescence measurements were performed at room temperature. All measurements were made with DEA buffer as the solvent and at a total volume of 3 mL in all cases. For the 1-naphthol assay, λ_{ex} = 332 nm, for 2-naphthol, λ_{ex} = 352 nm and for 4-methylumbelliferone, λ_{ex} = 365 nm.

ALP immobilized on planar support analysis: A Si chip with ALP immobilized on the surface was placed in the bottom of a cuvette. Buffer was added and the various substrates were introduced (3 mL total volume) and allowed to react without stirring. The fluorescence intensity was monitored in 2 minute intervals at the corresponding λ_{max} for each of the substrates.

Results and Discussion

The ability to bind enzymes to a solid support is attractive for a variety of reasons, as discussed above, but there are also a number of potential problems with this approach. Among the issues that are challenging to evaluate and control are the details of how the enzyme is bound to the solid support structure. There are a number of well-established methods for binding biomolecules to (polar) surfaces, all of which rely on the identity of the functional groups that

are present at the enzyme surface. The details of the binding can vary significantly depending on which amino acid functionality on the enzyme is used for this purpose, both in terms of possible changes in the tertiary structure of the enzyme upon binding and on the accessibility of the reactive binding pocket. It is thus possible to either enhance or diminish the reactivity of a surface bound enzyme depending on the identity of the enzyme and the manner in which it is bound to the support surface. In a previous report we have investigated the surface binding of glucose oxidase (GOx) to a silica inverse opal structure. We found that the surface bound enzyme exhibited higher reactivity than the solution phase enzyme, and that a nanoscale confinement effect was operative (*vide infra*) that served to enhance the activity for inverse opal-supported enzyme relative to the same system supported on a planar silica surface. In this work our focus is two-fold. We have chosen to use the enzyme alkaline phosphatase (ALP) because it is a promiscuous catalyst, reacting with a variety of phosphate monoesters, allowing the interrogation of the binding pocket by challenging the enzyme with a selection of different phosphates. In addition, because ALP is a structurally different enzyme than GOx, we anticipate being able to evaluate the generality, or not, of the surface-enhancement exhibited by the binding of GOx to our inverse opal structures. In the discussion that follows we briefly consider the rationale for the selection of the substrates used in this work and then consider the results for each. Comparison of solution phase results for ALP dephosphorylation of the substrates provides some information on the nature of the reaction. Subsequent comparison of the solution phase results to those for ALP bound to both inverse opal and silica surfaces allows for direct evaluation of the effect of surface immobilization for this enzyme when the well-established glutaraldehyde surface binding reaction is used (Fig. 4.1).

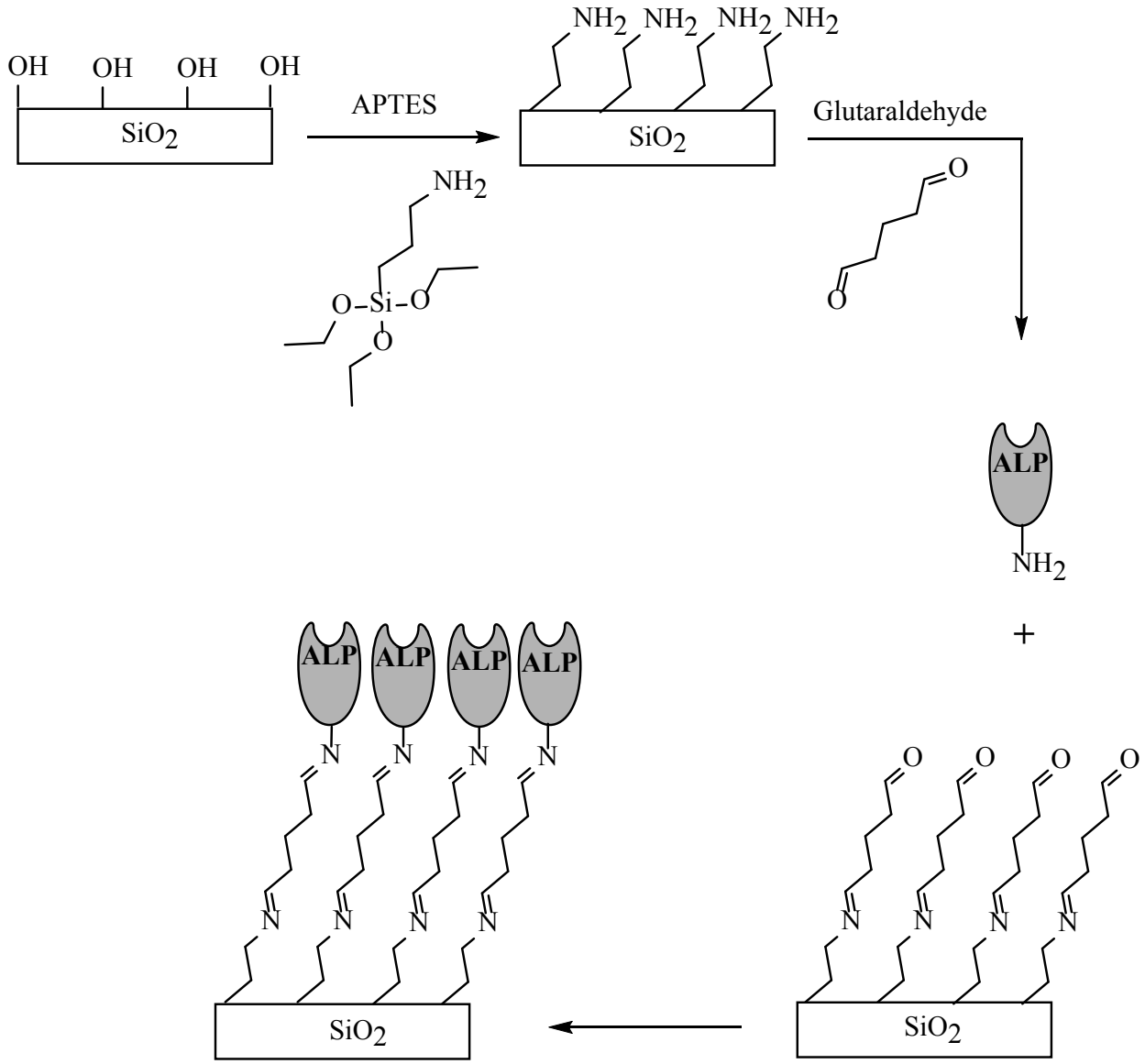

Figure 4.1: ALP immobilization chemistry used for planar and NS/PAS support experiments.

We have chosen three phosphate probes for these studies. These are 4-methylumbelliferyl phosphate (4-MBP), 1-nahpthyl phosphate (1-NP) and 2-naphthyl phosphate (2-NP). These substrates were chosen because they are characterized by very low fluorescence quantum yields and upon dephosphorylation the resulting alcohol products (Fig. 4.2) emit light efficiently. Thus detection of the reaction process is facile and sensitive. The excitation and emission spectra are shown in Figs. 4.3-4.5 for 4-MBP/4-methylumbelliferone, 1-NP/1-naphthol, and 2-NP/2-naphthol, respectively. From these data it is clear that the substrate molecules do not exhibit measureable fluorescence under the enzyme reaction conditions. Absorbance spectra for each R-PO_4/R-OH pair are shown in Fig. 4.6. The absorbance data indicate that each product was selectively excited, with minimal interference from the substrate molecules. In addition to these substrates providing for facile detection, the difference in chemical structure may provide some insight into the structure-dependence of the enzymatic reaction and it is this point we address next in the context of the reaction kinetics for solution phase reactions.

Solution phase ALP reactivity: We have determined the substrate concentration-dependence of the ALP enzymatic reaction rate with 4-MBP, 1-NP and 2-NP. The concentration-dependent time-evolution of the reactions and the concentration-dependence of the long-time fluorescence intensities are shown in Figs. 4.7-4.9. These data demonstrate that the reactions proceed rapidly in all cases, essentially reaching completion within two minutes after initiation. It is important to note that for 1-NP and 2-NP, the fluorescence intensities achieved at the completion of the reaction are not linear in substrate concentration-dependence. This finding is indicative of either nonlinearity in the concentration-dependence of 1- and 2-naphthol fluorescence or that the reaction proceeds to completion at lower substrate concentrations but does not achieve completion for substrate concentrations of *ca*. 10^{-4} M.

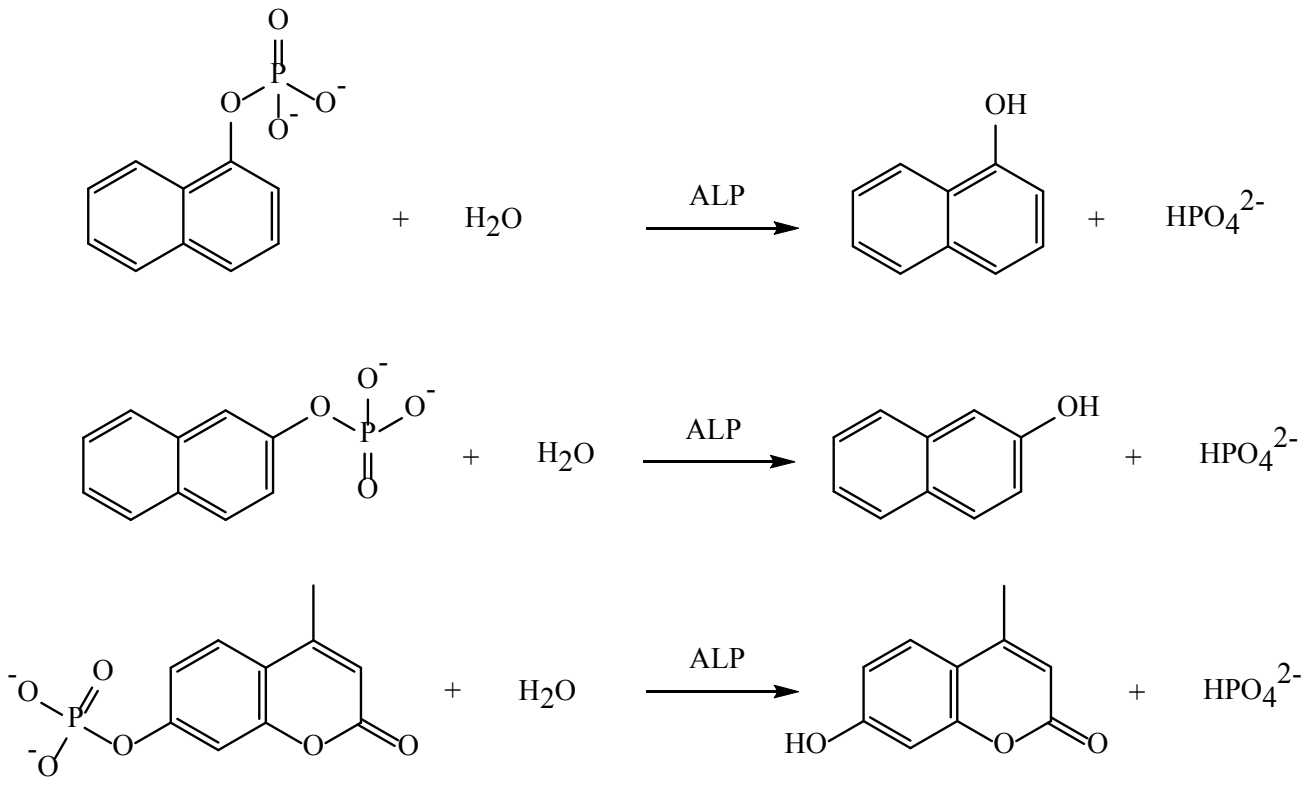

Figure 4.2: Reactions for ALP with 1-NP (top), 2-NP (middle), and 4-MBP (bottom).

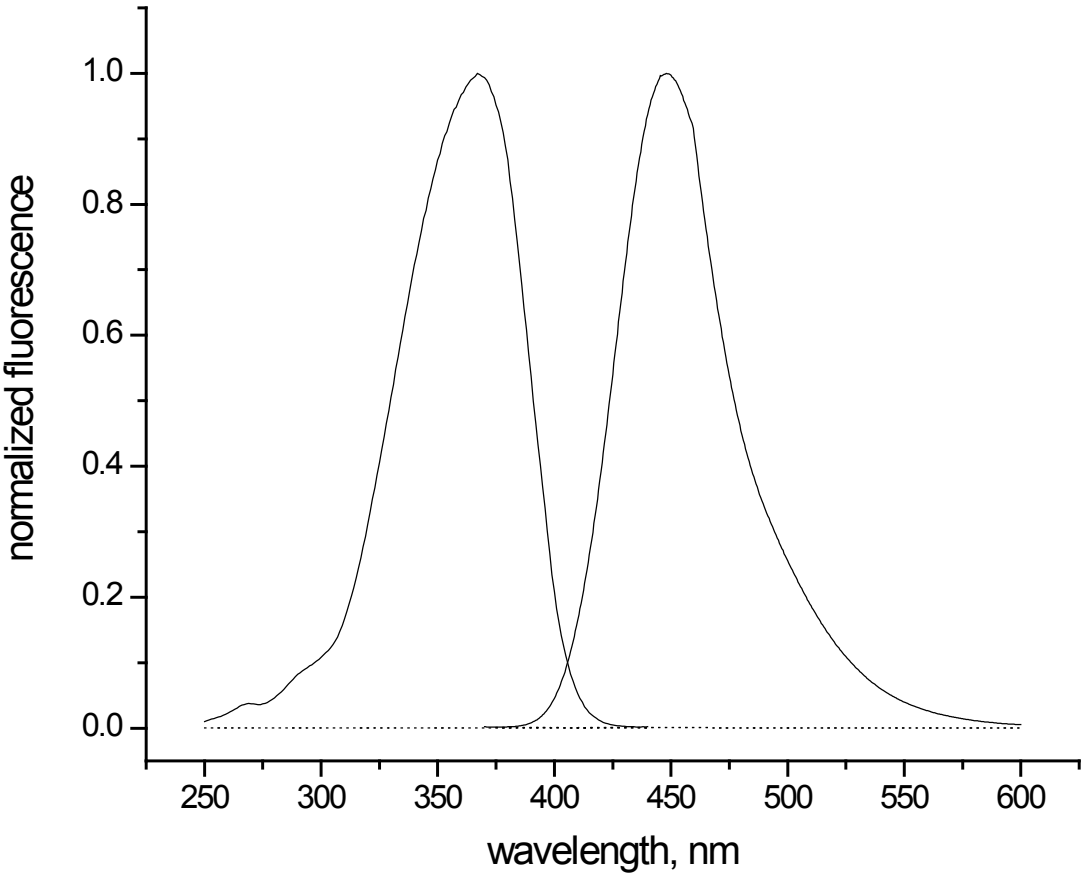

Figure 4.3: Fluorescence excitation and emission spectra for 4-MBP (dotted) and 4-MB (solid), λ_{ex} = 365 nm and λ_{em} = 448 nm for each.

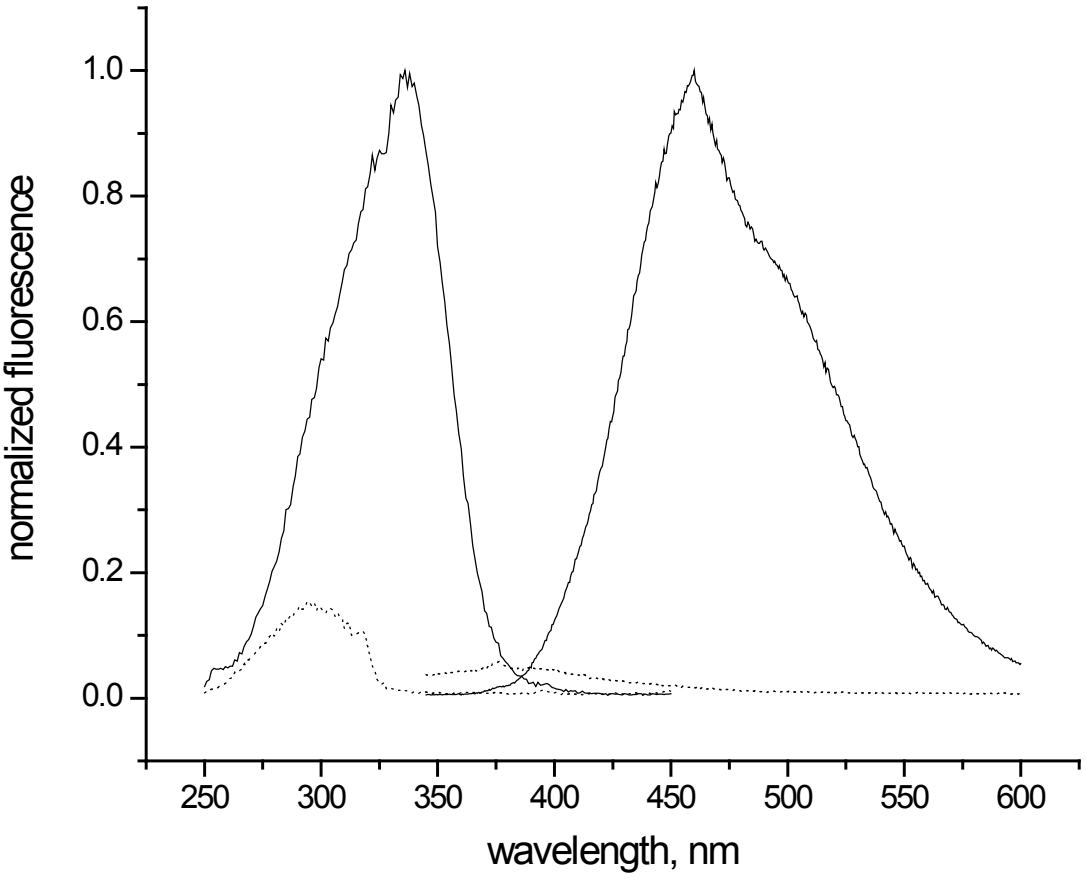

Figure 4.4: Fluorescence excitation and emission spectra for 1-NP (dotted) and 1-naphthol (solid), λ_{ex} = 332 nm and λ_{em} = 460 nm for each.

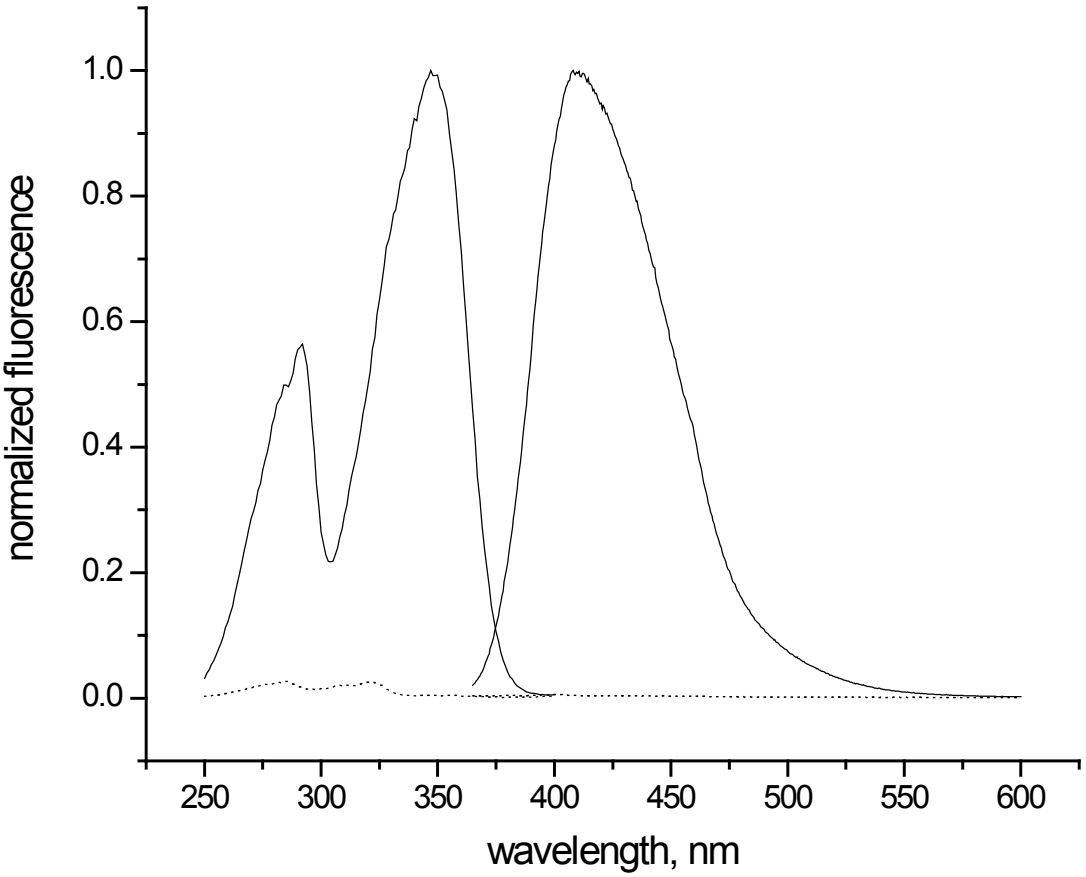

Figure 4.5: Fluorescence excitation and emission spectra for 2-NP (dotted) and 2-naphthol (solid), λ_{ex} = 352 nm and λ_{em} = 408 nm for each.

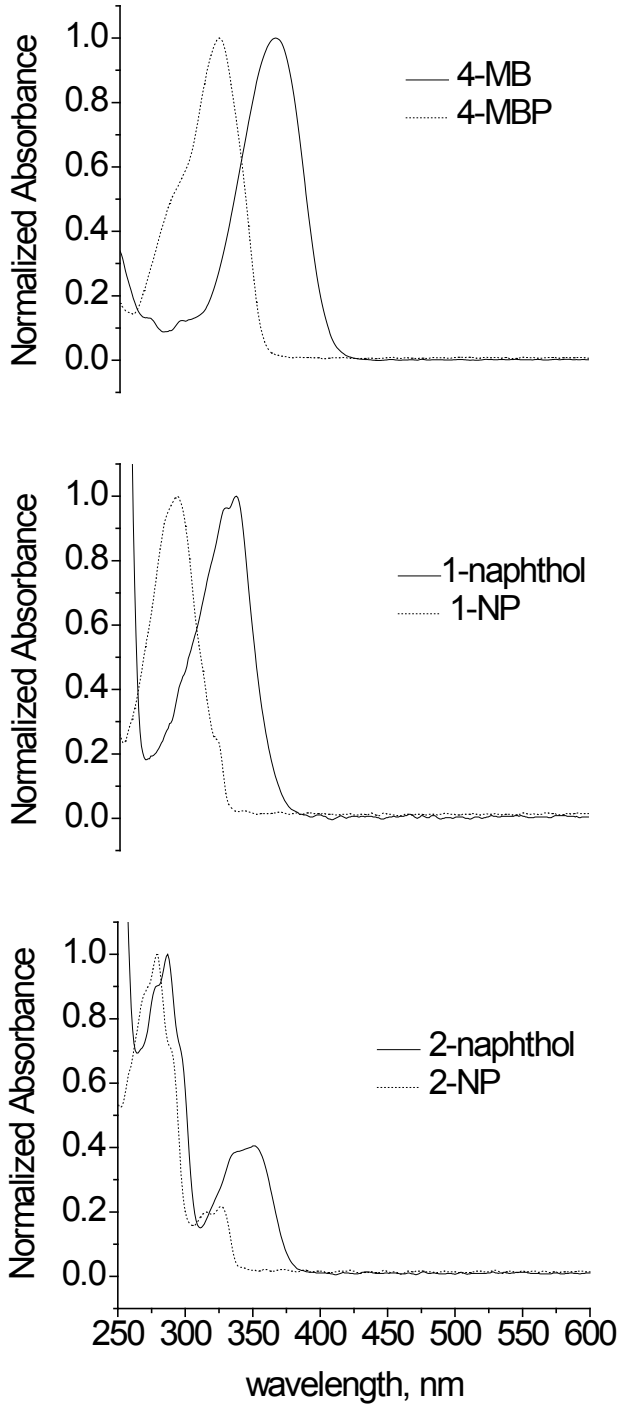

Figure 4.6: Absorbance spectra for 4-MB/4-MBP (top), 1-naphthol/1-NP (middle), and 2-naphthol/2-NP (bottom).

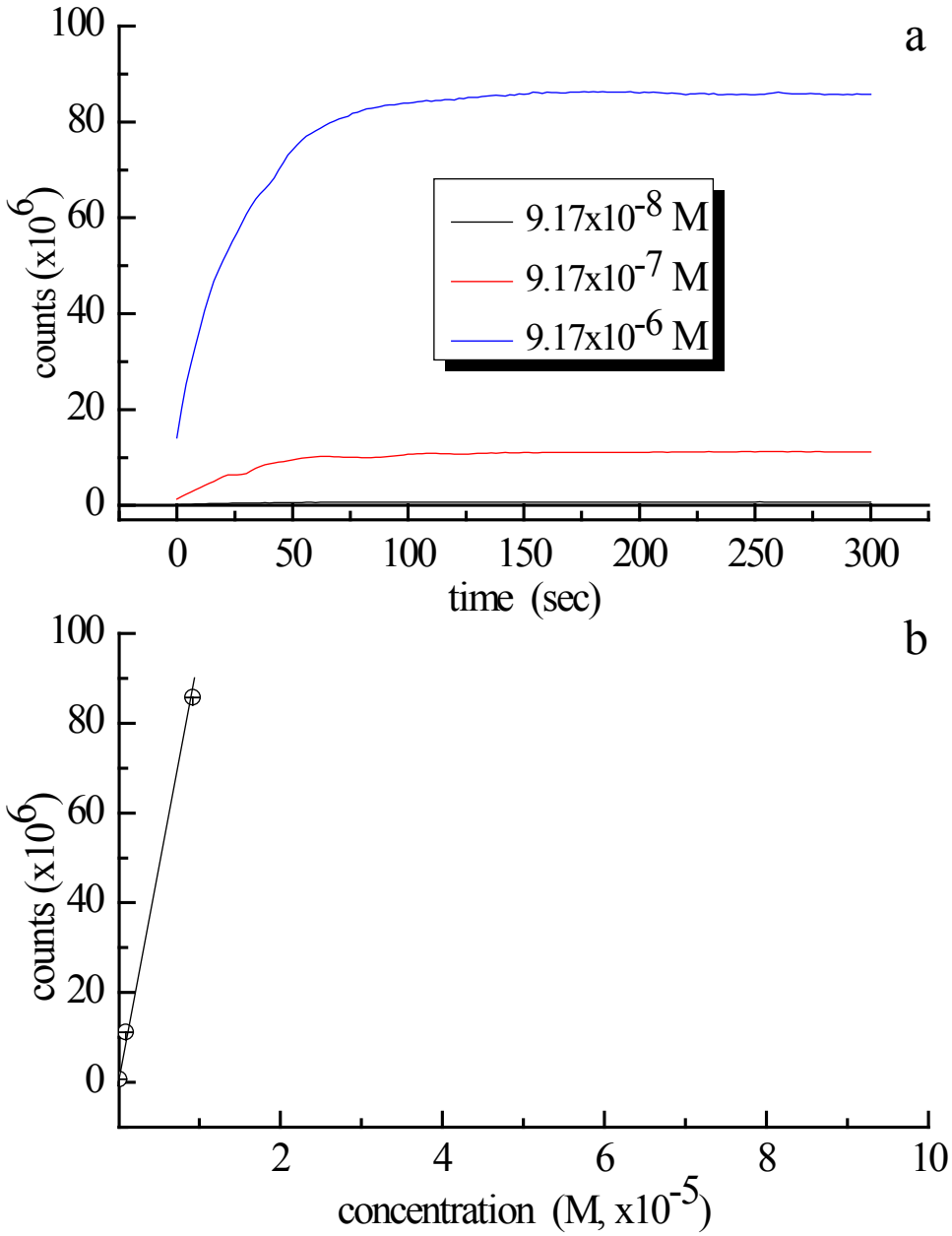

Figure 4.7: (a) Time-dependent fluorescence from the reaction of 4-MBP with ALP at different 4-MBP initial concentrations, as indicated in the legend. [ALP] = 2.08×10^{-7} M. (b) Concentration-dependence of long-time fluorescence intensity from the same reactions.

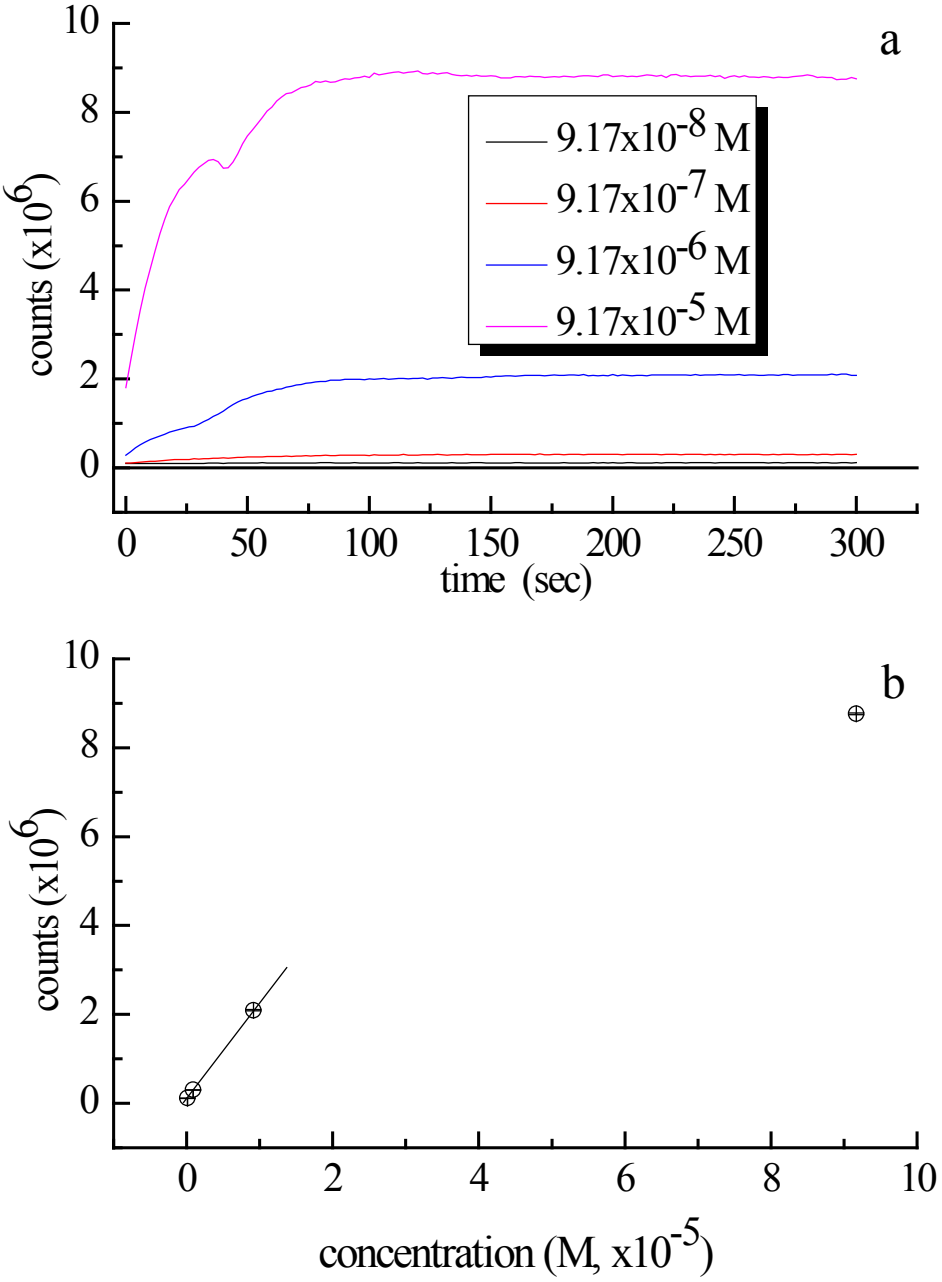

Figure 4.8: (a) Time-dependent fluorescence from the reaction of 1-NP with ALP at different 1-NP initial concentrations, as indicated in the legend. [ALP] = 5.21×10^{-7} M. (b) Concentration-dependence of long-time fluorescence intensity from the same reactions.

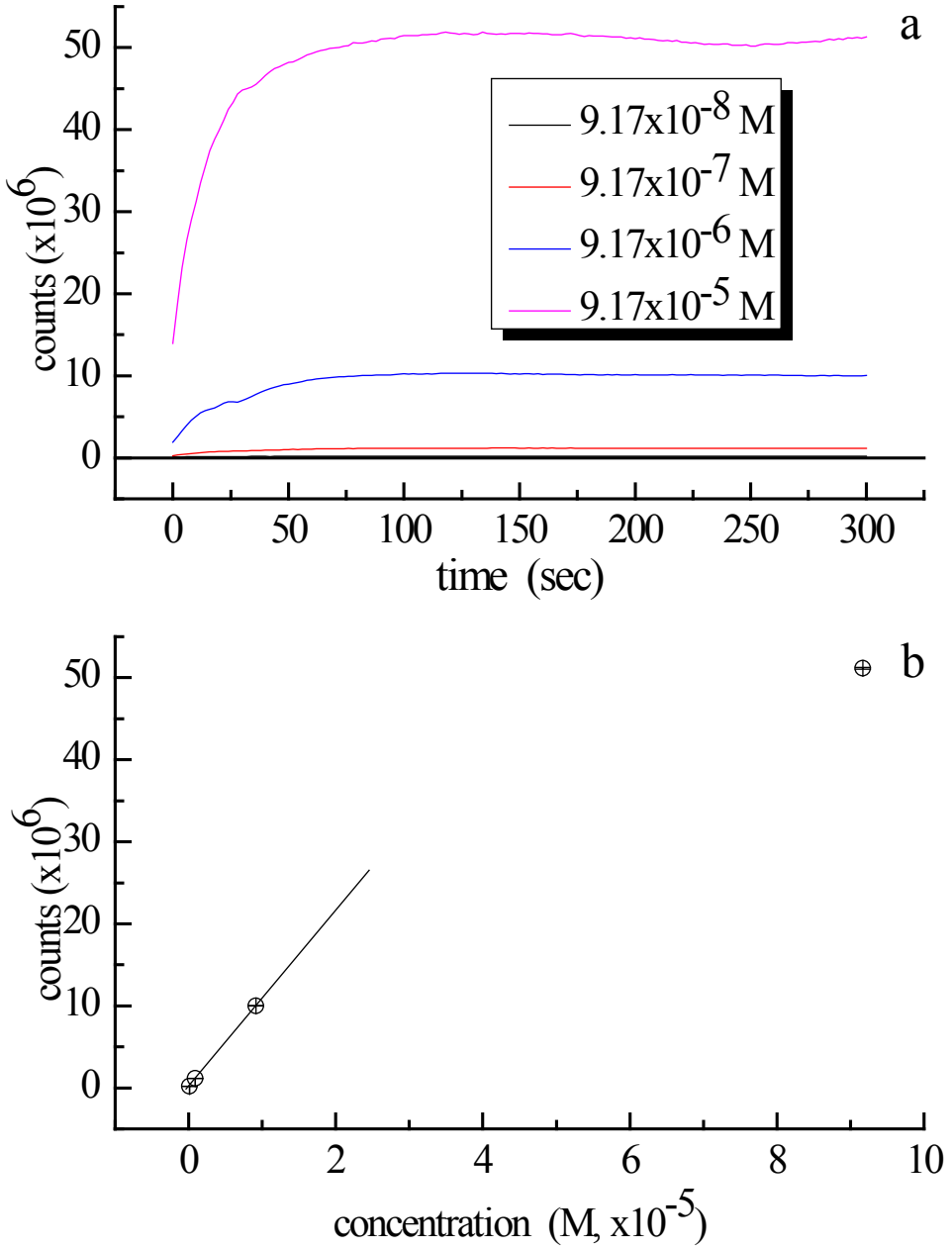

Figure 4.9: (a) Time-dependent fluorescence from the reaction of 2-NP with ALP at different 2-NP initial concentrations, as indicated in the legend. [ALP] = 5.21×10^{-7} M. (b) Concentration-dependence of long-time fluorescence intensity from the same reactions.

The functional form of the kinetic data is sufficiently complex that it is difficult to assign a detailed model for the reaction based on these results. One effective means of evaluating the kinetic information presented in Figs. 4.7-4.9 is to measure the initial rates of reaction. We present these data in Figs. 4.10-4.12. These data show clearly that the kinetics of reaction for 4-MBP with ALP are different than for 1-NP and 2-NP with ALP. For 4-MBP there appears to be a much less pronounced concentration dependent initial rate than is seen for either NP. We are aware that the concentration range over which we report the data for 4-MBP is smaller than it is for either 1-NP or 2-NP and this is for reasons of the fluorescence quantum yield of the reaction produces. With that caveat, at the low range of the concentrations we have studied, it appears that the initial rate for 4-MBP reaction with ALP is close to concentration-independent (Fig. 4.10). For 1-NP (Fig. 4.11) and 2-NP (Fig. 4.12) there is a much more pronounced concentration-dependence to the initial rates and for these two compounds the initial rates are similar for a given concentration. This finding suggests that the location of the phosphate functionality on the naphthyl phosphates is of secondary importance relative to the size of the substrate. We view this finding as somewhat surprising in light of the influence of the naphthyl substitution on the absorbance spectra (Fig. 4.6). The difference in spectral response for these two substrates is consistent with a different electron density distribution in their π and π^* states, yet the dephosphorylation reaction does not seem to be affected to a great extent. It is perhaps because the reaction involves the cleavage of σ-bond(s) and the π-electrons are not involved directly in the reaction.

It is also instructive to consider that the initial rates of reaction for 1-NP and 2-NP appear to exhibit an onset of saturation at higher substrate concentrations. Given that the upper concentration range of the substrate is less than 10^{-4} M and that there is no spectroscopic

evidence for aggregate formation, it appears that the presence of sufficient reaction product (1- and 2- naphthol) could serve to occupy the reactive site of ALP and thus diminish the achievable rate of reaction for this system.

It is clear from our solution phase data that the reaction of these substrates with ALP is facile and that the detection methodology we use is sufficiently sensitive for the purpose. It is also important to note that, based on the initial rate data (Figs. 4.10-4.12) that the kinetics of reaction for 4-MBP are different from those of the naphthyl phosphates. We believe that the reason for this difference lies in the structural differences of the substrates, although the extent to which structural issues influence the reaction kinetics is limited, as seen in the similarity of the initial rate data for 1-NP and 2-NP. With this information in hand, we examine next these same reactions where ALP is bound to inverse opal and planar silica support structures.

Surface-bound enzyme reactivity: One of the central issues of this work is the catalytic efficiency of surface-bound ALP relative to solution phase ALP. As noted above, the binding of an enzyme to a surface is likely to alter the reactivity of the enzyme but it is not clear, *a priori*, whether the reactivity will be increased or decreased upon attachment to a surface. In our previous work (Chapter 3) we observed enhanced catalytic activity for surface bound GOx relative to solution phase GOx, and there was a further reactivity dependence on the structure of the support matrix. In this work, as is described below, we find that the reactivity of ALP is reduced when it is bound to a surface, but the dependence of enzyme reactivity on the structure of the support matrix is similar to what was observed for GOx. These data, taken collectively, serve to provide a useful limit on the range of applicability of surface-binding of enzymes using glutaraldehyde linking chemistry.

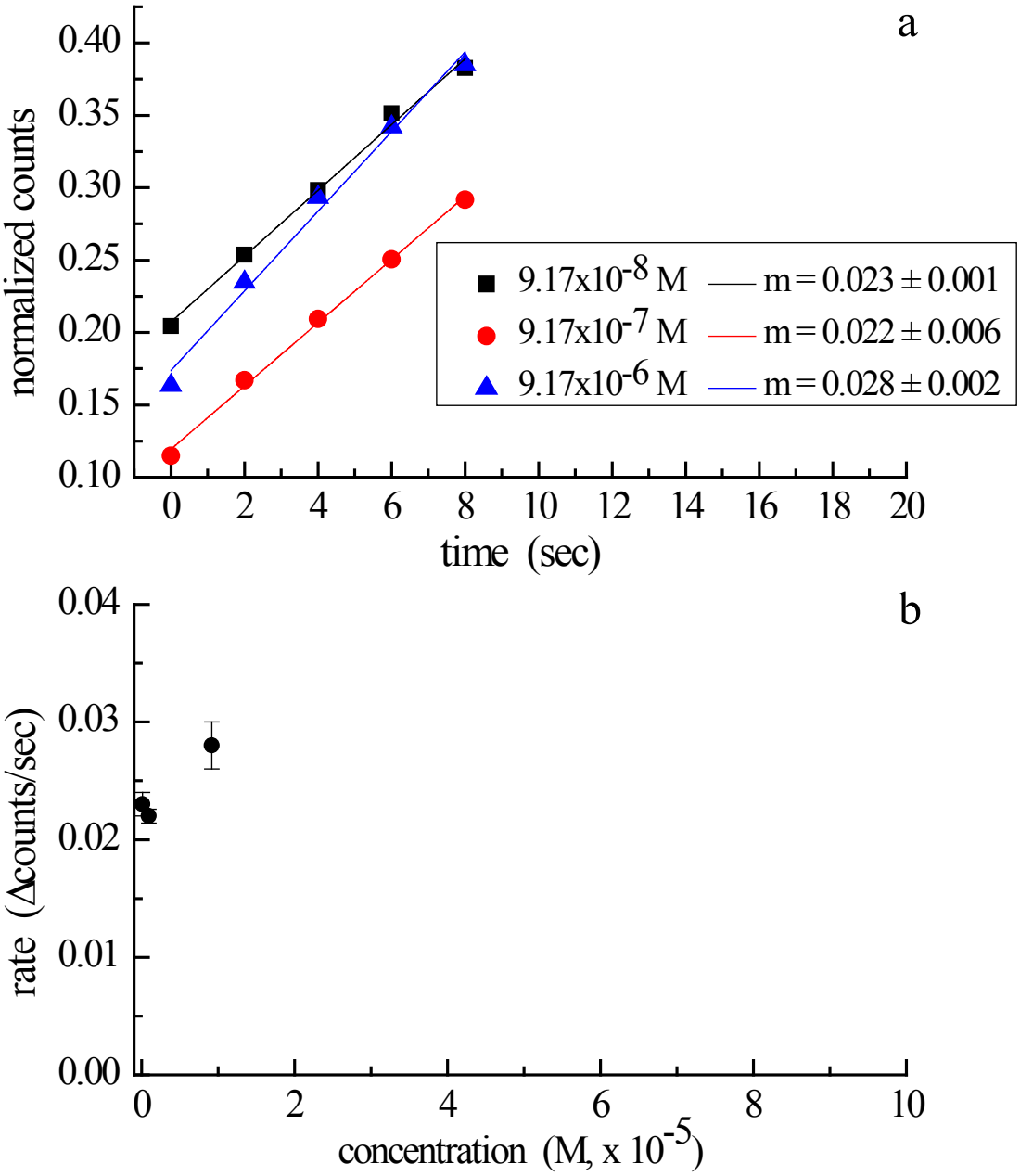

Figure 4.10: (a) Initial rate data for the reaction of 4-MBP with ALP at different 4-MBP initial concentrations, as indicated in the legend. [ALP] = 2.08×10^{-7} M. (b) Concentration-dependence of the initial rate data for the same reactions.

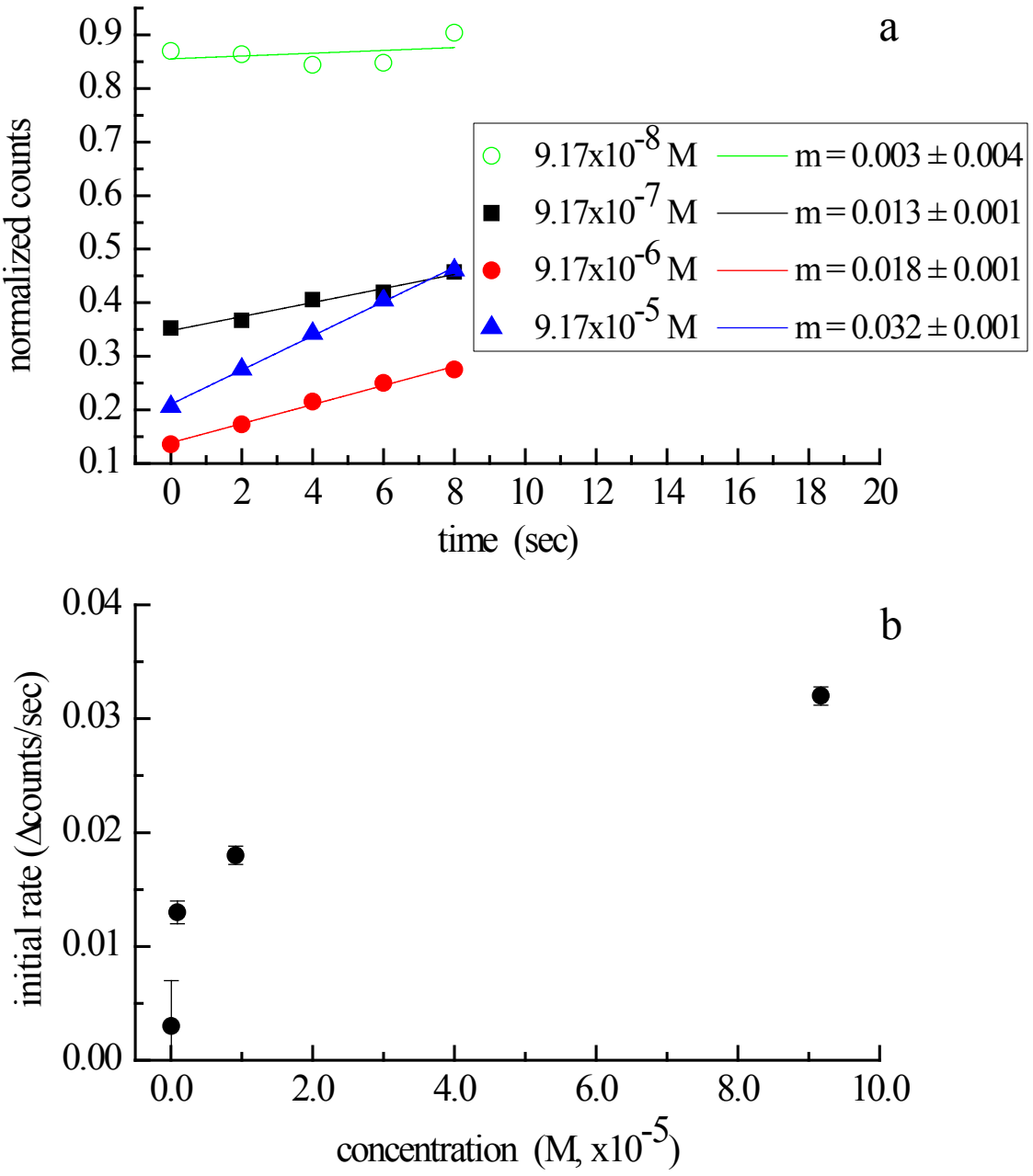

Figure 4.11: (a) Initial rate data for the reaction of 1-NP with ALP at different 1-NP initial concentrations, as indicated in the legend. [ALP] = 5.21×10^{-7} M. (b) Concentration-dependence of the initial rate data for the same reactions.

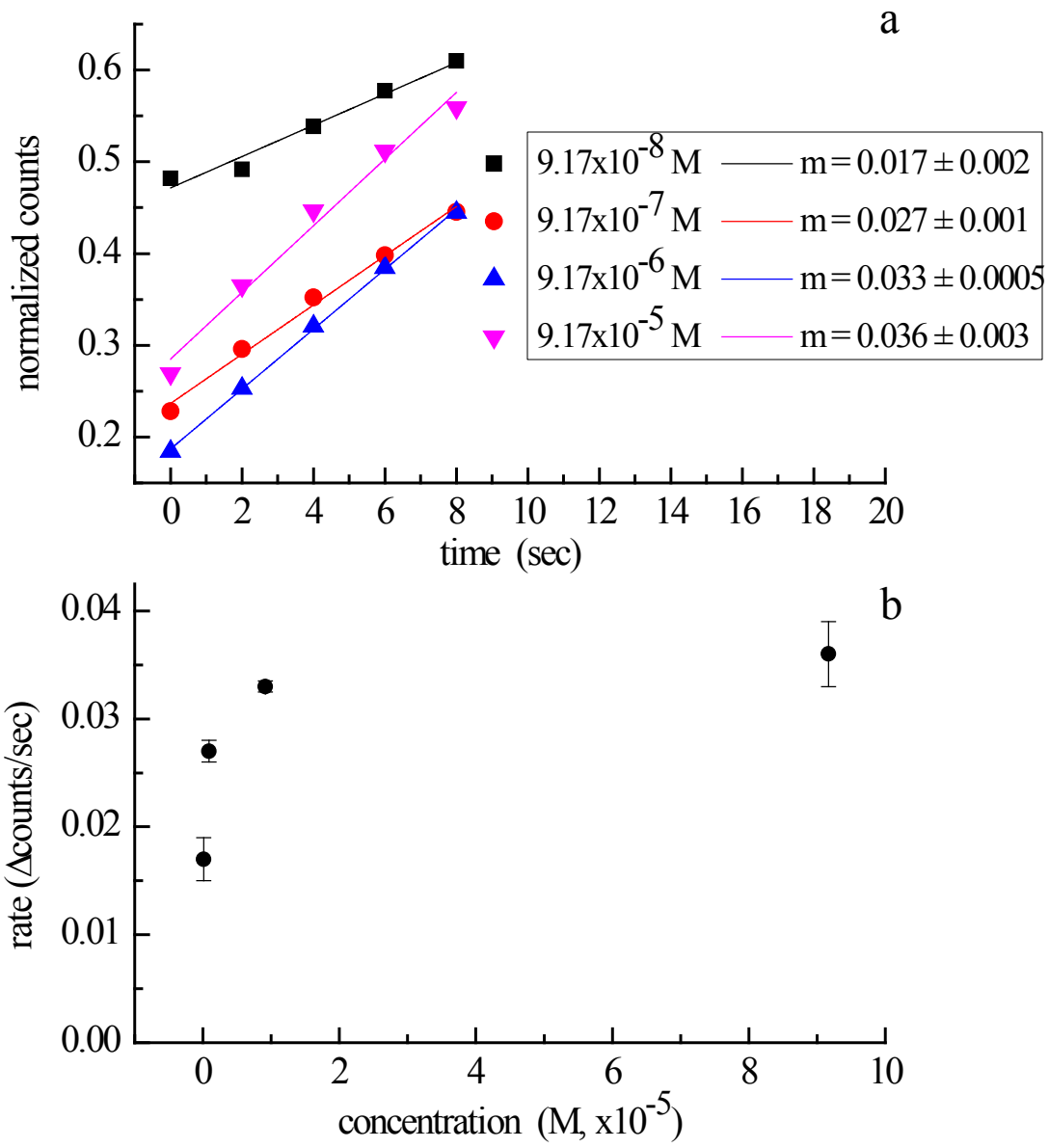

Figure 4.12: (a) Initial rate data for the reaction of 2-NP with ALP at different 2-NP initial concentrations, as indicated in the legend. [ALP] = 5.21×10^{-7} M. (b) Concentration-dependence of the initial rate data for the same reactions.

A schematic of the nanoporous solid/porous alumina support (NS/PAS) structure used here is shown in Fig. 4.13. The details of constructing this interface have been presented in Chapter 2 of this dissertation. ALP was bound to the NS using a glutaraldehyde linking reaction (Fig. 4.1) and a key issue for such systems is characterizing the loading density achieved with this process. We have chosen to use silica as a support material because of its surface functionality and consequent ease of surface-binding chemistry. Another key aspect in our choice of silica as a support matrix is its comparative inertness relative to a variety of metals (*e.g.* Au, Pt, Pd) and some oxides (*e.g.* Al_2O_3), which have been shown to denature other enzymes.[12] A critical limitation to the use of silica, however, lies in the ability to quantitate the amount of enzyme present on the surface. Because of the insulating nature of silica, electrochemical characterization is not possible and the inverse opal structure precludes quantitative spectroscopic measurements because of their diffractive properties at optical wavelengths. We have used thermogravimetric analysis previously (TGA) to quantitate the amount of GOx present on silica inverse opal structures, and we determined that the surface chemistry we used produced a coverage of *ca*. 0.77 monolayer. For ALP bound to silica inverse opals, however, we have not been able to acquire reliable TGA data. We believe that the reason for this limitation lies with the buffer system used, which contains diethanolamine. The DEA in the buffer produces residue upon heating, resulting in a mass loss well in excess of that achievable even with full monolayer coverage of ALP. Based on the surface binding chemistry we use, one monolayer of enzyme is the maximum coverage achievable and the geometric properties of the inverse opal structure allow for accurate calculation of surface area. For these reasons, we have estimated the surface coverage of ALP to be the same as that which we achieved for GOx. The number of ALP molecules on the surface was calculated using a radius

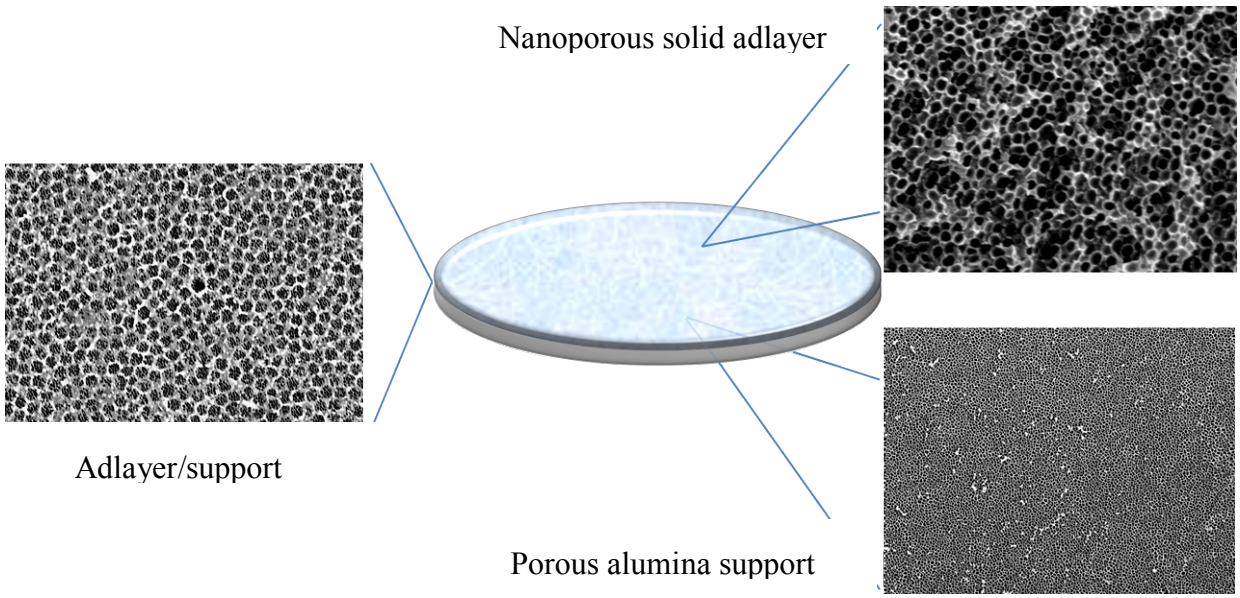

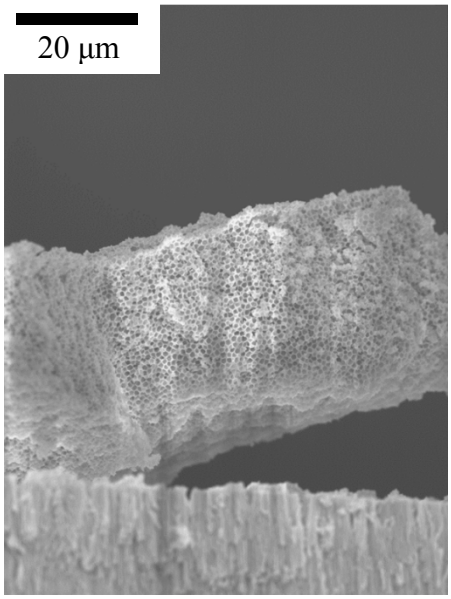

Figure 4.13: Overview of the construction of the NS/PAS supports used for ALP immobilization (top) and a cross-section SEM image of the NS/PAS interface (bottom).

of 7.7 nm which has been reported in the literature.[24] We recognize that this situation is far from ideal but, based on the observed reactivities for these systems, any reasonable deviation from the estimated surface coverage will not have a significant effect on the larger lessons learned from this work. In other words, even if our estimate of surface coverage is substantially too high, it will not alter the fact that the reactivity of bound ALP is much less than that of solution phase ALP.

In contrast to the solution phase measurements, studies of ALP bound to a silica nanoporous solid were performed under flowing conditions at a flow rate of 50 μL/min. We have performed flow-based experiments on both NS/PAS and PAS structures, where the latter porous alumina structure was reacted with ALP and the same glutaraldehyde linking chemistry used for binding of the enzyme to the nanoporous solid silica support. Our motivation for performing this latter study was to determine whether or not the enzyme activity was influenced by exposure to the alumina surface. As noted above, GOx was found to denature when exposed to the porous alumina support surface. We present these data in tabular form (Table 4.1).

The data presented in Table 4.1 provide a direct comparison of the reactivity of ALP toward the three substrates in four different structural formats, three with the enzyme surface-bound and the fourth in the solution phase. Because of the different structural formats, there are a number of specific points that needed to be addressed in order to make these different bodies of data comparable. For the solution phase measurements, as discussed above, the turnover rates were determined from the initial rate data, the detection sensitivity for each substrate (number of fluorescence counts per unit solution concentration) and the concentration of the enzyme. For our instrument, the sensitivity for 4-methylumbelliferone is 1.44×10^{13} counts/M, for 1-naphthol 4.91×10^{11} counts/M and for 2-naphthol 1.46×10^{11} counts/M (Table 4.1, Fig. 4.14). These

Table 4.1. Comparison of different substrates for various reaction formats. (Uncertainties are ±1σ)

	Substrate	[substrate] (M)	Rate (M/s)	[ALP] (M)	TO/sec
Solution Phase	4-MBP[a]	9.17×10^{-6}	6.00×10^{-6}	2.08×10^{-7}	28.8±8.9
	1-NP	9.17×10^{-6}	1.06×10^{-6}	5.21×10^{-7}	2.04±0.03
	2-NP	9.17×10^{-6}	9.35×10^{-6}	5.21×10^{-7}	17.9±3.3

	Substrate	[substrate] (M)	Initial slope (cts/s)	Calib. (cts/M)	Rate (M/s)	[ALP][b]	TO/sec
Planar	4-MBP	9.17×10^{-5}	6349	$(1.44\pm0.08)\times10^{13}$	4.41×10^{-10}	5.40×10^{-7}	$(8.16\pm4.62)\times10^{-4}$
	1-NP	9.17×10^{-5}	248	$(4.91\pm0.28)\times10^{11}$	5.05×10^{-10}	5.40×10^{-7}	$(9.35\pm5.46)\times10^{-4}$
	2-NP	9.17×10^{-5}	179	$(1.46\pm0.13)\times10^{11}$	1.23×10^{-9}	5.40×10^{-7}	$(2.27\pm0.56)\times10^{-3}$

	Substrate	[substrate] (M)	Rate (mol/s)[c]	ALP (mol)	TO/sec
PAS	4-MBP	6.52×10^{-5}	5.43×10^{-11}	2.82×10^{-9}	$(1.93\pm0.45)\times10^{-2}$
	1-NP	2.10×10^{-5}	1.75×10^{-11}	2.82×10^{-9}	$(6.02\pm1.33)\times10^{-3}$
	2-NP	5.26×10^{-5}	4.39×10^{-11}	2.82×10^{-9}	$(1.55\pm0.16)\times10^{-2}$

Table 4.1 (cont'd)

	Substrate	[substrate] (M)	Rate (mol/s)[b]	ALP (mol)	TO/sec
NS/PAS	4-MBP	3.94×10^{-5}	3.29×10^{-11}	3.04×10^{-9}	$(1.08\pm0.32)\times10^{-2}$
	1-NP	5.37×10^{-5}	4.47×10^{-11}	3.04×10^{-9}	$(1.47\pm0.03)\times10^{-2}$
	2-NP	7.04×10^{-5}	5.86×10^{-11}	3.04×10^{-9}	$(1.93\pm0.06)\times10^{-2}$

[a] N=2 for 4-MBP solution phase, N=3 for all other measurements.

[b] Determined by the number of moles of ALP bound to the silica surface and the volume of the system determined by the diffusion length (depth) and the geometric area of the surface.

[c] Rate calculated using the calibration factors given for the planar surface data and the flow rate of 50 μL/min.

sensitivity factors could, in principle, be calculated from the extinction coefficient and fluorescence quantum yields of the chromophores at the wavelengths of excitation and emission, and the throughput and gain factors for the fluorescence spectrometer, but none of these quantities are known reliably. Rather than use estimates, we determined these calibration factors experimentally (Fig. 4.14). With these data we determine the turnover rates for the substrate/ALP reactions, and show these data in Table 4.1.

Determining the turnover rate for the enzyme bound to the planar surface is accomplished by measuring the count rate for production of the product (Fig. 4.15) and converting that count rate to a concentration with the sensitivity factors given in Table 4.1 (*vide infra*). Determining the amount of enzyme present and the relevant volume of the reactive system involves two assumptions. Because the concentration of surface-bound ALP is not directly measurable, we estimate the surface loading to be 0.77 monolayer, as discussed above based on the surface chemistry used to attach the enzyme. The central issue in this determination is the relevant volume in which the reaction occurs. Because we operate under non-stirred conditions for these measurements, diffusion is, at best, the limiting factor in delivery of substrate to the enzyme. We thus assume the relevant distance from the enzyme-coated surface is the diffusion length, $l = 2(Dt)^{1/2}$. Taking $D = 10^{-5}$ cm^2/s, for t = 1 s, $l = 6.32 \times 10^{-3}$ cm. Under these assumptions we estimate the turn-over rates for the substrates used here at a planar ALP-covered silica surface. We note that, of all the experimental formats, the determinations for ALP bound to a planar silica surface is associated with the largest number of approximations and is thus characterized by the greatest uncertainty.

Quantitation of the turnover rates for the three substrates at the NS/PAS and PAS structures involves the measurement of product under flow-through conditions at a flowrate of

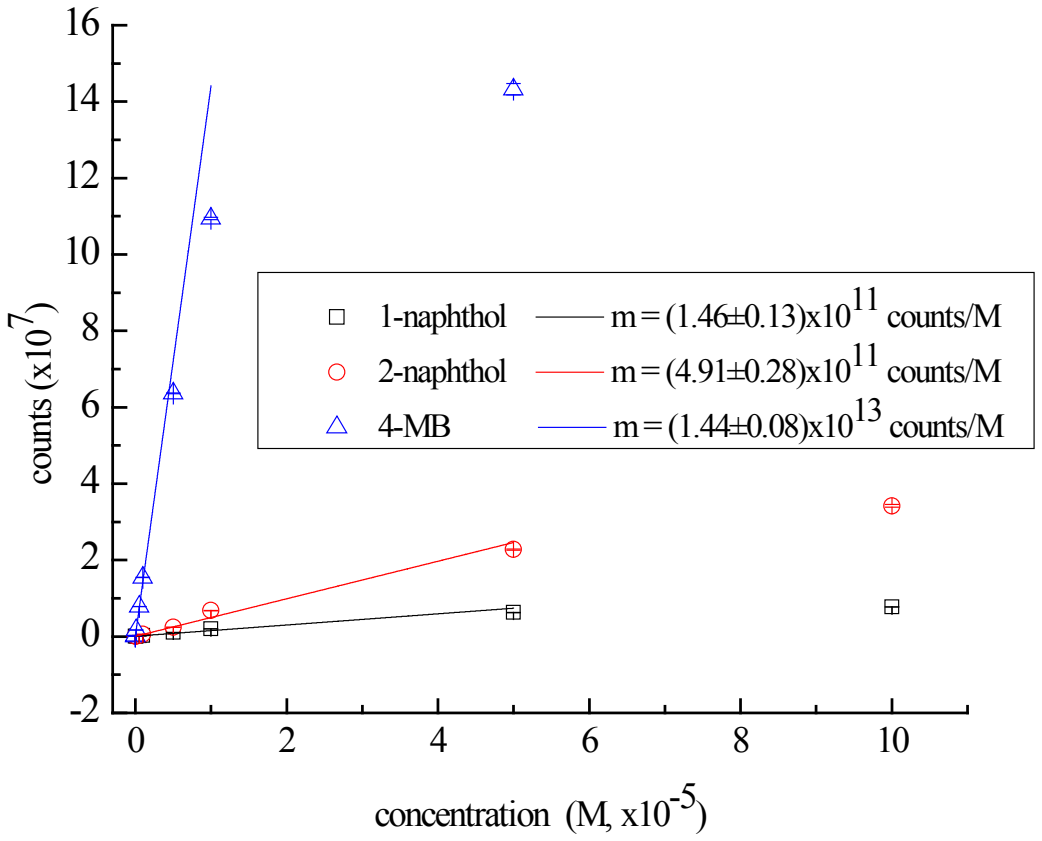

Figure 4.14: Calibration data for the reaction products used in this work. Slopes are the sensitivity factors for our system, given in counts/M and are best fits of data points contained in the linear range for each reaction product.

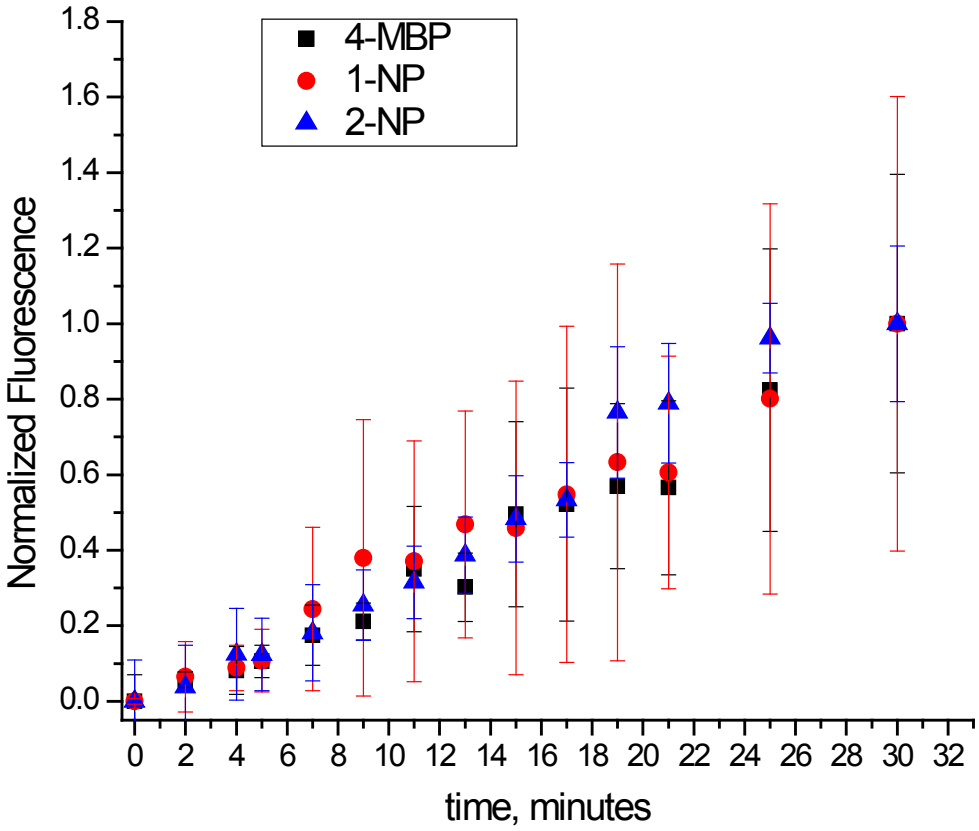

Figure 4.15: Time-dependent fluorescence data for ALP immobilized on planar silica for each of the three different substrates. The concentration of the substrate was 9.17×10^{-6} M for all cases.

50 μL/min in all cases. We determine the turnover rates for these experimental configurations based on the flowrate and the amount of product formed, assuming a surface coverage of 0.77 monolayer (*vide infra*). Because we use the same surface coverage for all of our surface-bound ALP data interpretation, the absolute turnover rates may be consistently biased by a small amount but comparison between the surface-bound experimental formats is valid.

Our turnover rate data are presented in Table 4.1 and are summarized in normalized form in Table 4.2. A number of important points emerge from these data. The first is that when comparing the reactivity of the different substrates for solution phase measurements we find that there is a noticeable structure-dependence on turnover rate. The turnover rate for 4-MBP and 2-NP differ by a factor of two and both are approximately an order of magnitude larger than that for 1-NP. Given the locations of the phosphate groups on these substrates, it is tempting to speculate that the shape of the binding pockets are such that 2-NP and the phosphate-containing ring of 4-MBP fit the ALP binding pockets better than 1-NP does. This result is interesting in light of the kinetic initial rate data (Figs. 4.10-4.12) which give similar concentration-dependencies for the two naphthyl derivatives and a distinctly different concentration-dependence for 4-MBP. The TO rate data thus are related to steric factors while the kinetic data are reflective of mechanistic differences between different classes of substrates. The fact that the 4-MBP and 1-NP TO rate results are so similar suggests that the rate-limiting factor, at least in the concentration range we have examined, is determined to some extent by delivery of the substrate to the enzyme. For the concentration of substrate and enzyme used, we estimate for 4-MBP and ALP that there should be on the order of 500 collisions between the two compounds per second, and the measured TO rate is *ca*. 5% of the collision rate. For 1-NP and 2-NP we estimate there to be *ca*. 700 collisions with ALP per second, and the TO rates for these two

Table 4.2. Relative turnover rates for the substrates and ALP in different formats. The turnover rates are normalized to a solution phase rate of 28.8/s for 4-MBP.

	Solution	**PAS**	**NS/PAS**	**Planar**
4-MBP	1	6.7×10^{-4}	3.8×10^{-4}	2.8×10^{-5}
1-NP	0.069	2.2×10^{-4}	5.1×10^{-4}	3.3×10^{-5}
2-NP	0.63	5.4×10^{-4}	6.7×10^{-4}	7.9×10^{-5}

substrates is *ca*. 0.3% and 2.6% of the collision rate, respectively. The issue that we cannot address is the probability of a reactive interaction taking place between the substrate and ALP based on geometric factors alone.

Comparison of the TO rates for surface-bound ALP to solution phase ALP for the substrates we have studied shows that the binding of the enzyme to a silica surface using glutaraldehyde binding chemistry results in a substantial loss of reactivity. This loss of reactivity could be associated either with the binding of the enzyme in such a way that access to the reactive site is blocked or with the enzyme being locked into a conformation that is less reactive than the solution phase conformation. If the latter explanation were operative, we would expect there to be a substantial difference in the reactivity of ALP when bound to silica and alumina and we find this not to be the case. The findings for ALP stand in contrast to those for GOx in this regard.[12] Further investigations using different enzyme binding chemistry may be able to provide more insight into this issue.

Despite the fact that the surface-binding of ALP reduces its reactivity relative to what it is in the solution phase, the issue of reactivity enhancement associated with nanoconfinement can still be evaluated for this system. As was discussed in Chapter 1, flowing substrate solution through a structure with features that have a characteristic length scale shorter than the diffusion length of the substrate gives rise to more opportunity for interaction between substrate and enzyme than if the enzyme were attached to a planar surface. The enhanced frequency of interactions leads to higher reactivity and thus the apparent enhancement. Comparing our data for the nanoporous structure(s) to that for the planar silica surface shows the enhancement effect expected on geometric grounds. This finding, while not surprising, provides further proof of the geometric enhancement in catalytic activity observed for nanoporous structures. We anticipate

that the enhancement could be increased with a decrease in the diameter of the characteristic void space in our nanoporous structures, but this enhancement would occur at the expense of the flow rate achievable and thus the throughput of the system. The optimum balance between reactivity enhancement and throughput depends on the kinetics of the enzyme used and is expected to be different for each enzyme-substrate pair. We have not attempted to identify this optimum operating point for either ALP or GOx and, in light of our findings for surface binding of ALP, finding the optimum for that system would serve no practical purpose.

Conclusions

We have reported on the reactivity of the enzyme alkaline phosphatase (ALP) with substrates 1-naphthyl phosphate, 2-naphthyl phosphate and 4-methylumbelliferyl phosphate, in solution and with the enzyme bound to planar and nanoporous silica structures. Our data demonstrate that both the mechanism and the rate of reactivity depend on the chemical identity of the substrate. Comparison of the solution phase data to that for surface bound enzyme demonstrates a substantial loss of reactivity upon surface attachment. There are two possible causes for this loss of reactivity; blocking of the enzyme reactive site by virtue of the way in which it is bound to the support structure, and loss of reactivity due to locking the enzyme into a less reactive conformation upon binding. The fact that the TO rate for ALP is the same for alumina and silica surfaces suggests that the former explanation is operative. Despite the loss of reactivity upon surface binding, we observe the geometrically-derived enzyme reactivity enhancement associated with nanoscale confinement. Our data, taken collectively, serve to underscore the importance of enzyme surface binding chemistry and geometric factors in achieving enhanced reactivity.

Literature Cited

Literature Cited

1. Díaz, J. F.; Balkus Jr, K. J. *Journal of Molecular Catalysis B: Enzymatic* **1996**, *2*, 115.

2. Yan, A.-X.; Li, X.-W.; Ye, Y.-H. *Applied Biochemistry and Biotechnology* **2002**, *101*, 113.

3. Borole, A.; Dai, S.; Cheng, C.; Rodriguez, M.; Davison, B. *Applied Biochemistry and Biotechnology* **2004**, *113*, 273.

4. Lei, C.; Soares, T. A.; Shin, Y.; Liu, J.; Ackerman, E. J. *Nanotechnology* **2008**, *19*, 1.

5. Lei, C.; Shin, Y.; Liu, J.; Ackerman, E. J. *Journal of the American Chemical Society* **2002**, *124*, 11242.

6. Kim, M. I.; Ham, H. O.; Oh, S.-D.; Park, H. G.; Chang, H. N.; Choi, S.-H. *Journal of Molecular Catalysis B: Enzymatic* **2006**, *39*, 62.

7. Wang, Y.; Caruso, F. *Chemical Communications* **2004**, 1528.

8. Kim, J.; Jia, H.; Lee, C.-w.; Chung, S.-w.; Kwak, J. H.; Shin, Y.; Dohnalkova, A.; Kim, B.-G.; Wang, P.; Grate, J. W. *Enzyme and Microbial Technology* **2006**, *39*, 474.

9. Minton, A. P. *Journal of Biological Chemistry* **2001**, *276*, 10577.

10. Zhou, H.-X.; Dill, K. A. *Biochemistry* **2001**, *40*, 11289.

11. Zhu, Y.; Cao, H.; Tang, L.; Yang, X.; Li, C. *Electrochimica Acta* **2009**, *54*, 2823.

12. Gornowich, D. B.; Blanchard, G. J. *The Journal of Physical Chemistry C* **2012**, *116*, 12165.

13. Walcarius, A.; Kuhn, A. *TrAC Trends in Analytical Chemistry* **2008**, *27*, 593.

14. Szamocki, R.; Velichko, A.; Mücklich, F.; Reculusa, S.; Ravaine, S.; Neugebauer, S.; Schuhmann, W.; Hempelmann, R.; Kuhn, A. *Electrochemistry Communications* **2007**, *9*, 2121.

15. Bon Saint Côme, Y.; Lalo, H.; Wang, Z.; Etienne, M.; Gajdzik, J.; Kohring, G.-W.; Walcarius, A.; Hempelmann, R.; Kuhn, A. *Langmuir* **2011**, *27*, 12737.

16. Wang, Z.; Etienne, M.; Kohring, G.-W.; Bon-Saint-Côme, Y.; Kuhn, A.; Walcarius, A. *Electrochimica Acta* **2011**, *56*, 9032.

17. Qu, F.; Nasraoui, R.; Etienne, M.; Côme, Y. B. S.; Kuhn, A.; Lenz, J.; Gajdzik, J.; Hempelmann, R.; Walcarius, A. *Electrochemistry Communications* **2011**, *13*, 138.

18. Kleppe, K. *Biochemistry* **1966**, *5*, 139.

19. Krishnaswamy, S.; Kittrell, J. R. *Biotechnology and Bioengineering* **1978**, *20*, 821.

20. Fosset, M.; Chappelet-Tordo, D.; Lazdunski, M. *Biochemistry* **1974**, *13*, 1783.

21. Subramanian, A.; Kennel, S. J.; Oden, P. I.; Jacobson, K. B.; Woodward, J.; Doktycz, M. J. *Enzyme and Microbial Technology* **1999**, *24*, 26.

22. Ehlert, N.; Müller, P. P.; Stieve, M.; Behrens, P. *Microporous and Mesoporous Materials* **2010**, *131*, 51.

23. Surinenaite, B.; Bendikiene, V.; Juodka, B. *Prog. Biotechnol.* **1998**, *15*, 577.

24. Ey, P. L.; Ferber, E. *Biochimica et Biophysica Acta (BBA) - Enzymology* **1977**, *480*, 403.

CHAPTER 5: Conclusions

Summary

Enzymes play an important role in many processes that span a multitude of different industries including food, beverage, drug discovery, chemical manufacturing, and biofuels. In 2010, the global market for industrial enzymes was estimated to be worth $3.3 billion.[1] Consequently, a great deal of research is aimed at optimizing various parameters for maximum enzyme efficiency (kg product/kg enzyme).[2,3] Immobilization of enzymes continues to be an area of focus because immobilizing the enzyme has several advantages, including increased enzyme stability,[4,5] the relative ease with which the enzyme can be recovered and reused, and in some cases enhancement in reactivity.[6-8] The goal of this project was to evaluate the utility of the inverse opal structure function as a flow-through catalyst support. To this end, an inverse opal structural format was designed and utilized as a support for immobilized enzymes that could be used in a flow-through mode. Chapter 2 outlined the procedure involved in creating a flow-through inverse opal matrix, and Chapters 3 and 4 provided experimental results on two different enzymes that were chosen to characterize this approach to catalyst immobilization and reaction. These results provide a useful initial point in evaluating the utility of inverse opal structures as enzyme supports, but there are limitations to this approach based on the enzyme used and the manner in which it is bound to the inverse opal structure.

Inverse opal structures have been created using a wide range of different materials, most commonly metals and inorganic oxides.[8-27] The moderately high surface area provided by these materials allows for a correspondingly high enzyme loading density. Most inverse opal structures are created on planar support structures, which don't allow for a facile flow-through

experimental configuration. For biocatalysis applications using a non-flow through format, the delivery of substrate to the enzyme is limited by diffusion, thereby not taking advantage of the full surface area provided by the multi-layer NS structure. The flow-through NS system that was described in Chapter 2 overcomes this limitation and allows for a reactant stream to be flowed through the matrix. Consequently, the number of substrate-enzyme interactions is increased, which can lead to an enhancement in enzyme reactivity.[8] However, the chemistry used to attach the enzyme to the support structure must leave the enzyme in an active form with the binding pocket readily accessible, or the activity may be diminished.[23]

Glucose oxidase (GOx) and alkaline phosphatase (ALP) were chosen as model enzymes to investigate whether or not an enhancement in activity could be observed for our flow-through inverse opal structure. The two enzymes are similar in size; however GOx has only one specific target substrate (β-D-glucose), while ALP dephosphorylates a wide range of phosphate monoesters. The results for GOx showed an enhancement in reactivity for the enzyme immobilized on a planar support relative to its reactivity in solution. This finding indicated an enhancement in reactivity due to the enzyme immobilization. The data also revealed an enhancement in reactivity for GOx immobilized on the NS structure relative to the reactivity of the enzyme on the planar support. These data demonstrated an enhancement due to the nanoconfinement of the enzyme within the NS matrix.[8] The concentration of oxygen at the support surface may have also contributed to the enhancement in turnover rate, however oxygen studies were not performed. Results for ALP, however, showed different behavior. The solution phase reactivity of ALP was higher than when it was used in immobilized reaction formats. While there was still an enhancement observed for the enzyme within the NS structure relative to

its reactivity when bound to a planar structure, the data illustrated the limitations involved with the immobilization process.[23]

There are a couple of limitations that are important to point out. The methods used for the immobilization process can determine the reactivity of the enzyme based on which functionalities are used in the covalent linkage between the enzyme and the support. As a result, each enzyme behaves differently for a given immobilization technique, making it challenging to determine the optimum immobilization chemistry for a given enzyme/support system. Another important issue is the quantitation of enzyme loading on the silica inverse opals. Thermo-gravimetric measurements were used for this work; however the ALP loadings were not able to be determined due to large mass losses associated with the buffer system. The incorporation of metals either within the dielectric matrix or the fabrication of a flow-through inverse opal using a conductive material will prove beneficial for the quantitation of the enzyme loading. A conductive NS matrix would allow electrochemical methods to be used for surface coverage evaluation.

Future Directions

While this work has illustrated the utility of NS structures as supports for enzyme immobilization, there is still work to be done. With an enhancement observed for an enzyme supported on an inverse opal structure, it is important to optimize the flow-through NS system to maximize the enzyme efficiency. The diffusion length vs. void size model indicates that as the diameter decreases, the number of substrate-enzyme interactions per unit time will increase. A relationship between pore size and flow rate would be useful to evaluate so that an enzyme could have an optimized set of parameters to maximize the reactivity. The optimized inverse opal structural parameters differ for each enzyme/substrate system and is also expected to depend on

the enzyme-attachment chemistry used. Thus it will also be useful to compare several immobilization reactions that will bind the enzyme to the support using different functionalities present on the outer "surface" of the enzyme. As mentioned previously, each enzyme may exhibit different levels of reactivity based on how the enzyme is immobilized. Other immobilization techniques have been investigated in the literature for planar supports,[28] and it would be useful to compare these immobilization methodologies for the flow-through NS system.

As noted above, a present limitation is the quantitation of the enzyme loading. The gravimetric analysis is not ideal for this measurement, because the mass losses are low and such measurements are characterized by a high background.[23] Consequently, exploration of alternative inverse opal matrix materials with an emphasis on conductive materials would be an important direction to move in. The use of electrochemistry to provide information on the surface coverage of the enzyme could also allow for additional characterization of how the enzyme is bound to the support, depending on the details of the enzyme electrochemistry. Devising flow-through metal NS structures or incorporating metal nanowires into the inverse opal structure could be useful avenues of investigation. Enzyme stability is another issue that requires evaluation. As discussed in Chapter 1, immobilization of the enzyme can increase its stability, and this issue would have to be characterized more thoroughly if this structural motif is to be considered for practical applications. In the work presented in this dissertation, long term stability was not addressed as most experiments were completed within a one- to two-week time-frame. In the future, the long term stability of enzymes immobilized within the NS structures must be addressed to calculate a measure of kg of product formed per kg of enzyme.

Overall Conclusions

In conclusion, creating a flow-through NS proved to be challenging. Due to the fragile nature of the material, careful consideration had to be taken when fabricating and handling these structures. While there are still some areas that need to be investigated further, this work has illustrated the potential and limitations for immobilizing enzymes on dielectric inverse opal structures. Once the various parameters are optimized, flow-through NS structures could prove to be a useful format for biocatalysis applications, but their expansion to industrial-scale operations would be problematic. It is most likely that this approach to enzyme immobilization and reactivity will find its greatest use in research laboratory or other small volume enzymatic reaction applications.

Literature Cited

Literature Cited

1. http://www.bccresearch.com/report/enzymes-industrial-applications-bio030f.html.

2. Sheldon, R. A. *Advanced Synthesis & Catalysis* **2007**, *349*, 1289.

3. Hwang, E. T.; Gu, M. B. *Engineering in Life Sciences* **2013**, *13*, 49.

4. López-Gallego, F.; Betancor, L.; Mateo, C.; Hidalgo, A.; Alonso-Morales, N.; Dellamora-Ortiz, G.; Guisán, J. M.; Fernández-Lafuente, R. *Journal of Biotechnology* **2005**, *119*, 70.

5. Zhou, H.-X.; Dill, K. A. *Biochemistry* **2001**, *40*, 11289.

6. Lei, C.; Shin, Y.; Liu, J.; Ackerman, E. J. *Journal of the American Chemical Society* **2002**, *124*, 11242.

7. Lei, C.; Soares, T. A.; Shin, Y.; Liu, J.; Ackerman, E. J. *Nanotechnology* **2008**, *19*, 1.

8. Gornowich, D. B.; Blanchard, G. J. *The Journal of Physical Chemistry C* **2012**, *116*, 12165.

9. Abramova, V.; Sinitskii, A. *Superlattices and Microstructures* **2009**, *45*, 624.

10. Cao, Y.; Wang, Y.; Zhu, Y.; Chen, H.; Li, Z.; Ding, J.; Chi, Y. *Superlattices and Microstructures* **2006**, *40*, 155.

11. Gladden, J. K.; Dole, M. *Journal of the American Chemical Society* **1953**, *75*, 3900.

12. Holland, B. T.; Blanford, C. F.; Do, T.; Stein, A. *Chemistry of Materials* **1999**, *11*, 795.

13. Holland, B. T.; Blanford, C. F.; Stein, A. *Science* **1998**, *281*, 538.

14. Holland, B. T.; Blanford, C. F.; Stein, A. *Science* **1998**, *281*, 538.

15. Turner, M. E.; Trentler, T. J.; Colvin, V. L. *Advanced Materials* **2001**, *13*, 180.

16. Yang, P.; Deng, T.; Zhao, D.; Feng, P.; Pine, D.; Chmelka, B. F.; Whitesides, G. M.; Stucky, G. D. *Science* **1998**, *282*, 2244.

17. Yu, H. M.; Yim, J.-H.; Choi, K. Y.; Lim, J. S. *The Journal of Supercritical Fluids* **2012**, *67*, 71.

18. Ma, J.; Parajuli, B. R.; Ghossoub, M. G.; Mihi, A.; Sadhu, J.; Braun, P. V.; Sinha, S. *Nano Letters* **2013**, *13*, 618.

19. Mu, W.; Hwang, D.-K.; Chang, R. P. H.; Ketterson, J. B. *Journal of Raman Spectroscopy* **2011**, *42*, 941.

20. Dimos, M. M.; Blanchard, G. J. *The Journal of Physical Chemistry C* **2010**, *114*, 6019.

21. Dimos, M. M.; Blanchard, G. J. *Journal of Electroanalytical Chemistry* **2011**, *654*, 13.

22. Dimos, M. M.; Blanchard, G. J. *The Journal of Physical Chemistry C* **2011**, *115*, 11247.

23. Gornowich, D. B.; Blanchard, G. J. *The Journal of Physical Chemistry C* **2013**, in preparation.

24. Qu, F.; Nasraoui, R.; Etienne, M.; Côme, Y. B. S.; Kuhn, A.; Lenz, J.; Gajdzik, J.; Hempelmann, R.; Walcarius, A. *Electrochemistry Communications* **2011**, *13*, 138.

25. Szamocki, R.; Reculusa, S.; Ravaine, S.; Bartlett, P. N.; Kuhn, A.; Hempelmann, R. *Angewandte Chemie International Edition* **2006**, *45*, 1317.

26. Szamocki, R.; Velichko, A.; Mücklich, F.; Reculusa, S.; Ravaine, S.; Neugebauer, S.; Schuhmann, W.; Hempelmann, R.; Kuhn, A. *Electrochemistry Communications* **2007**, *9*, 2121.

27. Walcarius, A.; Kuhn, A. *TrAC Trends in Analytical Chemistry* **2008**, *27*, 593.

28. Subramanian, A.; Kennel, S. J.; Oden, P. I.; Jacobson, K. B.; Woodward, J.; Doktycz, M. J. *Enzyme and Microbial Technology* **1999**, *24*, 26.